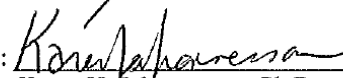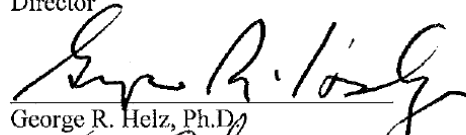TUNGSTEN SPECIATION, MOBILIZATION, AND SEQUESTRATION:

THIOTUNGSTATE STABILITY CONSTANTS AND EXAMINATION OF

(THIO)TUNGSTATE GEOCHEMISTRY IN ESTUARINE WATERS AND

SEDIMENTS

AN ABSTRACT SUBMITTED ON THE TENTH DAY OF NOVEMBER 2014

TO THE DEPARTMENT OF EARTH AND ENVIRONMENTAL SCIENCES

IN PARTIAL FULFILLMENT OF THE REQUIREMENTS

OF THE SCHOOL OF SCIENCE AND ENGINEERING

OF TULANE UNIVERSITY FOR THE DEGREE OF

DOCTOR OF PHILOSOPHY BY

_____

Tahmineh Jade Mohajerin Haug

APPROVED: _____

Karen H. Johannesson, Ph.D.

Director

_____

George R. Helz, Ph.D.

_____

George C. Flowers, Ph.D.

_____

Saugata Datta, Ph.D.

ABSTRACT

This dissertation combines laboratory experiments and analysis of field samples to examine tungsten (W) geochemistry. Data from low ionic strength experimental solutions at room temperature containing between 0.01 M to 0.0002 M total sulfide and 0.0027 M - 0.0001 M tungstate were analyzed using UV/VIS spectrophotometry. Stability constants have been determined for the formation of mono-thiotungstate log K_{01} = 3.43 ± 0.61, di-thiotungstate log K_{12} = 3.02 ± 0.61, tri-thiotungstate log K_{23} = 2.82 ± 0.02, and we estimated the tetra-thiotungstate log K_{34} ~ 2.34. Analysis of W, Mo, Mn, and Fe concentrations in estuarine surface and pore waters and sediments captured environmental samples from oxic and sulfidic conditions. Both surface waters and sediments demonstrated a positive correlation between W and Fe. Unlike Mo, which was depleted in sulfidic salt marsh pore waters, W was enriched in all pore waters in comparison to overlying waters. Thermodynamic modeling of W and Mo thioanion species in sulfidic pore water samples predicts ≤ 50% of tungstate (WO_4^{2-}) forms thiotungstate species and complete conversion of molybdate (MoO_4^{2-}) to tetrathiomolybdate (MoS_4^{2-}). Unlike tetrathiomolydate that is known to be more particle reactive than molybdate, increases in dissolved W coincide with increases in dissolved sulfide in pore waters, suggesting thiotungstates are less particle reactive than thiomolybdates at circum-neutral pH. Finally, sediment analysis suggests sequestration of W is dependent on surface water salinity in the intermediate marsh sediments, and long-term W entrapment occurs in sulfidic salt marsh sediments.
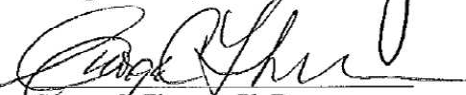
TUNGSTEN SPECIATION, MOBILIZATION, AND SEQUESTRATION:

THIOTUNGSTATE STABILITY CONSTANTS AND EXAMINATION OF

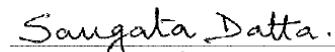(THIO)TUNGSTATE GEOCHEMISTRY IN ESTUARINE WATERS AND

SEDIMENTS
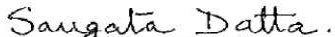
A DISSERTATION SUBMITTED ON THE TENTH DAY OF NOVEMBER

2014 TO THE DEPARTMENT OF EARTH AND ENVIRONMENTAL SCIENCES

IN PARTIAL FULFILLMENT OF THE REQUIREMENTS

OF THE SCHOOL OF SCIENCE AND ENGINEERING

OF TULANE UNIVERSITY FOR THE DEGREE OF

DOCTOR OF PHILOSOPHY BY

_____

Tahmineh Jade Mohajerin Haug

APPROVED: _____

Karen H. Johannesson, Ph.D.
Director

_____

George R. Helz, Ph.D.

_____

George C. Flowers, Ph.D.

_____

Saugata Datta, Ph.D.

UMI Number: 3680830

UMI

Dissertation Publishing

UMI 3680830

ProQuest®

ACKNOWLEDGMENTS

Table of Contents

LIST OF FIGURES

for core TBW-9; **d)** DTMP for W, Mo, and Mn is plotted against DOP for core TBW-1

Figure 4.6 Schematic model of proposed mechanisms controlling W mobilization and sequestration in northern Terrebonne Bay estuarine sediments. **a)** In marsh sediments underlying fresh water, W adsorbed to Fe oxides/oxyhydroxides (FeOx) are tranported from the water column to sediments. Release of W and Fe into overlying waters results in some re-precipitation of FeOx at the sediment-water interface, resulting in seasonal W and Fe enrichments in the sediments likely in the reactive fraction. **b)** During periods of marine water intrusion into the intermediate marsh, production of dissolved sulfide induces reducing conditions causing reductive dissolution of FeOx, releasing W and Fe. Although a portion of the relaeased W and Fe are remineralized in the pyrite fraction, some W and Fe escapes into overlying waters where they are transported laterally towards the coast causing a seasonal depletion in intermediate marsh sediments. **c)** In salt marsh sediments that are likely permanently sulfidic, both Fe and W are sequestered in the sediments.

Chapter 1

General Introduction

1.1 Importance of Tungsten

Research on tungsten (W) has focused on mining of W for commercial and industrial purposes, the role of W enzymes in biochemistry, and the potential for W toxicity. More recently, studies have attempted to understand W geochemistry in the environment. Tungsten occurs naturally in the environment and has a high melting point, high density, and high conductivity, making it well suited to a variety of applications. The boiling point of tungsten (i.e., ~5700°C) is higher than the estimated temperature of the sun's surface (5500°C), making W well suited for high-temperature applications such as heating elements in high-temperature furnaces and light bulb filaments. In addition to having the highest melting point of all metals, W also has excellent conductivity, thus W is incorporated into many electronic components including laser printers, window heating wires, and car horns. The hardness of tungsten carbide (close to that of diamonds) as well as tungsten's resistance to heat have made W alloys essential to a variety of cutting tools including household drill bits and dentists tools. Tungsten and its alloys are also used in common house hold items such as ball-point pen tips, snow tire studs, and fishing weights (Lassner and Schubert, 1999).

Occurrences of childhood leukemia clusters associated with high tungsten levels in the environment sparked recent interest in the toxicological effects of W on

human populations, as well as renewed efforts to understand the fate and transport of W in environment. Between the years 1997 and 2001, 16 cases of childhood leukemia were diagnosed in or near Fallon, Nevada, from a population of about 23,000, which is 23 times higher than the rate of childhood leukemia for the rest of Nevada during the same time period (CDC, 2003; Seiler, 2004; Koutsospyros et al., 2006). Groundwater that serves as a drinking water source for the affected population in Fallon, NV exhibited high W concentrations measuring up to 4.04 µmol/kg (0.742 mg W/kg), and tungsten in blood and urine samples of families that had been affected by the childhood leukemia outbreak were up to 15 times higher than the national average (Seiler et al., 2005). Two additional clusters of childhood leukemia in Sierra Vista, AZ, and Elk Grove, CA, were recognized around this same time period (Sheppard and Witten, 2003). These areas are all associated with active or inactive tungsten mines and/or associated processing operations (Koutsospyros et al., 2006). Trace element concentrations from tree rings in these three areas were measured during the early 1980's and then again between 1997 and 2003, and tungsten was the only element that consistently showed increasing concentrations since the early 1980's in all three childhood leukemia clusters (Sheppard and Witten, 2003; Sheppard et al., 2007, Sheppard et al., 2008). The exact cause of the childhood leukemia clusters has yet to be determined (Rubin et al., 2007; Seiler, 2012), but studies have shown adverse health effects associated with elevated tungsten exposure, such as tumor formation and DNA damage in rats, and higher incidence of seizures, stroke, cardiovascular disease, and breast cancer metastasis in humans (Marquet et al., 1997; Kalinich et al., 2005; Strigul et al., 2010; Strigul, 2010; Witten et al., 2012; Kelly et al., 2013; Tyrrell et al., 2013; Bolt et al., 2014).

Based on an earlier notion that W is essentially non-reactive and non-toxic there are no current regulation standards for W in drinking water or soils in the USA and European Union. In Russia, however, W is now classified as a highly dangerous contaminant in aquatic systems and maximum allowable concentrations of W (MACs) have been set at 272 nM (0.05 mg/L) for potable water, and 4.35 nM W (0.0008 mg/L) for waters used for fishing due to the toxic effects found for animal and fish embryos (Strigul et al., 2010). Adverse health effects associated with elevated tungsten exposure have highlighted the need to understand factors controlling mobility, solubility, and geochemical behavior of W in low temperature waters.

Tungsten in the environment has both natural and anthropogenic sources. Elevated levels of W exceeding 270 nM (0.05 mg/kg) in aqueous solutions have only been found in association with geothermal waters, solutions that have interacted with tungsten ore deposits, alkaline waters, nitrogenous fissure-vein geothermal waters from crystalline rocks, and in alkaline lakes in arid climates in which W is elevated due to evaporative concentration (Kletzin and Adams, 1996; Seiler et al., 2005). Anthropogenic sources include W use in ammunition leading to high concentrations in shooting ranges, especially on U.S. Military bases (Clausen et al., 2007, 2011; Clausen and Korte, 2009), and the use of W in semiconductor circuit boards, essential for electronic devices such as transistors, solar cells, and light-emitting diodes (LED's), has resulted in high W concentrations (i.e. > 2000 nM) in effluent from semiconductor manufacturers (Hsu et al., 2011).

1.2 Tungsten Biogeochemistry

Tungsten and molybdenum (Mo), both Group VIB transition elements, share

many chemical characteristics. Specifically, W and Mo exhibit similar coordination

chemistry, exist principally as oxyanions in the hydrosphere, have multiple oxidation

states, and appear to play broadly similar biogeochemical roles (Table 1.1; Baes and

Mesmer, 1976; Kletzin and Adams, 1996; Cotton et al., 1999; Sohrin et al., 1999;

Table 1.1: Chemical and physical similarities between tungsten and molybdenum, M= W or Mo. From Kletzin and Adams (1996).

	Tungsten (W)	Molybdenum (Mo)
Ionic radii for IV oxidation state (Å)	0.68	0.68
Electronegativity	1.4	1.3
pK_a of oxo acid (MO_4^{2-}/HMO_4^-)	4.60	3.87
M = O bond length (Å)	1.76	1.76

Stiefel, 2002). In oxic natural waters with pH above 4, Mo and W are most stable in

the hexavalent oxidation state occurring as oxyanions with the general form MO_4^{2-}

(M=W or Mo; Baes and Mesmer, 1976). The tungstate (WO_4^{2-}) and molybdate

(MoO_4^{2-}) oxyanions behave conservatively in rivers and ocean waters (Johannesson et

al., 2000; Sohrin et al., 1987, 1999; Arnórsson and Óskarsson, 2007; Firdaus et al.,

2008). Despite the prevalence of W and Mo oxyanions in the hydrosphere, both

elements have complex speciation that can affect their biogeochemical cycling

(Strigul, 2010 and references therein). In addition to having multiple oxidation states,

in low pH waters at high W concentrations, W can form numerous ill-defined

(hetero)polytungstates that can coexist with the monomeric forms (Table 2.5; Baes

and Mesmer, 1976; Cruywagen, 2000). Toxicological studies have demonstrated that

polytungstate species are more harmful than monomeric tungstate for organisms

including fish, algae, and earthworms (Strigul et al., 2009, 2010; Strigul, 2010), and

experimental studies suggest polytungstates are more mobile than tungstate (Bednar et

al., 2008). Although polytungstates may occur in acidic waters such as those associated with acid mine drainage, for natural waters with pH > 6 and W concentrations < 4 μM, including the estuarine waters examined in this study, tungstate occurs as a monomeric species (Baes and Mesmer, 1976).

In biological systems, Mo, and to a lesser extent W, are incorporated into metal sulfide groupings in enzymes that are crucial to carbon, nitrogen, and sulfur cycles on Earth (Müller and Diemann, 1981; Dobbek, 2011; Gonzalez et al., 2013). Tungsten can substitute for Mo in molybdoenzymes, and W is the heaviest element known to occur in biomolecules (Gonzalez et al., 2013). The antagonistic effects of W-substituted Mo-enzymes, which generally display little or no catalytic activity, are thought to be due to the higher redox potential of Mo-enzymes compared to W-enzymes (Stiefel, 2002; Gonzalez et al., 2013). The higher solubility and lower redox potential of W(VI) compared to Mo(VI) has also been established in laboratory studies and is supported by rarity of minerals such as tungstenite (WS_2) in low temperature systems (Hsu, 1977; Ivanova, 1986; Kletzin and Adams, 1996).

Despite the many similarities between W and Mo, including similar molar contents in the upper continental crust (~10 µmol/kg; Hu and Gao, 2008), molar Mo concentrations in seawater are ~2000 times higher than W concentrations (Sohrin et al., 1987, 1999; Firdaus et al., 2008). The processes responsible for this large fractionation of W and Mo that occurs as both metals are transferred from continental rocks to the oceans are poorly understood (e.g., Firdaus et al., 2008; Kashiwabara et al., 2013). One possibility is the apparently stronger affinity of W for ferromanganese oxides/oxyhydroxides compared to Mo (Gustafson, 2003; Xu et al., 2006; Kashiwabara et al., 2013), which could explain the preferential removal of W in the

low salinity region of estuaries compared to Mo (Van der Sloot et al., 1985; Hoede et al., 1987; Van der Sloot et al., 1989; Mohajerin et al., in prep).

1.3 Statement of Purpose

The objective of this study is to evaluate mechanisms controlling W geochemical behavior, and specifically how sulfidic conditions in natural waters affect W geochemistry and cycling. The chief hypothesis that informed the current study is that like Mo, W undergoes sulfidation reactions in natural, sulfidic waters, and the consequential formation of thiotungstate anions controls the effective solubility of W in these sulfidic waters by interaction with iron sulfide minerals. The specific goals of this dissertation are:

1- **Measure stability constants for the formation of thiotungstates in order to predict W speciation in oxic and sulfidic natural waters.**

2- **Quantify the effects of variable dissolved sulfide concentrations on dissolved W concentrations in low temperature, natural waters to compare thiotungstate behavior with tungstate behavior in the environment.**

3- **Determine environmental conditions and mechanisms controlling W mobilization and sequestration between sediments and natural waters.**

To accomplish the first goal laboratory experiments were designed to determine stability constants for thiotungstates. After adding tungstate to sulfidic aqueous solutions under anoxic conditions, 5 experimental solutions were analyzed for up to 735 days. Like molybdate, in sulfidic waters, WO_4^{2-} goes through a step-wise formation to WS_4^{2-} as described in the following reaction:

$$WO_xS_{4-x}^{2-} + H_2S \leftrightarrow WO_{x-1}S_{5-x}^{2-} + H_2O \hspace{3cm} (1)$$

in which $1 \leq x \leq 4$ (Aymonino et al., 1969a,b; Müller et al., 1969; Mohajerin et al., 2014a). First pure samples were synthesized to measure molar absorbtion coefficients for each thiotungstate species. Thiotungstate stability constants were then computed using UV/Vis spectrophotometry to measure the concentration of mono-, di-, tri-, and tetrathiotungstates over time. Total dissolved sulfide ($\sum S^{2-}$) was measured using titration with silver nitrate ($AgNO_3$), which was used to calculate dissolved [H_2S]. Determination of thiotungstate stability constants was then computed using the following equation:

$$Q_{ij} = \frac{[WO_{x-1}S_{5-x}^{2-}][H_2O]}{[WO_xS_{4-x}^{2-}][H_2S]} \qquad (2)$$

in which Q is the concentration product for each thiotungstate anion formation reaction (eq. 1) and [] indicates concentrations in mol/L. Using the Q values that had plataued from solutions at equilibrium yeilded the stability constants for each thiotungstate, which are about two orders of magnitude less than analogous thiomolybdate species. The calculated thiotungstate stability constants were then used to model naturally euxinic waters. Our results indicate 0.3 mM H_2S is required to convert 50% of tungstate to thiotungstate species.

In order to study how tungstate speciation affects W geochemical behavior, natural water samples were collected in order to capture conditions favorable to thiotungstate occurrence as well as waters in which tungstate is predicted to predominate. Surface and pore waters were collected from northern Terrebonne Bay estuary in southeast Louisiana near the Gulf of Mexico for two sampling periods-August 2013 and April 2014. Measurements of dissolved W in estuarine surface and

pore waters were evaluated along with dissolved Mo, Fe, and Mn concentrations, pH values, and dissolved sulfide concentrations. In the examined waters, W and Mo were both enriched in pore waters with low sulfide concentrations, pH ~7.8, underlying surface waters. In sulfidic pore waters however, unlike Mo, which was depleted compared to surface waters, W was enriched and had a positive association with increasing dissolved sulfide concentrations in pore waters.

In the fourth chapter, sediments from the two sediment cores collected in April 2014 as well as one sediment aliquot from August 2013 underlying fresh surface waters were analyzed. Sediment digestions provide comparison of W content in intermediate marsh sediments, characterized by fresh and brackish water vegetation, to permanently sulfidic salt marsh sediments. Total digestions were employed to determine whether or not W was sequestered in the associated estuarine sediments. Results from total sediment digestions indicate seasonal Fe redox cycling in this estuary effects W mobilization and sequestration. A commonly used sequential leaching technique was used to measure the distribution of W, Mo, Fe, and Mn in operationally defined reactive and pyrite phases and show that like Mo, W has a high degree of pyritization. Finally, the fifth chapter summarizes the conclusions for each goal presented in this chapter.

Chapter 2: Tungsten speciation in sulfidic waters: Determination of thiotungstate formation constants and modeling their distribution in natural waters

Abstract

Using UV/VIS spectrophotometry the equilibrium constants for the formation of monothiotungstate, WO_3S^{2-} ($WO_4^{2-} + H_2S \leftrightarrow WO_3S^{2-} + H_2O$; log K_{01}= 3.08 ± 0.11),

dithiotungstate, $WO_2S_2^{2-}$ ($WO_3S^{2-} + H_2S \leftrightarrow WO_2S_2^{2-} + H_2O$; log K_{12} = 3.22 ± 0.22),

trithiotungstate , WOS_3^{2-} ($WO_2S_2^{2-} + H_2S \leftrightarrow WO_3S^{2-} + H_2O$; log K_{23} = 2.76 ± 0.10),

and tetrathiotungstate , WS_4^{2-} ($WO_3S^{2-} + H_2S \leftrightarrow WS_4^{2-} + H_2O$; log K_{34} ~2.36) were

determined. The equilibrium constants describing the formation of thiotungstates are approximately two orders of magnitude less than the equilibrium constants for the formation of the analogous thiomolybdates. These equilibrium constants for thiotungstates were used to model tungstate speciation in sulfidic waters. The model predicts that thiotungstate species are negligible in most natural waters, but are likely to be important in circum-neutral, anoxic waters with ≥ 0.1 mM S(-II) concentrations. Natural waters that are conducive to thiotungstate formation include the Black Sea, Tyro and Bannock Basins, and pore waters with high rates of sulfate reduction such as those common in salt marshes. Preliminary field investigations indicate that thiotungstate formation may lead to increased W solubility.

2.1 Introduction

      The need to understand the fate and transport of tungsten (W) in the environment has been prompted by recent findings linking W to adverse health effects (Marquet et al., 1997; Koutsospyros et al., 2006; Butcher, 2011; Strigul et al., 2010; Witten et al., 2012). For example, studies using rodent models have related exposure to high doses of W to tumor formation and DNA damage (Kalinch et al, 2005; Kelly et al., 2013). In humans, Tyrrel et al. (2013) demonstrated that elevated urinary W concentrations (i.e. 1.36 nM compared to 0.71 nM) are associated with stroke and cardiovascular disease. As industrial uses of W increase the amount of W released into natural waters (Hsu et al., 2011), comprehending mechanisms controlling W fate and transport in the hydrosphere are needed.

      The biogeochemistry of tungsten (W) in the environment is poorly understood, and existing data for W in natural waters, in particular, are limited (Koutsospyros et al., 2006; Kashiwabara et al., 2013, and references therein). Nevertheless, recent studies indicate that elevated tungsten concentrations in natural waters are associated with reducing conditions, high alkalinity, and high concentrations of solid phase tungsten associated with iron oxides (Seiler et al., 2005; Cutler, 2011; Johannesson et al., 2013). Furthermore, W concentrations in groundwater from the Carrizo Sand aquifer in south Texas, are strongly correlated with dissolved sulfide concentrations ($r = 0.95$, $p < 0.001$), suggesting that W mobilization and transport in some groundwater flow systems may be influenced by dissolved sulfide (Johannesson et al., 2013).

Tungsten generally exhibits similar geochemistry to other oxyanion-forming trace elements like molybdenum (Mo) and arsenic (As) in that it is strongly adsorbed onto Fe(III) oxides/oxyhydroxides and surfaces of other minerals at low to circumneutral pH, but desorbs from these minerals as pH increases (Gustafsson, 2003; Koschinsky and Hein, 2003; Seiler et al., 2005; Arnórsson and Óskarsson, 2007; Bednar et al., 2008, 2009; Johannesson and Tang, 2009; Kashiwabara et al., 2013; Johannesson et al., 2013). More specifically, W and Mo share many chemical characteristics. For example, W and Mo have the same atomic radii, exhibit similar coordination chemistry, exist principally as oxyanions in the hydrosphere, and occur mainly in the +IV and +VI oxidation states in natural systems (Baes and Mesmer, 1976; Kletzin and Adams, 1996; Cotton et al., 1999; Sohrin et al., 1999).

In oxic natural waters with pH above 4, hexavalent W and Mo predominate and occur as oxyanions of the form MO_4^{2-} (M=W or Mo; Baes and Mesmer, 1976), which commonly behave conservatively in natural waters (Sohrin et al., 1987, 1999; Arnórsson and Óskarsson, 2007; Firdaus et al., 2008). In non-polluted river waters W concentrations are generally an order of magnitude less than Mo, and W measurements vary widely (i.e. 22 pM to 1 µM, with the 1 µM likely associated with hydrothermal springs; Johannesson et al., 2000; Firdaus et al., 2008). The mean residence time for W in the ocean has been estimated to be between 14,000 to 61,000 years, much lower than the estimated 740,000 to 800,000 year residence time of Mo, with the lower estimates of both W and Mo possibly skewed by polluted rain water samples (Sohrin et al., 1998; Firdaus et al., 2008). Reports of W in seawater have chiefly focused on the western Pacific Ocean, but are generally consistent with a mean W concentration of ~50 pM that is

conservative throughout measured water columns (Sohrin et al., 1987,1998, 1999;

Firdaus et al., 2008). Thus, in spite of the roughly similar molar concentrations in the

upper continental crust (Mo/W = 1.3 ± 0.5; Hu and Gao, 2008 and references therein),

molar ratios of Mo/W in seawater are ~2000 (Firdaus et al., 2008). The processes

responsible for this large fractionation of W and Mo that occurs as both metals are

transferred from continental rocks to the ocean are poorly understood (e.g., Firdaus et al.,

2008; Kashiwabara et al., 2013). One possibility is the apparently stronger affinity of W

for ferromanganese oxides/oxyhydroxides compared to Mo (Gustafson, 2003; Xu et al.,

2006; Kashiwabara et al., 2013). For example, using the generalized two-layer model of

Dzombek and Morel (1990), Gustafsson (2003) determined that the intrinsic surface

complexation constants for tungstate (WO_4^{2-}) adsorption onto ferrihydrite (log K_1^{int} =

19.31; log K_2^{int}= 6.4) exceed those for molybdate (MoO_4^{2-}) adsorption onto ferrihydrite

(K_1^{int} = 17.96; K_2^{int} = 3.14), demonstrating the greater affinity of W for ferric

oxides/oxyhydroxides.

Despite the prevalence of W and Mo oxyanions in the hydrosphere, both

elements have complex speciation that can affect their biogeochemical cycling. In

addition to having multiple oxidation states, in low pH waters and high W concentrations,

W forms (hetero)polytungstate species, which are more toxic and can coexist with the

monomeric tungstate oxyanion, WO_4^{2-} (Table 2.5; Baes and Mesmer, 1976; Cruywagen,

2000; Bednar et al., 2008, 2009; Strigul et al., 2009, 2010; Strigul, 2010). In biology, W

and Mo play similar biochemical roles in catalytic reactions, although in eukaryotes and

bacteria Mo-enzymes (critical in the cycling of C, N, and S) dominate, whereas

analogous W-enzymes predominate in archea (Kletzin and Adams, 1996; Stiefel, 2002; Andreesen and Makdessi, 2008; Bevers et al., 2009; Gonzalez et al., 2013).

Laboratory investigations have also presented evidence that, like Mo, W forms thioanions in sulfidic solutions (Aymonino et al., 1969a,b ; Müller et al., 1969; Kulmukhamedov et al., 1991). Specifically, the formation of mono- and dithiotungstates (i.e., WO_3S^{2-} and $WO_2S_2^{2-}$, respectively) follows the general thiotungstate formation reaction:

$$WO_xS_{4-x}^{2-} + H_2S \leftrightarrow WO_{x-1}S_{5-x}^{2-} + H_2O \tag{1}$$

in which $1 \leq x \leq 4$ (Aymonino et al., 1969a,b; Müller et al., 1969). To the best of our knowledge, however, no studies have examined the formation of thiotungstates in natural waters, nor demonstrated the formation of tri- or tetrathiotungstates (i.e., WOS_3^{2-} and WS_4^{2-}). This study was motivated by the observation that W in the Carrizo Sand aquifer where S(-II) = 40 μM is ≥ 16 times the W concentration of the groundwater where S(-II) is generally ≤ 2 μM (Johannesson et al., 2013). Groundwater from the Carrizo Sand aquifer is an important drinking water resource in south Texas. Given the possibility of adverse health effects arising from excess W in bodily fluids (Marquet et al., 1996; Butcher, 2011; Tyrell et al., 2013), understanding the geochemical processes controlling W in drinking waters is vital. Furthermore, the reactivity of thiotungstate anions in natural waters with regards to minerals is largely unknown, which hampers our ability to predict the mobilization and transport of W in sulfidic waters.

Although the exact mechanisms for Mo enrichment in sulfidic sediments are complex and still under investigation, there is general consensus that formation of thiomolybdates is the first step in the removal of Mo from euxinic waters (Helz et al.,

1996; Erickson and Helz, 2000; Zheng et al., 2000; Bostick et al., 2003; Vorlicek et al., 2004; Tribovillard et al., 2006; Dahl et al., 2013; Chappaz et al., 2014). The evolving consensus differs from earlier models that proposed direct reduction of Mo(VI) to Mo(IV) and subsequent precipitation to explain Mo removal from sulfidic waters (e.g., Emerson and Huested, 1991; Calvert and Pedersen, 1993; Crusius et al., 1996). Reduction of thiomolybdates, however, may be a key mechanism for thiomolydate removal (Helz et al., 2011; Dahl et al., 2013; Chappaz et al., 2014). Given the lower redox potential of W compared to Mo (Tsigdinos, 1978; Ivanova, 1986; Kletzin and Adams, 1996), it is not clear whether thiotungstates are scavenged from sulfidic waters in a manner similar to that of the thiomolybdates. Although measurements of W in marine sediments are scarce, reported values of 30 ppm to > 100 ppm W in recent sediments from the euxinic Black Sea (Pilipchuk and Volkov, 1966) are higher than bottom sediments underlying oxic seawater (0.5- 5.35 ppm W; Krauskopf 1970; Hoede et al., 1987), suggesting that W may accumulate in sediments of anoxic basins.

This contribution investigates tungstate-thiotungstate conversions in experimental sulfidic aqueous solutions and presents equilibrium constants for the stepwise formation of four thiotungstate species relevant to natural waters. The measured equilibrium constants enable us to evaluate the possibility that thiotungstate formation could be responsible for changing the sorptive interactions of W with solid phases in the Carrizo aquifer, and thus be related to the observed increase in dissolved W (Johannesson et al., 2013). Finally, these formation constants are used to model thiotungstate formation in sulfidic, natural waters and speculate on the geochemical behavior of thiotungstates.

2.2 Materials and Methods

2.2.1 Materials

Doubly deionized, ultrapure water (i.e., Milli-Q, 18.2 MΩ cm) was deoxygenated by bubbling nitrogen (Airgas, 99.999%) through a gas diffusion tube for at least 45 minutes. Sulfide-bearing aqueous solutions were prepared under a hood by bubbling high-purity H_2S (Airgas, > 99.5%) through deoxygenated water for several minutes and were then sealed and transferred into the anoxic chamber. Stock tungstate solutions were made from sodium tungstate dihydrate (i.e., $Na_2WO_4 \cdot 2H_2O$; Strem Chemicals) dissolved in deoxygenated, Milli-Q water.

2.2.2 Experimental solutions

The five experimental solutions used to determine the thiotungstate equilibrium constants are listed in Table 2.1. Solution compositions were prepared to capture a range of S(-II)/W concentration ratios that could occur in natural waters. Studies over a range of pH values were hampered by the sluggish formation of thiotungstates at pH ≥ 7, and the attempt to avoid polytungstate formation at low pH values.

Preparation of thiotungstate solutions was conducted in a glove box or in a glove bag under an anoxic- N_2 atmosphere using Ridox oxygen scavenger (Fisher Scientific) for oxygen removal. Experimental solutions were prepared by mixing known amounts of tungstate stock solutions with freshly prepared dissolved sulfide solutions in deoxygenated water. The pH, total sulfide, and thiotungstate concentrations were measured immediately and for increasing time intervals (Table 2.1 and Electronic Annex in *Geochimica et Cosmochimica Acta*) using the approaches described below. Solutions were anoxically sealed either in capped Wheaton glass vials inside the glove box, or

Table 2.1: Composition of experimental solutions used to calculate K_{ij}

Solution ID Date created	Reactants	Concentrations	pH range	Ionic strength Total volume	Log K values determined	Time to reach equilibrium
TW1 7 March 2012	$Na_2WO_4 \cdot 2H_2O$ S (-II) initial S (-II) range	0.1 mM 11 mM [a]11 mM- 5.1 mM	4.52-4.92	0.32 mM 500 mL	Log K_{12} = 3.86 ± 0.2 Log K_{34} = 2.33 ± 0.03	~ 20 min. ~735 days
TW-B 28 March 2012	$Na_2WO_4 \cdot 2H_2O$ Initial S(-II) aq S(-II) range NH_3/NH_4^+ buffer	0.1 mM 6.6 mM 6.6 – 5.9 mM 10 mM	6.84- 6.90	6.7 mM 500 mL	Log K_{23} = 2.76 ± 0.1	107 – 288 days (stayed at equilibrium with respect to WOS_3^{2-})
TW4 11 April 2012	$Na_2WO_4 \cdot 2H_2O$ Initial S(-II) aq	1.176 mM 5.927 mM	5.22- 5.28	3.6 mM 100 mL	Log K_{12} = 3.17 ± 0.03	~ 20 min.
C1 25 Oct. 2012 cuvette mix	$Na_2WO_4 \cdot 2H_2O$ Initial S(-II) aq	0.1 mM 3.06 mM	5.13-5.4	0.33 mM 4.55 mL	Log K_{01} = 3.05 Log K_{12} = 3.10 ± 0.1	< 1 min. 30-60 min.
C2 5 Nov. 2012 cuvette mix	$Na_2WO_4 \cdot 2H_2O$ Initial S(-II) aq	0.1 mM 4.157 mM	5.31	3.4 mM 4.55 mL	Log K_{01} = 3.11 ± 0.04	1-3 min.

[a]Sulfide concentration measured 5.8 mM the second day, degassing likely occurred shortly after preparation.

flame sealed in glass ampules using techniques described in Helz and Dolor (2012). The sealed solutions were then kept at room temperature (21 ± 1.5°C) until analysis.

To collect scans of the short-lived monothiotungstate, 1 cm cuvettes with septum tops were used for two of the experiment solutions. Briefly, a known volume and concentration, of aqueous sulfide (determined by titration) was added to deoxygenated water in a cuvette. Then, a known volume and concentration of tungstate was injected into a cuvette through the septum. A UV/Vis spectrophotometric scan was recorded both before tungstate injection, and immediately after the introduction of tungstate to capture

monothiotungstate formation. In addition to possible oxidation, some degassing of H_2S occurred in the glove box as solution aliquots were being measured or sealed for later measurement. Thus, some changes in total sulfide concentration and pH occurred as shown by the pH and sulfide ranges in Table 2.1.

2.2.3 Measurements

All pH measurements were made inside the glove box with a double junction pH meter (Oakton pHTestr 30) that was calibrated and checked with certified reference pH buffers (pH 4, 7, and 10) the day of use to ensure accuracy of ± 0.05. Total sulfide concentrations in experimental solutions were measured using potentiometric titration (Metrohm 836 Titrando) with 0.01 M or 0.001 M $AgNO_3$ utilizing a Ag_2S coated titrode for sulfide analysis (Metrohm Ti Application Note No. T-32). Measurements of solutions with known S(-II) concentrations (e.g. sulfide standard Aqua Solutions) showed an average of $\leq 5\%$ error in sulfide concentrations.

2.2.4 Measurement of thiotungstate concentrations

Using matching cuvettes with Milli-Q water as a blank, the absorbance of the experimental solutions for 270 nm $\leq \lambda \leq$ 500 nm was recorded (HACH DR5000). Lower wavelengths (i.e. $\lambda < 270$ nm) were not employed because of interference from the absorbance of sulfide and the ammonium buffer. Concentrations of thiotungstates were determined in the experimental solutions by applying Beer's Law to UV/Vis spectrophotometric scans and by assuming that the absorbance was additive (i.e.,

$$\frac{A_{\lambda obs}}{d} = \varepsilon_{\lambda WO_3S^{2-}} c_{WO_3S^{2-}} + \varepsilon_{\lambda WO_2S_2^{2-}} c_{WO_2S_2^{2-}} + \varepsilon_{\lambda WOS_3^{2-}} c_{WOS_3^{2-}} + \varepsilon_{\lambda WS_4^{2-}} c_{WS_4^{2-}}$$, where $A_{\lambda obs}$ is the

absorbance at a given wavelength (λ), d is the pathlength (cm), ε_λ is the molar absorption coefficient at λ for a given species (Fig. 2.1), and c is the concentration of the given

species (M)). Employing our measured molar absorption coefficients (ε_λ) for all four

thiotungstates (Fig. 2.1; described below), the concentration values (c) were used as

adjustable parameters to fit the above equation to our individual wavelength UV/Vis

scans using classical least squares (270-500 nm; Montgomery et al., 2012; Electronic

Annex- CLS and constrained CLS). To measure equilibrium concentrations for each

thiotungstate species, analyses of solutions occurred for up to 735 days. The sealed

ampules were opened in the glove box at increasing time intervals to measure pH, sulfide,

and thiotungstate concentrations. Using this method for a solution with known

thiotungstate concentrations, calculated concentrations were within 10% of actual

concentrations for each thiotungstate species.
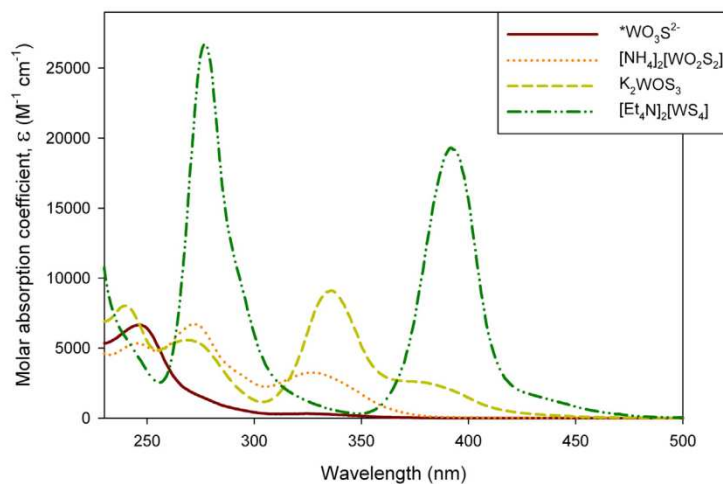
Figure 2.1: UV/Vis molar absorption coefficients as a function of wavelength for synthesized thiotungstate salts measured in this study. *Absorption coefficients for the WO_3S^{2-} species were measured from the C1 and C2 solutions as described in the text.

2.2.5 Determination of molar absorbance coefficients

To determine the molar absorption coefficients (i.e., ε in M^{-1} cm^{-1}) for $WO_2S_2^{2-}$, WOS_3^{2-}, and WS_4^{2-} for wavelengths between 230-500 nm, first pure $(NH_4)_2WO_2S_2$, K_2WOS_3, and $(Et_4N)_2WS_4$ salts were synthesized using previously described methods (Müller et al., 1970; McDonald et al., 1983; Basu et al., 2009). Next, each thiotungstate salt was analyzed using X-ray powder diffraction (XRD), and its composition was verified by comparison with the peak positions for the pure material provided in the International Centre for Diffraction Data (ICDD) database (Appendix A). Absorbance data were then recorded for wavelengths between 230 nm to 500 nm in 1 cm cuvettes for a series of standard solutions for each thiotungstate salt (Appendix B, Table B.1), and ε (M^{-1} cm^{-1}) was calculated using Beer's Law (above). Plotting the absorbance at a given wavelength against concentration and setting the y intercept to 0, the slope of the line is equal to the molar absorption coefficient, (i.e., $\varepsilon = A_\lambda/(dc) +0$). The molar absorption coefficients were established by this method for all wavelengths from 230 – 500 nm for each thiotungstate species (Fig. 2.1; Electronic Annex). Our values for the maximum molar absorption coefficients are similar to previous reports (Table 2.2). Monothiotungstate has been shown to exist only in solution, and pure monothiotungstate (WO_3S^{2-}) salt has not been isolated, but the absorption maxima (i.e., λ_{max} Table 2.2) have been reported (Müller et al., 1969; Aymonino et al., 1969a; Tsigdinos, 1978). Spectrophotometric scans in this study as well as those by Aymonino et al. (1969a,b) indicate that an isosbestic point exists between WO_3S^{2-} and $WO_2S_2^{2-}$ (dithiotungstate) at ~255 nm; thus, ε must be identical for both species at this wavelength (Fig. 2.1). Employing the molar absorption coefficient of dithiotungstate ($WO_2S_2^{2-}$), the concentration of monothiotungstate was determined using Beer's Law (Appendix B).

After obtaining the wavelength scans for several pure monothiotungstate solutions, the

molar absorption coefficients for monothiotungstate were then calculated as described

Table 2.2: UV/Visible spectroscopic absorption maxima, λ_{max} (in nm), and corresponding molar absorption coefficients, ε (in M^{-1} cm^{-1}), for thiotungstate anions.

	Müller et al. (1969)		McDonald et al. (1983)		This study	
	λ_{max}	ε (M^{-1} cm^{-1})	λ_{max}	ε (M^{-1} cm^{-1})	λ_{max}	ε (M^{-1} cm^{-1})
WS_4^{2-}	392	18500	393	15710	392	19300 ± 80
	277	28500	277	24500	277	26700 ± 670
WOS_3^{2-}	375	3000	375	3200	[a]374	2610 ± 10
	335	11300	336	11400	336	9110 ± 20
	270	7200	268	2860	269	5570 ± 20
	243	9700	240	9900	240	8020 ± 20
$WO_2S_2^{2-}$	327	4000	326	4050	327	3260 ± 200
	273	6900	272	8290	272	6740 ± 360
	244	3900	246	5700	245	5330 ± 160
WO_3S^{2-}	327				325	316 ± 30
	244				246	6660 ± 910

[a] Not a peak, but does show a shoulder around this wavelength.

previously.

2.2.6 Stability constant calculations

The concentration product, *Q*, for each thiotungstate anion formation reaction

(eq. 1) was calculated using the thiotungstate concentrations, computed with Beer's Law,

for each time of observation using:

$$Q_{ij} = \frac{[WO_{x-1}S_{5-x}^{2-}][H_2O]}{[WO_xS_{4-x}^{2-}][H_2S]} \tag{2}$$

in which [] indicates concentrations in mol/L. The value at which Q_{ij} plateaus is the

equilibrium constant for the reaction under the experimental conditions (Erickson and

Helz, 2000). Substituting activity for concentration, in equation 2, the activity

coefficients for the oxy-thiotungstates, which have the same charge, can be assumed to

cancel. Furthermore, the activity coefficients for $H_2S_{(aq)}$ and H_2O will be ~1 considering

the low ionic strength of our solutions (Table 2.1). Therefore, at equilibrium $Q_{ij} \rightarrow K_{ij}$. The

different activity products are indicated using, Q_{ij}, in which i indicates the number of

sulfur atoms in the reactant and j gives the number of sulfur atoms in the product. Thus,

Q_{12}, is the activity product for the conversion of monothiotungstate (WO_3S^{2-}) to

dithiotungstate ($WO_2S_2^{2-}$). The concentration of H_2S was calculated using $pK_a = 6.98$,

$K_a = \dfrac{[HS^-][H^+]}{[H_2S]}$, as the first ionization constant for H_2S (Butler and Cogley, 1998) and a

mass balance equation:

$$[H_2S] = \sum S^{2-} - [HS^-] - 4[WS_4^{2-}] - 3[WOS_3^{2-}] - 2[WO_2S_2^{2-}] - [WO_3S^{2-}] \qquad (3)$$

recognizing that $[H_2S]$ is related to the total sulfide concentrations in our solutions. Total

sulfide, pH, and the individual thiotungstate concentrations are known for each

experiment. Thus, $[HS^-]$ and $[H_2S]$ can be calculated for each scan. Calculations for Q_{ij}

were conducted for each solution at each measurement over time, and K_{ij} was computed

by averaging the Q_{ij} values calculated during equilibrium for a given thiotungstate

species.

     Measurements of solution TW1 (Table 2.1) over 735 days indicate that the

solution was slowly reaching equilibrium with respect to tetrathiotungstate. The true K_{34}

value was estimated by a nonlinear least squares fit (R Core Team 2013) to

$$Q_{34} = K_{34}\,(1 - e^{-bt}), \qquad\qquad (4)$$

where K_{34} is the asymptotic value of the plot of Q_{34} versus t, b is an apparent decay

constant, and t is time in days. Measurements that have small separations in time were

grouped to avoid redundancy and ensure appropriate weighting of the data (see Electronic

Annex for details). Computationally identical parameter estimates were obtained with

diverse starting points for the nonlinear fitting procedure, indicating a unique fit.

2.2.7 Calculating empirical rate constants

Applying methods described by Erickson (1998) and Erickson and Helz (2000), the forward reaction rates for the formation of each thiotungstate anion were calculated for each experimental solution (Table 2.1). First, we determined that the reactions were first order with respect to W and H_2S. Plotting $y = \ln(C_{eq} - C_t)$, where C_{eq} is the equilibrium concentration for the thiotungstate and C_t is the concentration of that thiotungstate at a given time, versus time on the x-axis showed linearity for each thiotungstate reaction, ($R^2 \geq 0.97$; e.g., Appendix Fig. C.1). Because the formation of each thiotungstate anion was first order with respect to W and H_2S, the following differential equation describes how the concentration of the species changes with time, considering both the forward and reverse reactions:

$$\frac{d[WO_{x-1}S_{5-x}^{2-}]}{dt} = k_f[H_2S]_t[WO_xS_{4-x}^{2-}]_t - k_b[WO_{x-1}S_{5-x}^{2-}]_t \tag{5}$$

where k_f is the forward rate constant for the reaction as written in eq. 1, and k_b is the rate constant for the corresponding reverse reaction. The formation constant is related to the forward and reverse rate constants by the following expression: $K = \dfrac{k_f}{k_b}$. We used this relationship to fix k_b in eq. 5 using the formation constants provided in Table 2.3. Because total sulfide was much greater than the W concentration for each solution, $[H_2S]$ was assumed to be constant. Simultaneous numerical integration of eq. 5 for each (thio)tungstate species was done with Scientist® (Micromath) to solve for the forward rate constants (k_f), minimizing the sum of the squared differences between the calculated and measured concentrations for all observation times for each solution. Details are provided in Erickson and Helz (equations 2-4; 2000).

2.3 Results

2.3.1 Thiotungstate formation constants

Following eq. 1, as time progresses, changes in the thiotungstate concentrations are measureable using UV/Vis spectrophotometry. For example, Fig. 2.2 shows the spectral changes and calculated concentrations, respectively, for solution TW4 (Table 2.1) over a period of 22 minutes as thiotungstate formation progresses from monothiotungstate to dithiotungstate (eq. 1). The stabilization of mono- and dithiotungstate concentrations after ~15 minutes demonstrate equilibrium with respect to dithiotungstate formation (Fig. 2.2b). Wavelength scans used to determine thiotungstate concentrations, and pH, sulfide, and thiotungstate concentrations as a function of time that were used to calculate the Q_{ij} values are provided in the Electronic Annex.

Figure 2.3 depicts the calculated log Q_{ij} (eq. 3), as solutions approach and attain equilibrium with the mono-, di-, tri-, and tetrathiotungstate anions. The solid horizontal lines represent average K_{ij} values, and the dotted lines represent the standard deviation (Fig. 2.3). Table 2.3 provides the thiotungstate formation constants calculated in this study. The K_{01} value in Table 2.3 is the mean ($\pm\sigma$) of the activity products (Q_{01}) at equilibrium with respect to monothiotungstate formation from solutions C1 and C2 (Table 2.1). K_{12} represents the mean ($\pm\sigma$) of the activity products at equilibrium with respect to dithiotungstate in solutions TW1, TW4, and C1 (Table 2.1). Note, the considerably higher K_{12} value from solution TW1 was obtained from measurements that were taken shortly before WO_3S^{2-} concentrations became undetectable, hence values presented in Table 2.3 are based on a weighted mean. K_{23} is the mean of the activity products at equilibrium with respect to trithiotungstate in solution TW-B (Table 2.1).

Using solution TW1, the estimated equilibrium constant for WS_4^{2-} is $K_{34} = 231$ with a

standard error of 17 and a 95 percent confidence interval of [199, 280] (constructed using
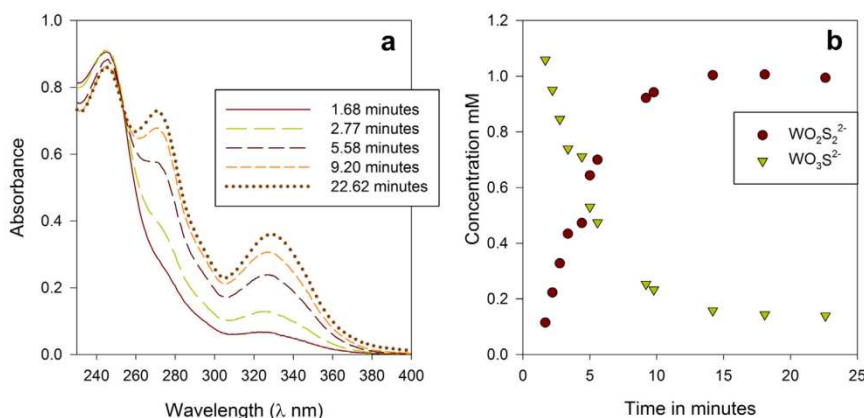
Figure 2.2: a) Selected UV/VIS scans of solution TW4 (Table 2.1) depicting formation of $WO_2S_2^{2-}$ from WO_3S^{2-}. **b)** Calculated concentrations (using Beer's Law) of mono- and di-thiotungstates in TW4 over the same time period presented in panel (a). For the relatively short time period presented here, the tri- and tetra-thiotungstate anion concentrations were negligible.

Table 2.3- Conditional, first order approximations of formation constants for thiotungstates

$WO_4^{2-} + H_2S \leftrightarrow WO_3S^{2-} + H_2O$	$\text{Log } K_{01} = 3.08 \pm 0.11;$ [a]$(\text{Log } K_{01} = 3.4)$
$WO_3S^{2-} + H_2S \leftrightarrow WO_2S_2^{2-} + H_2O$	$\text{Log } K_{12} = 3.22 \pm 0.22$
$WO_2S_2^{2-} + H_2S \leftrightarrow WOS_3^{2-} + H_2O$	$\text{Log } K_{23} = 2.76 \pm 0.1$
$WOS_3^{2-} + H_2S \leftrightarrow WS_4^{2-} + H_2O$	$\text{Log } K_{34} \sim 2.36$ (extrapolated)

[a] From Blokhin and Kopyrin (2003), equilibrium formation constant for WO_3S^{2-} in 1 M ammonium nitrate, converted to K at infinite dilution and to be in terms of H_2S instead of HS^-.

resampling near the estimated optimum). The apparent decay constant $b = 3.04 \pm 0.44 \times$

10^{-3} day^{-1} was used to obtain the best fit of a Q_{34} asymptote to our measurements. The

correlation coefficient between the observed and predicted values is $r = 0.98$. The estimated formation constant $K_{34} = 231 \pm 17$ is consistent with the last observed $Q_{34} = 216 \pm 16$ calculated at 735 days. Our results indicate that thiotungstate formation constants are similar in magnitude to those recently determined for the formation of thioperrhenates, ReO_3S^-, and ReS_4^- (Helz and Dolor, 2012) and are about 2 orders of magnitude less than the corresponding thiomolybdate formation constants (Erikson and Helz, 2000).

2.3.2 Rate of thiotungstate formation

The empirical rate laws for the forward rate constants for each thiotungstate anion determined for solutions TW1 and TW-B are presented in Table 2.4. The calculated thiotungstate concentrations over time that were used to calculate rate constants are given in the Electronic Annex. The reaction rates for each successive thiotungstate species decrease dramatically with time (Fig. 2.3) and are greater at lower pH values, suggesting thiotungstates are acid catalyzed, as is the case with thiomolybdates (Erickson and Helz, 2000). Previous research suggested that thiomolybdates form faster than thiotungstates (Aymonino et al., 1969b). No rates, however, have been published for thiotungstate formation. Our study demonstrates that, whereas thiomolybdates attained equilibrium with respect to MoS_4^{2-} after ~60 days (Erickson and Helz, 2000), it took ~2 years to approach equilibrium with respect to WS_4^{2-} (Fig. 2.3d). Although the rate constants presented depend on the solution composition and cannot be extrapolated to natural waters, these constants describe the relative rates of formation of the different thiotungstates and allow for a semi-quantitative comparison to thiomolybdate formation rates.

Table 2.4: Empircal forward rate constants from two solutions.

k_f formula	TW1	pH	TW-B	pH
$WO_4^{2-} + H_2S \rightarrow WO_3S^{2-} + H_2O$	$236000\ M^{-1}\ day^{-1}$	4.52	$101000\ M^{-1}\ day^{-1}$	6.84
$WO_3S^{2-} + H_2S \rightarrow WO_2S_2^{2-} + H_2O$	$38300\ M^{-1}\ day^{-1}$	4.52	$708\ M^{-1}\ day^{-1}$	6.91
$WO_2S_2^{2-} + H_2S \rightarrow WOS_3^{2-} + H_2O$	$350\ M^{-1}\ day^{-1}$	4.69–4.74	$7.92\ M^{-1}\ day^{-1}$	6.90–6.99
$WOS_3^{2-} + H_2S \rightarrow WS_4^{2-} + H_2O$	$<0.6\ M^{-1}\ day^{-1}$	4.61–5.11	Not determined	–
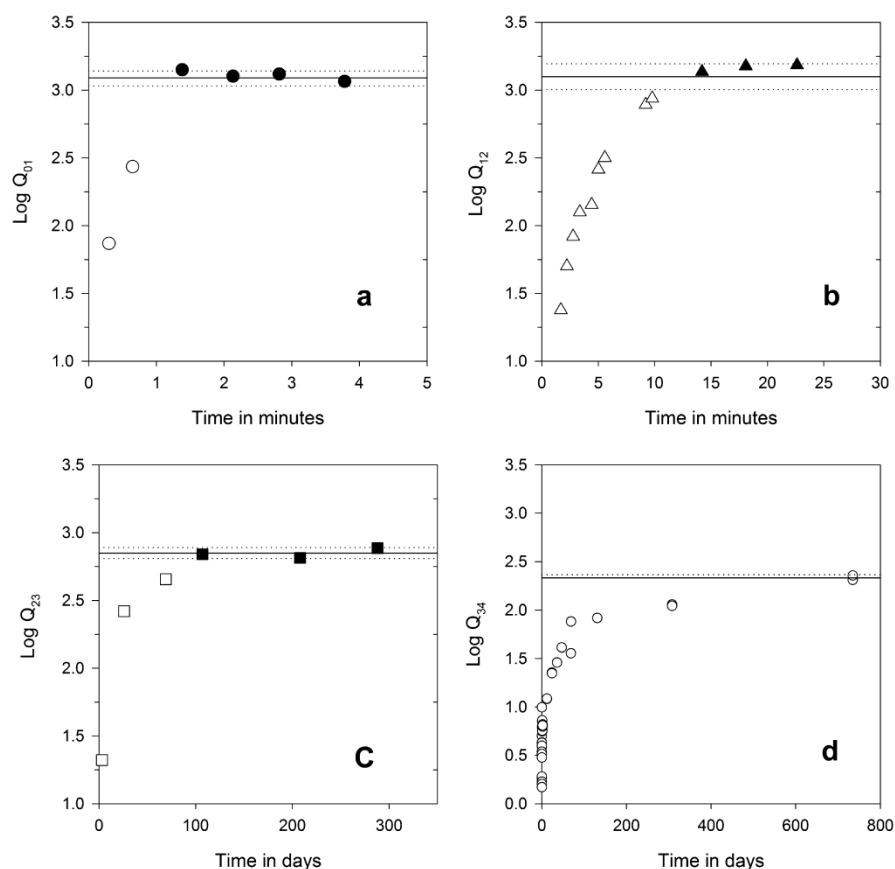
Figure 2.3: Calculated activity products for representative solutions. *Q* values taken to be at equilibrium are shown in the figures as filled symbols and were used to calculate *K* values. **a)** from solution C2, **b)** from solution TW4, **c)** from solution TW-B, and **d)** TW1. Solid line indicates average K_{ij} value, and dotted lines show standard deviation (σ).

2.4. Discussion

2.4.1 Reported thiotungstate formation constants

Figure 2.4 (conditions described below in section 2.4.2) illustrates W speciation

as a function of $H_2S_{(aq)}$ based on the findings we have presented. Specifically, relatively

high sulfide concentrations that increase with increasing pH are required to attain

equilibrium with respect to thiotungstates. The values in Table 2.3 are from solutions that

had measurable amounts of reactants at equilibrium, the concentration of the reactants

was greater than the concentration of the products (eq. 1), and were not expected to form

polytungstates (Table 2.5).

Previous investigations of thiotungstate anion formation are scarce in the

literature. Blokhin and Kopyrin (2003) measured the equilibrium constant for the

formation of the monothiotungstate anion from the tungstate anion (i.e., K_{01}) in 1 M

ammonium nitrate solutions buffered at pH 9.2 and 9.7. These researchers report a log

$K_{01} = 3.4$, for the formation of monothiotungstate, which is similar to our estimate of log

$K_{01} = 3.08 \pm 0.11$ (Tables 2.3). The reported equilibrium constants of Kulmukhamedov et

al. (1991) for thiotungstates and thiomolybdates are inconsistent with previously reported

values, which are all in reasonable agreement (Harmer and Sykes, 1980; Brule, 1982;

Erickson and Helz, 2000; Blokhin and Kopyrin, 2003). Hence, the formation constants

determined by Kulmukhamedov et al. (1991) are not reported here. No values have

previously been reported for tri- and tetrathiotungstates.

4.2 Tungsten speciation and geochemical behavior in sulfidic waters

Tungsten speciation was modeled using Geochemist's Workbench® (release 9.0; Bethke,

2008; Bethke and Yeakel, 2013), and the Lawrence Livermore database (Delaney and

Lundeen, 1989) provided with the software (i.e., thermo.dat). The database was modified

by addition of the equilibrium constants for the formation of the four thiotungstate species determined in this contribution, and the dissociation constants for tungstic acid (H_2WO_4) and several polytungstates species at infinite dilution (Table 2.5). The objective of the model was to evaluate the geochemical conditions under which thiotungstates are likely to form, and other ion pairs involving W were not included. Figure 2.4 illustrates W speciation as a function of sulfide, Lines are added to show predicted W speciation for 4 natural waters (i.e. Carrizo Sand aquifer, Black Sea, a salt marsh porewater, and Tyro Basin). Polytungstates and tungstic acids are negligible (<0.01%) under these conditions.

Table 2.5: Formation constants of aqueous species and scheelite solubility added to GWB database for modeling

Reaction	Log K at 25° C	References
$WO_4^{2-} + H^+ \rightarrow HWO_4^-$	3.6	Smith and Martell (2004)
$WO_4^{2-} + 2H^+ \rightarrow H_2WO_4$	5.8	Smith and Martell (2004)
$WO_4^{2-} + H_2S \rightarrow WO_3S^{2-} + H_2O$	3.08	This study
$WO_3S^{2-} + H_2S \rightarrow WO_2S_2^{2-} + H_2O$	3.22	This study
$WO_2S_2^{2-} + H_2S \rightarrow WOS_3^{2-} + H_2O$	2.76	This study
$WOS_3^{2-} + H_2S \rightarrow WS_4^{2-} + H_2O$	2.36	This study
$7WO_4^{2-} + 8H^+ \rightarrow W_7O_{24}^{6-} + 4H_2O$	65.19	Cruywagen and van der Merwe (1987)
$7WO_4^{2-} + 9H^+ \rightarrow HW_7O_{24}^{5-} + 4H_2O$	76.59	Rozantsev and Sazonova (2005)
$6WO_4^{2-} + 7H^+ \rightarrow HW_6O_{21}^{5-} + 3H_2O$	63.83	Smith and Martell (2004)
$6WO_4^{2-} + 6H^+ \rightarrow H_2W_6O_{22}^{6-} + 2H_2O$	53.68	Rozantsev and Sazonova (2005)
$12WO_4^{2-} + 14H^+ \rightarrow H_2W_{12}O_{42}^{10-} + 6H_2O$	123.38	Rozantsev and Sazonova (2005)
$12WO_4^{2-} + 18H^+ \rightarrow H_2W_{12}O_{40}^{6-} + 8H_2O$	149.59	Rozantsev and Sazonova (2005)
$10WO_4^{2-} + 16H^+ \rightarrow W_{10}O_{32}^{4-} + 8H_2O$	129.63	Rozantsev and Sazonova (2005)

Table 2.6: Parameters for speciation model

Location	pH	S(-II) mM	WO_4^{2-} (nM)	Ionic strength (M)
[a]Carrizo	8.54	0.39	1.30	0.15
[b]Black Sea	7.38	0.4	0.05	0.45
[c]Cocodrie	6.9	1.83	0.9	0.2
[d]Tyro Basin	6.75	2.1	0.05	5.3

[a] Parameters from SMA74R-2 in Johannesson et al. (2013; Table 2.4) were employed.
[b]Data for pH and salinity from Goyet et al. (1991), sulfide from Neretin et al., 2001.
[c]Porewater concentrations from Cocadrie, a Louisiana salt marsh.

[d]Tyro Basin parameters from DeLange et al. (1990). Note that the ionic strength exceeds the cutoff for the B dot model used in GWB.

Tungstate anions are known to form polytungstates species at low pH and at high W concentrations (Baes and Mesmer, 1976; Cruywagen, 2000; Strigul, 2010). To determine polytungstate formation in our experimental solutions, geochemical modeling using the reactions presented in Table 2.5 predict that polytunsgstate species are 4 to 5 orders of magnitude less abundant in three of our experimental solutions (Table 2.1) than the other (thio)tungstate species. The model predicts that polytungstates (i.e., the $HW_6O_{21}{}^{5-}$ species) could have formed in solution TW4 (Table 2.1), but would have only accounted for ≤ 4% of the total W in solution. Polytungstate formation, however, would only interfere with calculations of tungstate ($WO_4{}^{2-}$), and solution TW4 was only used to calculate the formation constant for dithiotungstate, based on measured concentrations of mono- and dithiotungstate. Furthermore, summing the total tungsten concentrations measured in all of the solutions (Electronic Annex), > 99% of the initial tungstate added was converted to thiotungstate anions shortly after mixing. In addition, the geochemical model (Table 2.5) predicts that thiotungstates are more likely to form in our modeled natural waters than polytungstate species (Fig. 2.4 and Table 2.7).

Table 2.7: Results of speciation modeling in percent total dissolved W in natural waters

Location	WO_4^{2-}	WO_3S^{2-}	$WO_2S_2^{2-}$	WOS_3^{2-}	WS_4^{2-}	Other W species
Carrizo	>99	<1	0	0	0	0
Black Sea	89	9	1	<1	0	0
Cocodrie	22	17.5	34	23	3.5	0
Tyro Basin	11	17	37	27	8	0

Modeled W speciation in natural waters include sulfidic groundwater from the
Carrizo Sand aquifer (Texas, USA; Johannesson et al., 2013), porewater from a salt
marsh along the Louisiana Coast, and simulated waters from modern euxinic basins (i.e.,
Black Sea and Tyro Basin). The parameters used to predict W speciation for these waters
are listed in Table 2.6. No data on W concentrations in the Black Sea or Tyro Basin has
been reported, thus we employed the average seawater W concentration of 50 pM (Sohrin
et al., 1999; Firdaus et al., 2008).

 The pH of groundwater from the Carrizo Sand aquifer recharge zone is ~ 6.5,
with S(-II) < 1 μM, and W < 80 pM. Groundwaters in this aquifer flow southeast toward
to Gulf of Mexico and wells ~60 km from the recharge zone are ~1350 m deep. The
groundwaters become both more alkaline and sulfidic down flow, and W concentrations
rise correspondingly, reaching ~1300 pM at the well furthest away from the recharge
zone (i.e., well SMA74R-1; Johannesson et al., 2013; Table 2.6). Our initial hypothesis
that thiotungstate formation could be related to the increase of dissolved W with S(-II) in
the Carrizo Sand aquifer (i.e., Johannesson et al., 2013) is not supported by the current
study, which predicts that less than 0.5% of W occurs as thiotungstates in the sulfidic
groundwaters (Fig. 2.4; Table 2.7). Consequently, the elevated W concentrations that
characterize the reducing, sulfidic groundwaters of the confined Carrizo Sand aquifer are
likely the result of pH-related desorption and quantitative reductive dissolution of Fe(III)
oxides/oxyhydroxides, important scavengers of WO_4^{2-}, within the aquifer sediments (e.g.,
Koschinsky and Hein, 2003; Kashiwabara et al., 2013; Johannesson et al., 2013).

At the bottom of the Black Sea, the model predicts that the thiotungstate anions
account for ~10% of the total W in solution, predominately as monothiotungstate

(WO_3S^{2-}; Table 2.7). Pilipchuk and Volkov (1966) reported W enrichment in recent

Black Sea sediments, which could reflect scavenging of dissolved W from sulfidic waters

and subsequent sequestration in the sediments. Due to the low concentrations of W

typically measured in seawater (i.e. ~50 pM; Sohrin et al., 1987, 1999), it is not clear that

authigenic W enrichment could be detected in recent sediments. Using the equation for

authigenic accumulation rate (i.e. $F_{au} = \Delta W(H/\tau)$ in which $F_{au}=$ authigenic accumulation

rate (nmol W/cm^2 yr), $\Delta W =$W removed from the water column (nM), H= height of the

water column (m), and τ = replacement rate of the water (years); described in Emerson

and Huested (1991), and the reported 100 ppm W in the Black Sea sediments (Pilipchuk

and Volkov, 1966) we determined that a concentration of ~10 nM W is required if all the

W is removed. The highest report of W in rivers is > 120 nM, (Johannesson et al., 2000),

but the few reports on W in seawater and terrestrial water indicate that seawaters are

depleted with respect to W (Van der Sloot et al., 1985, 1989; Hoede et al., 1987; Firdaus

et al., 2008). Therefore, the published values for W content in Black Sea sediments are

conceivable, but somewhat dubious. In coastal environments receiving terrestrial waters

with high flushing times, however, it seems plausible that an authigenic W signal could

be detected.

  To examine the actual behavior of W in sulfidic waters, we collected porewaters

from a local salt marsh in Cocadrie, Louisiana. Interstitial waters underlying saline waters

can have high sulfide concentrations due to the reduction of sulfate (Lord and Church,

1983; Howarth, 1984; Luther and Church, 1988; Brüchert et al., 2003). For example, S(-

II) concentrations in porewaters from an intertidal salt marsh on Sapelo Island in Georgia

range from 1 to 13 mM (Koretsky et al., 2005), and we have measured S(-II)

concentrations up to 1.8 mM in porewaters from the salt marsh along the Louisiana coast (Mohajerin et al., 2014c). Modeled speciation of W in one porewater sample indicates almost 80% of dissolved W would form thiotungstates (Table 2.7). Although intermediate thiotungtates are likely to predominate in this porewater, > 98% of Mo likely occurs as MoS_4^{2-} (Erickson and Helz, 2000). Tungsten concentrations in Cocodrie porewaters collected in August 2013, exhibited strong and significant correlations with Mo (r = 0.86, p < 0.0001; Mohajerin et al., 2014c), but in porewaters collected at the same site in April 2014, W and Mo had a negative association. Furthermore, unlike Mo concentrations that were depleted in sulfidic porewaters, W concentrations demonstrated a positive association with dissolved sulfide for porewaters with similar pH values. The combination of field sampling and analysis along with the predictions from geochemical modeling suggest that thiotungstates are likely to be important in sulfidic porewaters and may be more soluble than tungstate under sulfidic conditions.

In contrast to Cocodrie field results, measurements of W and Mo from the euxinic Tyro and Bannock basins suggest dissolved W may be scavenged in euxinic waters. The concept that Mo is scavenged in the water column and deposited in sediments is supported by studies demonstrating low dissolved Mo concentrations in sulfidic waters and Mo enrichment in sediments of anoxic basins (e.g., Emerson and Huested, 1991; Calvert and Pedersen, 1993; Crusius et. al, 1996; Sundby et al., 2004). Our geochemical model predicts that almost 90% of dissolved W would occur as thiotungstate species in the anoxic waters of the Tyro Basin (Fig. 2.4; Table 2.7). Investigations of suspended particulate matter (SPM), rich in Al and Fe, from the anoxic, hypersaline Tyro Basin indicate that the content of both Mo and W in SPM increase from <10 and < 0.5 ppm,

respectively, in the oxic surface waters to 190 and 19 ppm, respectively, at the oxic

seawater-anoxic brine interface (Van der Sloot et al., 1990). Tungsten and Mo are also

elevated in SPM collected from the oxic-anoxic interface in the Bannock Basin, which
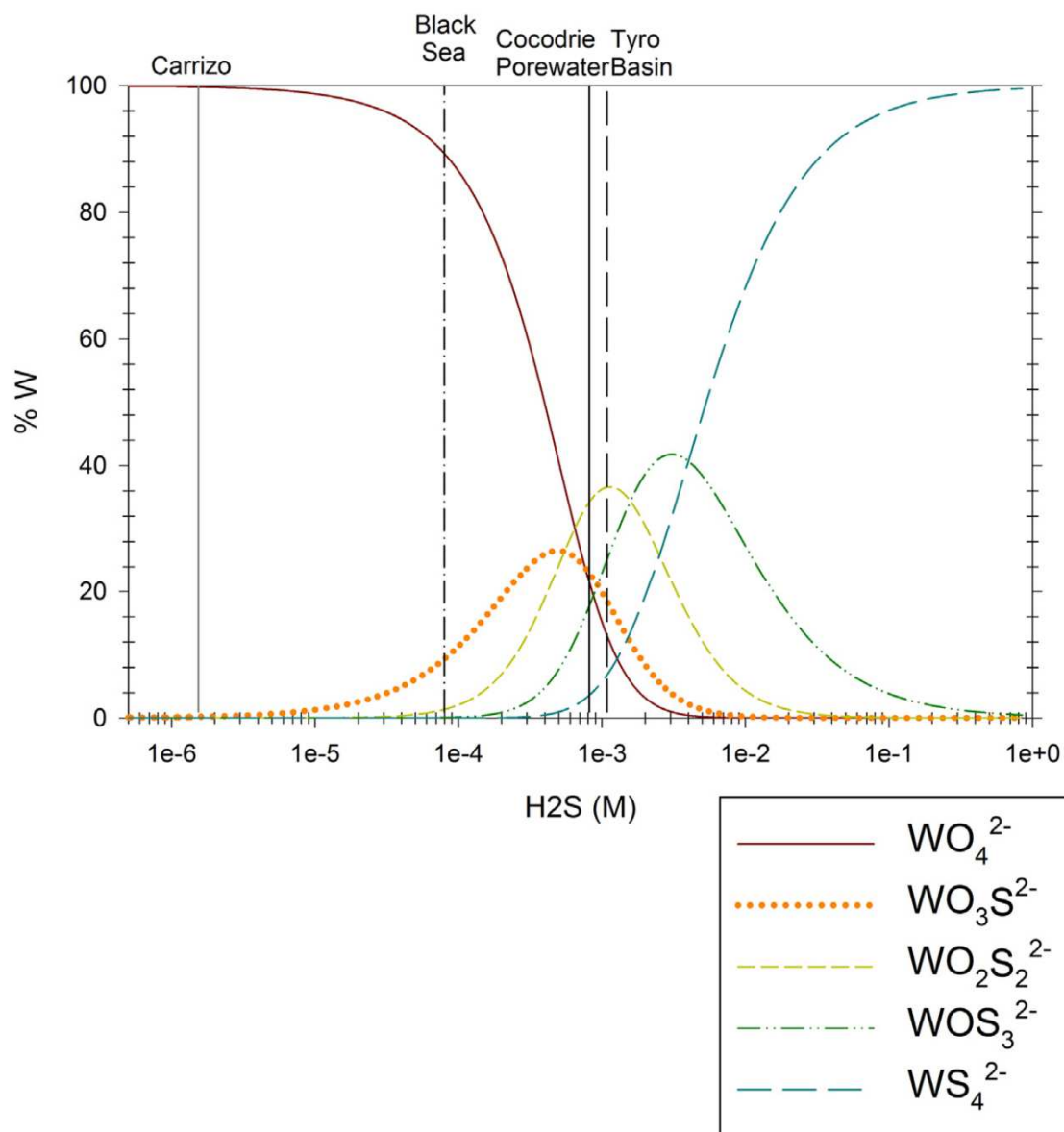
Figure 2.4: Modeled (oxo)thiotungstate speciation using 50 pM W, pH = 7, I =0.7M, and stability constants in Table 2.5. The percentage of total tungsten is on the y-axis and H_2S concentration is on the x-axis on a log scale. Lines indicate maximum reported sulfide concentrations from the Carrizo Sand aquifer S(-II) and pH from Johannesson et al. (2013), Black Sea, pH from Goyet et al. (1991) and S(-II) from Neretin et al. (2001), Pore

water (this study); Tyro Basin pH and S(-II) from De Lange et al. (1990). Only W species that account for $\geq$ 1% of the total dissolved W are depicted.

has similar pH and S(-II) concentrations to the Tyro Basin (Table 2.6; Van der Sloot et al., 1990; DeLange et al., 1990). Dissolved Mo concentrations in both the Tyro and Bannock Basins exhibit a sharp decline at the oxic-anoxic interface, suggesting that Mo is removed from the anoxic water column via scavenging by SPM. Although measurements of dissolved W from these basins were not reported, the higher concentration of W on SPM at the anoxic interface, and the likelihood that thiotungstates predominate in these waters suggests thiotungstates could be particle reactive.

2.4.3 Comparison of Mo and W in euxinic waters

Two mechanisms have been proposed to account for the removal of aqueous MoO_4^{2-} from sulfidic waters including Mo(VI) reduction to Mo(IV) and subsequent precipitation of MoS_2, and thiomolybdate formation followed by processes that may include Mo(VI) reduction or complexation with other ligands such as polysulfides, organic matter, or iron sulfides minerals (Zheng et al., 2000; Bostick et al.,2003; Vorlicek et al., 2004; Helz et al., 2011; Dahl et al., 2013; Chappaz et al., 2014). We submit that both of these mechanisms play a weaker role in the geochemistry of W in sulfidic waters. First, Mo(VI) is more readily reduced than W(VI) to form MS_3 and MS_2 (M = Mo or W) minerals (Ivanova, 1986; Kletzin and Adams, 1996; Stiefel, 2002). Reduction of W(VI) to W(IV) is unlikely to occur in low temperature, near surface environments, thus preventing W removal by precipitation of WS_2, and our measurements of thiotungstate formation constants imply that W(VI) also has a lower affinity than

Mo(VI) to form thioanions. Specifically, the geochemical model predicts that thiotungstates require sulfide concentrations that are ca. 40-fold higher than those required to form thiomolybdate (compare with Fig. 2.5 of Helz et al., 1996 with Figure 2.4, this study). Nevertheless, anoxic waters do occur in sediment porewaters from salt marshes and in some anoxic basins (e.g., Tyro Basin) that are sufficiently sulfidic for thiotungstates to form. In these environments, the formation of thiotungstates may facilitate W sequestration in sulfidic sediments similarly to the processes leading Mo removal in these environments, but more research on dissolved W in sulfidic waters and W in sulfidic sediments is necessary.

2.5 Conclusions

Formation constants for thiotungstate anions were determined using UV/Vis spectrophotometric techniques. The thiotungstate formation constants were used in geochemical modeling to investigate formation of thiotungstates in sulfidic natural waters. The formation constants and geochemical modeling indicate thiotungstate formation is favored by increasing dissolved sulfide concentrations and decreasing pH. The results also indicate that W has a lower affinity for sulfide complexation than Mo, requiring about 40-fold higher sulfide concentrations to form than thiomolybdates. The thiotungstate formation constants suggest that intermediate thiotungstates are likely to predominate in water columns with high sulfide concentrations (i.e. mM S(-II)), in contrast to the predicted sharp transition of molybdate to tetrathiomolybdate. The positive association between dissolved W concentrations and S(-II) in interstitial waters, suggests thiotungstates could be more soluble than tungstate, but W from euxinic water columns suggest increased thiotungstate particle reactivity (Van der Sloot et al., 1990). As

industrial uses for W increase, and W concentrations become elevated in effluent (Hsu et al., 2011), natural scavenging of W in sulfidic porewaters in environments such as salt marshes may reduce the bioavailability of this contaminant. Future investigation of W, Mo, and sulfide concentrations in euxinic waters and sulfidic sediments are needed to elucidate the effect of thiotungstate formation on the fate and transport of W in the hydrosphere.

Acknowledgements

Chapter 3:

Geochemical differences of tungsten and molybdenum in coastal waters: The effects of speciation on sequestration and mobilization

"Molybdenum and tungsten are similar chemically, although there are differences between them in various types of compounds that are not easy to explain." (p. 920; Cotton et al., 1999).

Abstract

Concentrations of dissolved tungsten (W) and molybdenum (Mo) are reported for surface waters and pore waters of a Louisiana estuary transect for two sampling periods. We also present pH, salinity, dissolved iron (Fe) and manganese (Mn) concentrations as well as dissolved oxygen in surface waters and dissolved sulfide in pore waters. The data demonstrate a positive correlation between dissolved (i.e., < 0.45 μm) W with dissolved Fe in surface waters, and the likelihood of W sequestration into estuarine sediments. Although the estuarine sediments are also a sink for Mo, conservative mixing of terrestrial and marine water is the primary control on Mo concentrations in surface waters. Compared to low salinity surface waters (i.e., < 1 ‰), underlying pore waters with dissolved sulfide concentrations ~2.5 μM and pH ~7.8 have ~100 fold enrichment of dissolved W, whereas dissolved Mo pore water concentrations exhibit ~3 fold enrichment relative to overlying surface waters. In contrast to Mo, W is enriched in all pore waters compared to overlying surface waters. These data suggest W may be removed from the

water column and deposited into sediments at a higher rate than Mo in this estuary.

Molybdenum is depleted in all pore waters underlying brackish (i.e., salinity > 1 ‰)

surface waters. Dissolved Mo concentrations decrease in pore waters with $[H_2S_{(aq)}] \geq 11$

µM, and remain at low (i.e., 0.5 -10 nM) concentrations, whereas W concentrations in

pore waters increase with increasing sulfide concentrations. Prediction of thioanion

formation in sulfidic pore waters suggests that thiotungstates may be more soluble than

thiomolybdates.

3.1 Introduction

Tungsten (W) and molybdenum (Mo) are considered chemical analogs

due to their numerous chemical similarities that include 1) formation of oxyanions

(MO_4^{2-}, M = Mo or W) in the (VI) oxidation state in most natural oxic waters (Baes and

Mesmer, 1976; Smith and Martel, 2004); 2) conservative behavior in oxic, circum-neutral

pH waters (Sohrin et al., 1987, 1999; Arnórsson and Óskarsson, 2007); 3) adsorption to

Fe/Mn oxides/oxyhydroxides at pH ~4-7, and desorption at higher pH values

(Johannesson et al., 1992, 2013; Gustafsson, 2003; Seiler et al., 2005; Mohajerin et al.,

2014b); and 4) thioanion formation in sulfidic waters (Müller et al., 1969; Erickson and

Helz, 2000; Mohajerin et al., 2014a). The chemical behavior of W and Mo are both

conservative in ocean water columns (Sohrin et al., 1987, 1989, 1999), but under certain

conditions they exhibit differences. For example, although W and Mo have similar molar

concentrations in the upper continental crust (Mo/W = 1.3 ± 0.5; Hu and Gao, 2008, and

references therein), Mo/W molar ratio in seawater is ≈ 2000 (Sohrin et al., 1987, 1999;

Firdaus, 2008). Although considerable research has been devoted to Mo, fewer studies

have focused on W. For example, Gaillardet et al. (2005) calculated a world river average

for Mo using 20 measurements reported worldwide, whereas W was calculated from one

report containing 30 measurements from California streams.

Table 3.1: Dissolved tungsten and molybdenum concentrations in natural waters

	W (nM)	Mo (nM)	Mo/W	Reference
Carson River (SW USA)	8.21- 1000	54.2 - 318	0.5 - 12	Johannesson et al., 2000
Scheldt River (Belgium, Holland)	5 - 10	10 - 40	2 - 4	Hoede et al., 1987
Sacramento River (California, USA)	0.23 – 3.07	1.56 – 27.1	12 - 131	Taylor et al., 2012
Surface waters from Skagafjördur (Iceland)	0.027 - 1.84	0.1 – 28.24	*6.3 -18 *ave. river	Arnórsson and Óskarsson, 2007
Karelian Rivers (NW Russia)	0.016-0.109	0.521- 4.17	30 - 40	Pokrovsky and Schott, 2002
Mississippi River (SE USA)	0.18 – 0.3	12.09 – 13.96	47 - 67	This study
Yodo River and estuary (0 ‰≤S≤ 13‰; Japan)	0.03 – 3.3	2 - 69	77 (river)	Sohrin et al., 1989; Firdaus et al., 2008
Solo (Indonesia)	0.12 - 0.2	15 - 24	120 - 125	Hoede et al., 1987
World River Ave. (range)	0.543 (0.54 – 980)	4.38 (1.16 – 28.03)	8	Gaillardet et al., 2005
Java Sea	0.2	92	460	Van der Sloot et al., 1989
Bali Basin	0.13	95	731	Van der Sloot et al., 1989
North Sea (Southern Bight)	0.1	120	863	Van der Sloot et al., 1989
N. Pacific Ocean	0.053 - 0.06	97 - 115	~2000	Sohrin et al., 1999
Mean Ocean Residence time	14,000 – 61,000 years	440,000 – 800,000 years		Firdaus et al, 2008; Miller et al., 2011

Table 3.1 demonstrates the wide range of W and Mo concentrations measured in

natural waters. In Iceland, measurements in streams with high rock to water ratios

suggest that W and Mo dissolve from the underlying basalt nearly quantitatively (Mo/W:

6.4 local basalt ≈ 6.3 in water), but peat soil waters are depleted in W compared to Mo

(Mo/W = 18; Arnórsson and Óskarsson, 2007). Relatively high W concentrations in the

Carson River likely reflects the occurrence of W mines in the watershed, input from

hydrothermal waters that are naturally enriched in tungsten (Kishida et al., 2004),

evaporative concentration, and alkaline conditions that promote desorption of both W and

Mo from Fe/Mn oxides/oxyhydroxides (Johannesson et al., 2000; Seiler et al., 2005).

One mechanism leading to the different W and Mo seawater concentrations could

be that compared to Mo, W exhibits a stronger affinity for Fe/Mn oxides/oxyhydroxides

(Gustafsson, 2003; Kashiwabara et al., 2013). Ferromanganese oxides in the ocean

exhibit relatively higher enrichment of W over Mo (Takematsu et al., 1990; Kuzendorf

and Glasby, 1991; Koschinsky and Hein, 2003; Kashiwabara et al., 2013), and laboratory

experiments indicate WO_4^{2-} is a strong competitor of MoO_4^{2-} for adsorption onto goethite

(Xu et al., 2006). In addition, Van der Sloot et al. (1989) estimated total annual discharge

of W to be 76.15 kilomoles with 11% in the dissolved fraction (i.e., < 0.45 µm) compared

to 1280 kilomoles Mo, ~80% of which was in the dissolved fraction in the River Solo

located in Indonesia. Thus, the overall input of W to the ocean from terrestrial waters

may be less than Mo.

Preferential scavenging of W compared to Mo by Fe/Mn

oxides/oxyhydroxides is likely one of the mechanisms contributing to their differing

concentrations in oxic waters (Gustaffson, 2003; Kashiwabara et al., 2013; Johannesson

et al., 2013; Mohajerin et al., 2014b), but unlike Mo, it is unclear if W is also scavenged

from sulfidic waters. Groundwaters in the Carrizo sand aquifer demonstrate a positive

correlation between increases of dissolved sulfide with increasing dissolved W

concentrations (Johannesson et al., 2013). In the Tyro and Bannock basins, however,

measurements of W in suspended particulate matter are higher in the euxinic (i.e., anoxic

and sulfidic) waters compared to the oxic overlying water, similar to Mo, suggesting W

may be scavenged from the water column in sulfidic waters. Several proposed

mechanisms of Mo removal from euxinic water begin with formation of

tetrathiomolybdate (MoS_4^{2-}; Helz et al., 1996; Erickson and Helz, 2000; Zheng et al.,

2000; Vorlicek et al., 2004; Algeo and Lyons, 2006; Tribovillard et al., 2006; Helz et al.,

2011; Dahl et al., 2013; Chappaz et al., 2014), but laboratory experiments demonstrate

that thiotungstates form more slowly than thiomolybdates, stability constants (i.e.,

$WO_xS_{4-x}^{2-} + H_2S \leftrightarrow WO_{x-1}S_{5-x}^{2-} + H_2O$) are approximately two orders of magnitude less

than stability constants for analogous thiomolybdates, and thiotungstates require ~40 fold

higher dissolved sulfide concentrations to form than thiomolybdates (Aymonino et al.,

1969b; Erickson and Helz, 2000; Mohajerin et al., 2014a).

Sediments and pore waters from sulfidic environments such as euxinic

basins, some estuaries that experience seasonal anoxia, and coastal marine marshes, can

be sinks or sources for many trace elements, such as Mo. Diagenetic processes re-

mineralize oxides/oxyhydroxides into more refractory sulfide phases such as pyrite that

adsorb or co-precipitate trace metals (e.g., Church et al, 1996; Huerta-Diaz and Morse,

1992). Trace metals can be released from sediments under conditions that lead to pyrite

oxidation such as sediment resuspension or spatial changes in the redoxocline due to

seasonal cycles (Morse, 1994). Estuarine studies demonstrate conservative mixing of Mo

(Van der Sloot et al., 1985, 1989; Audry et al., 2007; Rahaman et al., 2010), as well as

both positive and negative fluxes of Mo from the water column to the sediments due to

adsorption/desorption reactions, removal by organic-rich particulates, or fixation in

reducing sediments (Dalai et al., 2005; Dellwig et al., 2007; Morford et al., 2007). The

sparse data available for W in estuaries demonstrates that W exhibits reactive behavior, such that W concentrations have a non-linear relationship with salinity for two estuarine transects that could be due to removal of W by suspended particulate matter (SPM; Van der Sloot, 1985, 1989; Hoede et al., 1987). Studies of W in estuary pore waters, however, are lacking hindering our understanding of what mechanisms may be controlling W in natural waters.

In this study, we present new data for W and Mo in surface waters and underlying sediment pore waters for an estuarine-tidal marsh system in coastal Louisiana. To the best of our knowledge, the W data represent the only such data for the Western Hemisphere, and the first reported estuarine pore water W concentrations. The W and Mo data presented here are employed to investigate possible controls on these two transition metals in coastal marine settings.

3.2 Study Area

The study area, referred to here as the northern Terrebonne Bay estuary, is located ~100 km southwest of New Orleans, LA, and ~90 km west of the Mississippi River mouth (Fig. 3.1). The study transect is located in a broad, shallow, bar-built estuary surrounded by barrier islands that restrict seawater flow (Prager, 1992; Schroeder and Wiseman, 1999). Cat Island Pass is the dominant connection between Terrebonne Bay and the Gulf of Mexico, but shallow passes exist along the entire barrier island chain and exchange with the open ocean is increasing with time (McKee et al., 1994). Terrebonne Bay is shallow (i.e. 1.2 m – 2.75 m), well-mixed environment with salinity that is driven
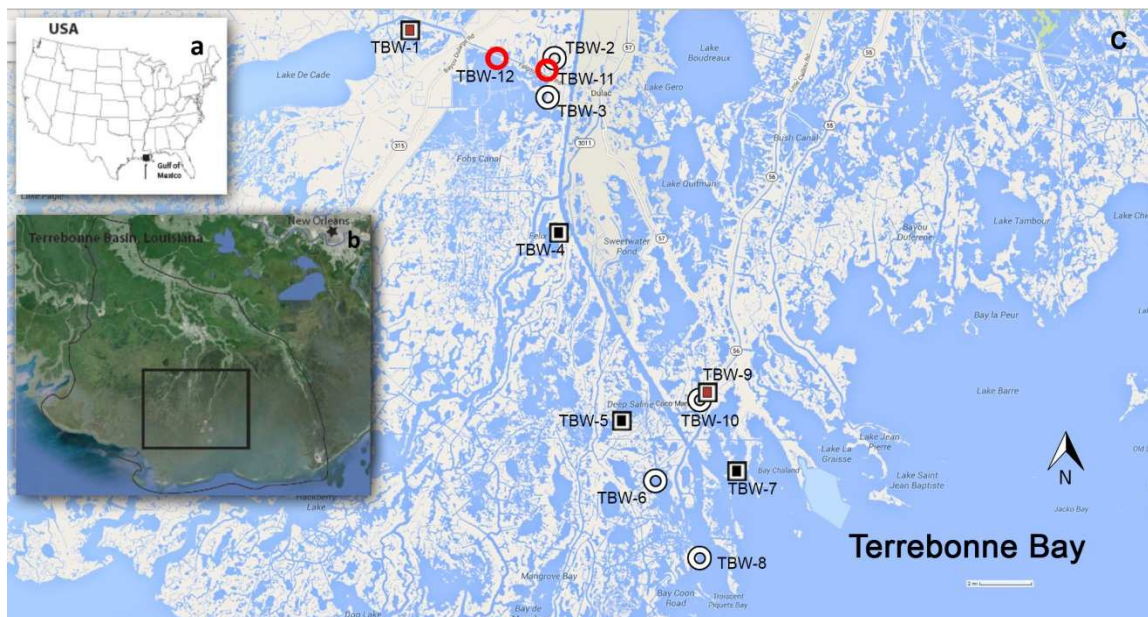
Figure 3.1: a) Map of the United States of America, arrow points to our study site in Louisiana near the Gulf of Mexico; **b**) Close up of Terrebonne Basin with a square capturing the study area and star indicating location of New Orleans near the Mississippi River. **c**) Image of study area. Open white circles represent sample sites where only surface waters were collected in August 2013 and April 2014, red circles show locations only sampled in April 2014. Filled black squares show sites where both core and surface water samples were collected in August 2013. Filled red squares illustrate the two points in which surface waters and cores were collected in both August and April. Images from Google Earth (**b**) and Google Maps (**c**).

by seasonal changes in run-off from the Mississippi River and cold fronts that flush water out of the bay to the continental shelf (Wiseman et al., 1990; Inoue and Wiseman, 2000; Feng and Li, 2010). Water column salinities are vertically homogeneous, but lateral salinity gradients occur in Terrebonne Bay with fresher terrestrial waters near the coast and more saline water near the Gulf of Mexico (Solis and Powell, 1999). As an abandoned outlet of the Mississippi River, active delta development in this basin last occurred between 800 to 1200 BP (Penland et al., 1987).

Fresh water is predominantly from precipitation and local runoff, with minor contributions from the Atchafaylaya River via the Gulf Intracoastal Waterway (Prager, 1992; Rablais, 1995). Terrestrial waters are transported into the bay via the

Houma Navigation Canal (HNC), a structure that allowed salt-water intrusion that destroyed most of cypress swamps north of Falgout Canal (Beasley, 1995; Bianchi et al., 2009). Residence time of the fresh-water fraction (i.e. salinity = 0 ‰) of Terrebonne Bay is estimated to be 125 days, reflecting the relatively low fresh water input to the bay (Solis and Powell, 1999). Circulation in Terrebonne Bay is primarily controlled by wind-driven flow and to a lesser degree from daily micro-tidal events (i.e., 0.2 m - 0.4 m tides with currents of 0.01m/s and 0.025 m/s, respectively; Prager, 1992; Adams et al., 1997; Solis and Powell, 1999). During cold front passages, northwesterly winds flush bay waters onto the continental shelf in less than 40 hours, and waters return 10-25 hours following the passage of the front when the wind changes to the more typical southeasterly direction (Feng and Li, 2010). Intermediate marshes near Falgout Canal in northern Terrebonne Bay estuary are characterized by freshwater and brackish water vegetation (Baustian and Turner, 2006). Vegetation in the salt marshes is dominated by *Spartina alterniflora* and *Spartina patens,* but deterioration of the barrier islands, subsidence, and relative sea level rise are converting the salt marshes to open estuaries (Prager, 1992; Nyman et al., 1995; Lindstedt, 2005), which contributes to reduced, sulfidic sediments and vegetation loss (Nyman et al., 1995; Wang, 1997; Day et al., 2011).

3.3 Methods

3.3.1 Sample collection

Water samples from freshwater and saltwater marshes were collected to examine surface waters with varying degrees of salinity. Surface waters and pore waters were collected on August 8, 2013 and April 30, 2014 along a ~35 km transect beginning in Falgout Canal

and terminating near Terrebonne Bay by the Gulf of Mexico (Figs. 3.1 & 3.2). The water column depth at these sites was on average ~2 m. The first surface water and core samples were collected in an intermediate marsh in Falgout Canal (TBW-1, Fig. 3.2a) that is generally isolated from the coastal bay (Cahoon et al., 1995). Two more fresh surface water samples were taken along the HNC (TBW-2 and TBW-3). The remaining water samples were collected from minor bayous (i.e., sluggish tributaries) in marshes exhibiting salinity from 3-22‰. The April 2014 sampling campaign was affected by winds that pushed saltwater up the HNC, such that a freshwater–saltwater front could be seen at the intersection of Falgout canal and HNC (Fig. 3.2b). Consequently, surface waters collected in April 2014 were generally more saline that the samples collected at corresponding locations in August 2013.

Sediment cores were collected in small, natural waterways to minimize anthropogenic contamination. To examine the influence of sulfidic pore waters on W geochemistry, cores were collected in intermediate and salt marshes. In August 2013, two sediment cores were taken in the upper regions of the estuary where sulfide concentrations in pore waters were expected to be minimal, and three cores were collected in more saline sites to capture areas where sulfate reduction was expected to be substantial. In April 2014, one core was collected at TBW-1, and another one in the salt marsh, at TBW-9 (Fig. 3.1c). Sediment cores were collected using a push core sampler and clean 2 mm thick acrylic tubes. Although this salt marsh is known to be habitat for various macrofauna (Lindstedt, 2005; Fry, 2008), no evidence of bioturbation was observed in our samples. Some vegetation (roots and buried shoots), however, were observed in the collected sediment cores. Recovered cores were capped and immediately

Figure 3.2: Photographs of field site on April 30, 2014 **a**) Freshwater end-member site TBW-1; **b**) Mixing line of saltwater in Houma Navigation Canal (left) and freshwater from Falgout Canal (right); **c**) Salt marsh by TBW-9

sealed in anaerobic bags under a carbon dioxide atmosphere and stored on ice for

transport back to the laboratory at Tulane University. The sealed cores were transferred

into a nitrogen-filled glove box that evening. Cores were sectioned into 50 mL

polyethylene tubes within the glove box. Pore waters were obtained by centrifugation of

sediment core sections under nitrogen.

Pore water pH was measured on recovered pore water inside the glove box. Pore

water sulfide concentrations were determined using the methylene blue method (Hach,

1997; method 8131) in which sealed cuvettes were measured spectrophotometrically

outside the glove box and diluted as needed with deoxygenated doubly distilled (Milli-Q

18 MΩ) water. A refractometer was used to estimate pore water salinity using ~0.25 mL

of pore water. In the glove box, remaining interstitial waters were filtered (0.45 μm

polyethersulfone Whatman syringe filter) and collected in trace metal clean HDPE bottles

or trace metal clean 50 mL polyethylene centrifuge tubes. The filtered pore waters were

then removed from the glove box and acidified with ultra-pure nitric acid (Fisher Optima)

at a class 100, laminar flow clean bench for subsequent trace metal analysis.

Surface water samples were collected in HDPE (August) or Teflon (April)

bottles cleaned using procedures described in Johannesson et al. (2004). Trace metal

clean sampling and handling techniques including wearing polyethylene gloves,

conditioning each bottle 3 times with sample water before collection, double bagging all

water samples in clean zip-lock style polyethelyne bags, and handling the samples under

a clean bench, were employed for sample collection and processing. Surface water

samples were collected ~5 cm below the water surface using a peristaltic pump with acid

cleaned Teflon® tubing attached to a 0.45 μm in-line filter (Gelman Sciences, Pall Corp.

polyethersulfone membrane). The filtered water samples were stored in a cooler on ice in the field and acidified with ultrapure (Fisher Optima) nitric acid within a class 100 laminar flow clean bench after returning to the lab. In August, temperature and pH were measured in the field for surface water samples using an Oakton pHTestr 30 meter calibrated with NIST certified pH 4, 7, and 10 buffers. For the August collection, one aliquot of surface waters was not acidified and was used to measure chloride concentrations using a chloride ion selective electrode (accumet®). Salinity was calculated as S‰ = 1.80655 Cl‰ (UNESCO, 1962 referenced in Pilson, 1998). In April, a calibrated YSI multiprobe sonde was employed to measure pH, dissolved oxygen, temperature, and salinity (measured via conductivity) at the surface (0. 25 m) and 0.5 m depth intervals. Seasonal trends in DO were obtained for Terrebonne Bay and at a station in the Cocodrie salt marsh using data provided by LUMCON's environmental monitoring stations from an EXO sonde and a Vaisala WXT520 all-in-one sensor (LUMCON weather station, 2014).

3.3.2 Trace metal analysis

Tungsten, Mo, Fe, and Mn were measured directly using Inductively Coupled Plasma Mass Spectroscopy (ICP-MS) employing standard curves prepared from certified standards (Peak Performance®). Surface and pore waters were diluted 1.5 to 20-fold with 2% Fisher Optima ultra-pure nitric acid in doubly distilled (Milli-Q) water to minimize matrix effects. Instrument drift was corrected for with the use of internal standards that included Rh for W and Mo, and Sc for Fe and Mn. Measurements of known standards (Peak Performance®) and certified reference materials SLRS-4 (river water) and SLEW-3 (estuary water) were generally within 10% for Mo, Fe, and Mn (Tables 3.2a and 3.2b).

No certified reference waters could be found for W. Detection limits reported in Tables 3.2a and 3.2b represent concentrations detectable in diluted waters. Thus, the actual detection limit for each sample was dependent on the dilution factor as shown in the tables. Measurement of W by ICP-MS was optimized by employing methods described in Clausen et al. (2010) and confirmed by Mohajerin et al. (2014b). Analytical error for trace metal analysis was propagated using standard procedures and includes analytical (ICP-MS) precision, error of the slope from the standard curve, and weighing error from dilutions (e.g., Lindberg, 2001). For the August samples, concentrations for W and Mo were also measured using elemental isotope dilution mass spectrometry (IDMS; Alonso and Rodríguez-González, 2013; see Appendix D for IDMS methods and Tables D.1 and D.2 for results). April samples were also measured using standard additions. Standard additions calculations were on average 93% of dilution concentrations (results presented in Appendix E), and average percent spike recovery (± σ) for 24 water samples are provided in Table 3.2b. Because measurement of Fe, Mn, and Mo in SLEW-3 certified estuarine water using the dilution approach were more accurate than the IDMS approach, only the dilution data are presented and discussed in this manuscript. One exception is the Mo pore water concentration data obtained from the sediment cores collected in August 2013, where isotope dilution was employed. We use IDMS for these analyses because we suspect that the high Mn concentration of these pore waters likely caused $^{55}Mn^{40}Ar$ interference.

Table 3.2a: August 2013 quality control

Sample	182 W nM	184 W nM	95 Mo nM	55 Mn µM	56 Fe µM
certified SLRS 4 ug/L	-	[a]0.07 ± 0	[a]	2.19 ± 0.21	0.061 ± 0.003	1.84 ± 0.09
Measured SLRS-4	0.07 ± 0.02	0.06 ± 0.01	2.41 ± 0.09	0.06 ± 0.001	1.84 ± 0.08
Certified SLEW3	-	-	53.15	0.029 ± 0.004	0.01 ± 0.001
Measured SLEW3	0.31 ± 0.05	0.31 ± 0.05	69.51 ± 1.7	0.029 ± 0.001	< 0.02
Standard 1 actual	5.44	5.44	10.42	0.018	0.018
Standard 1 measured	5.19 ± 0.08	5.25 ± 0.07	11.1 ± 0.2	0.018 ± 0.001	0.021 ± 0.001
Standard 2 actual	0.54	0.54	1.04	0.002	0.002
Standard 2 measured	0.53 ± 0.02	0.51 ± 0.01	1.08 ± 0.06	0.003 ± 0.001	0.01 ± 0.06
Detection Limit (DL)	0.03	0.03	0.05	.001	.002
Surface water DL	0.3	0.3	0.5	0.01	0.02
Pore water DL	0.6	0.6	1	0.02	0.04

[a] 184W reported value (13 ppt) in SLRS-4 from Yeghicheyan et al. (2001)

Table 3.2b: April 2014 quality control

Sample	^{182}W nM	^{184}W nM	^{100}Mo nM	^{55}Mn μM	^{56}Fe μM
Certified SLEW3	na	na	53.15	0.029 ± 0.004	0.01 ± 0.00
Slew3 measured	0.15 ± 0.01	0.14 ± 0.01	48 ± 2	0.027 ± 0.001	0.013 ± 0.001
Standard 1 actual	5.44	5.44	208.42	0.364	0.358
Standard 1 measured	5.6 ± 0.1	5.66 ± 0.08	206 ± 3	0.38 ± 0.01	0.37 ± 0.02
Standard 2 actual	0.07	0.07	2.61	0.005	0.004
Standard 2 measured	0.09 ± 0	0.08 ± 0.01	2.63 ± 0.1	0.005 ± 0	0.007 ± 0
Standard 3 actual	-	-	1042.1	1.82	1.791
Standard 3 measured	-	-	1020 ± 90	1.8 ± 0.2	1.9 ± 0.2
Detection Limit	0.03	0.03	0.1	0.0002	0.004
Surface water DL	0.045	0.045	0.15	0.0003	0.006
Pore water DL	0.27	0.27	0.9	0.0018	0.036
Ave. spike recovery	100% ±24%	90% ± 6%	89% ± 9%	74% ± 17%	104% ± 14%

3.3 Data analysis

To estimate thiotungstate and thiomolybdate speciation along with mineral saturation

states, we employed the SpecE8 program of Geochemists Workbench® (version 9.0;

Bethke, 2008) along with a modified version of the Lawrence Livermore National

Laboratory (LLNL) thermodynamic database provided with the software that includes the

reactions presented in Table 3.3.

3.4 Results

3.4.1 Surface waters

Concentrations of W, Mo, Fe, and Mn in surface waters along with pH, salinity,

dissolved O_2, and temperature are presented in Table 3.4 for the August 2013 samples

and Table 3.5 for the samples collected in April 2014. Trace element concentrations in

surface and pore waters are plotted versus salinity in Fig. 3.3. Data for the northern

Terrebonne Bay estuary agree with previous studies that demonstrate non-conservative,

reactive behavior for dissolved W (Van der Sloot et al., 1985, 1989), and generally

conservative mixing of Mo in estuaries (Audry et al., 2007; Rahaman et al., 2010;

Scheiderich et al., 2010). In August 2013, W concentrations reached a maximum of 0.4

nM at S ~10 ‰, then decreased to 0.13 nM W at S > 15 ‰, similar to previous studies in

unpolluted waters in Indonesia (W: 0.1 – 0.34 at S < 15 ‰ and W ≤ 0.16 nM at S > 15 ‰

near the Java Sea; Van der Sloot et al., 1989). In April 2014, W exhibited little change

with salinity (i.e., 0.05 nM – 0.1 nM), comparable to dry season W concentrations that

remain ~0.1 nM for the entire salinity range in the River Solo estuary (Van der Sloot et

al., 1989). For comparison, the industrialized Scheldt estuary that empties into the

Southern Bight of the North Sea, W concentrations range from ~2 nM to 11 nM between

Table 3.3: Formation constants of aqueous species added to GWB for pore water speciation modeling

Species	Log K (I=0, 25°C)	Reference
$WO_4^{2-} + H^+ \rightarrow HWO_4^-$	3.6	Smith and Martell, 2004
$WO_4^{2-} + 2H^+ \rightarrow H_2WO_4$	5.8	Smith and Martell, 2004
$WO_4^{2-} + H_2S \rightarrow WO_3S^{2-} + H_2O$	3.08	Mohajerin et al., 2014a
$WO_3S^{2-} + H_2S \rightarrow WO_2S_2^{2-} + H_2O$	3.38	Mohajerin et al., 2014a
$WO_2S_2^{2-} + H_2S \rightarrow WOS_3^{2-} + H_2O$	2.79	Mohajerin et al., 2014a
$WOS_3^{2-} + H_2S \rightarrow WS_4^{2-} + H_2O$	2.36	Mohajerin et al., 2014a
$7WO_4^{2-} + 8H^+ \rightarrow W_7O_{24}^{6-} + 4H_2O$	65.19	Cruywagen and van der Merwe, 1987
$7WO_4^{2-} + 9H^+ \rightarrow HW_7O_{24}^{5-} + 4H_2O$	76.59	Rozantsev and Sazonova, 2005
$6WO_4^{2-} + 7H^+ \rightarrow HW_6O_{21}^{5-} + 3H_2O$	63.83	Smith and Martell, 2004
$6WO_4^{2-} + 6H^+ \rightarrow H_2W_6O_{22}^{6-} + 2H_2O$	53.68	Rozantsev and Sazonova, 2005
$12WO_4^{2-} + 14H^+ \rightarrow H_2W_{12}O_{42}^{10-} + 6H_2O$	123.38	Rozantsev and Sazonova, 2005
$12WO_4^{2-} + 18H^+ \rightarrow H_2W_{12}O_{40}^{6-} + 8H_2O$	149.59	Rozantsev and Sazonova, 2005
$10WO_4^{2-} + 16H^+ \rightarrow W_{10}O_{32}^{4-} + 8H_2O$	129.63	Rozantsev and Sazonova, 2005
$MoO_4^{2-} + H^+ \rightarrow HMoO_4^-$	4.24	Smith and Martell, 2004
$MoO_4^{2-} + 2H^+ \rightarrow H_2MoO_4$	8.24	Smith and Martell, 2004
$MoO_4^{2-} + H_2S \rightarrow MoO_3S^{2-} + H_2O$	5.19	Erickson and Helz, 2000
$MoO_3S^{2-} + H_2S \rightarrow MoO_2S_2^{2-} + H_2O$	4.80	Erickson and Helz, 2000
$MoO_2S_2^{2-} + H_2S \rightarrow MoOS_3^{2-} + H_2O$	5.00	Erickson and Helz, 2000
$MoOS_3^{2-} + H_2S \rightarrow MoS_4^{2-} + H_2O$	4.88	Erickson and Helz, 2000
$FeS_{(mackinawite)} + 0.6[MoS_4^{2-}] + 1.2\,[H^+] \rightarrow 0.6[H_2S]_{(aq)} + FeMo_{0.6}S_{2.8(s)}$	11.7	Helz et al., 2011
$Fe^{2+} + WO_4^{2-} \rightarrow FeWO_{4\,(ferberite)}$	10.65	Robie et al., 1978
$Fe^{2+} + HS^- \rightarrow FeS_{(mackinawite)} + H^+$	3.5	Rickard, 2006

0 - 15 ‰ salinity, and subsequently decrease to < 1 nM for S > 15‰, suggesting a possible low to mid-salinity source of W in the estuary (Van der Sloot et al., 1985). Iron concentrations exhibited a similar distribution to W as a function of salinity at our study site, with Fe concentrations peaking in August 2013 at ~7 ‰ salinity (Fig. 3.3b,c).

Molybdenum concentrations increased linearly with salinity, from 8 nM in the fresh waters to 78 nM near Terrebonne Bay where S = 22.6‰ (Fig. 3.3a; r = 0.99, p < 0.0001). Extrapolating from these Mo data for the northern Terrebonne Bay estuary to a typical open ocean seawater salinity of 35‰ results in Mo concentrations of ~95 nM for the April 2014 data and ~116 nM for the August 2013 data, both of which are similar to

measured values of Mo in seawater (~110 nM; Sohrin et al., 1989, 1999; Firdaus et al., 2008) and the Gulf of Mexico (98 nM: Yao and Byrne, 1999). Extrapolation to S = 0‰ results in a freshwater endmember with Mo ~10 nM, which is consistent with Mo measured in the Mississippi River and other fresh water samples from northern Terrebonne Bay estuary in August 2013 (Table 3.4).

Manganese surface water concentrations were greater in April than in August (i.e., 0.2 - 1.4 µM in August 2013 vs. 0.12 – 3.43 µM in April 2014). Surface water pH averaged 7.98 µM ± 0.45 µM (± σ standard deviation) in August and 7.5 µM ± 0.2 µM in April. As expected, the temperature of surface waters in the northern Terrebonne Bay estuary were generally greater in August 2013 than in April 2014. Although the salinity of samples near Terrebonne Bay was greater in August than April, salinity of the samples near Falgout Canal were greater in April 2014 (Tables 3.4; 3.5). Vertical measurements of temperature and salinity collected in April were consistent with a non-stratified oxic water column (Appendix F).

Table 3.4: Surface water samples collected in August 2013.

Sample	Dissolved O$_2$ μM	Temp. °C	pH	[a]Salinity ‰	[c]W nM	Mo nM	Mn μM	Fe μM
[b]Mississippi River	nd	nd	nd	nd	0.29 ± 0.08	13 ± 1	0.04 ± 0.05	0.05 ± 0.02
TBW-1	256.26	31	7.71	0.29	<0.3	9.1 ± 0.3	0.41 ± 0.01	0.59 ± 0.02
TBW-2	206.26	29.8	7.30	0.05	<0.3	10.1 ± 0.3	0.73 ± 0.02	0.11 ± 0.01
TBW-3	193.76	32.8	7.33	0.13	<0.3	10.2 ± 0.5	0.28 ± 0.01	0.21 ± 0.01
TBW-4	306.26	36.7	7.76	0.66	<0.3	12.6 ± 0.4	0.21 ± 0.00	1.03 ± 0.03
TBW-5	406.27	34.8	8.34	7.24	0.36 ± 0.06	31.3 ± 0.9	0.87 ± 0.01	2.52 ± 0.04
TBW-6	462.52	35.4	8.35	11.22	0.40 ± 0.03	44.2 ± 0.6	0.19 ± 0.0	0.01 ± 0.00
TBW-7	262.51	33.9	7.86	22.58	<0.3	78 ± 2	1.40 ± 0.02	0.12 ± 0.00
TBW-8	531.27	34.4	8.25	21.86	<0.3	76 ± 1	0.67 ± 0.01	0.63 ± 0.01
TBW-9	537.52	34	8.61	6.05	0.35 ± 0.03	29.9 ± 0.6	0.53 ± 0.01	3.13 ± 0.05
TBW-10	456.27	32.8	8.56	6.76	<0.3	30 ± 2	1.10 ± 0.01	3.30 ± 0.06

[a]Salinity was calculated from Cl⁻ concentration. [b]Two Mississippi River samples were collected, one in June and one in July, 2013, concentrations represent the average ±1σ. Other parameters were not measured. [184]W values reported

Table 3.5: Surface water samples collected in April 2014.

Sample	Dissolved O$_2$ μM	Temp. °C	pH	[a]Salinity ‰	W nM	Mo nM	Mn μM	Fe μM
TBW-1	508.78	24.4	7.59	1.27	0.06 ± 0	12.7 ± 0.5	1.39 ± 0.04	0.42 ± 0.01
TBW-2	361.27	24.6	7.30	4.04	0.09 ± 0.01	21.5 ± 0.7	3.0 ± 0.1	0.29 ± 0.01
TBW-3	411.90	24.4	7.26	5.3	0.07 ± 0.01	25.0 ± 0.8	3.2 ± 0.1	0.39 ± 0.01
TBW-4	384.40	25.7	7.27	7.37	0.07 ± 0.01	29 ± 2	2.11 ± 0.06	0.137 ± 0.004
TBW-5	453.78	27.4	7.53	12.5	0.07 ± 0.01	40.2 ± 0.7	0.93 ± 0.03	0.39 ± 0.01
TBW-6	453.78	27.4	7.51	12.5	0.07 ± 0.01	43.9 ± 0.8	0.48 ± 0.01	0.29 ± 0.01
TBW-7	566.29	26.8	7.78	12.1	0.05 ± 0.01	44. ± 1	0.165 ± 0.005	0.037 ± 0.001
TBW-8	571.91	26.4	7.95	20.57	0.06 ± 0.01	56 ± 2	0.122 ± 0.004	0.020 ± 0.001
TBW-9	365.02	28.6	7.45	10.28	0.06 ± 0.01	40 ± 1	1.0 ± 0.1	0.21 ± 0.01
TBW-10	384.40	26.7	7.39	10.34	0.06 ± 0.01	40 ± 1	0.89 ± 0.03	0.108 ± 0.004
TBW-11	378.77	24.8	7.39	3.95	0.07 ± 0.01	20 ± 1	3.4 ± 0.1	0.37 ± 0.02
TBW-12	408.78	25.1	7.54	2.39	0.1 ± 0.01	17.3 ± 0.4	2.1 ± 0.2	0.25 ± 0.02

[a]Salinity was measured using conductivity. [184]W values reported

3.4.2 Pore waters

Concentrations of W, Mo, Fe, and Mn in pore waters from the study site are presented in

Tables 3.6 (August 2013) and 3.7 (April 2014) along with corresponding dissolved

sulfide concentrations, salinity, and pH values. In August 2013, pore waters underlying

fresh surface waters (i.e., S < 1 ‰; TBW-1 and TBW-4) that had relatively low dissolved

sulfide concentrations (≤ 2.5 µM) and pH ~7.8 exhibited the highest W and Mo

concentrations (W: 14.3 - 24.5 nM; Mo: 30 - 45 nM). Dissolved iron in these low sulfide,

mildly alkaline pore waters ranged from 1.6 to 3.8 µM, and Mn varied from 6.9 to 8.1

µM. Pore waters underlying brackish surface waters (i.e., salinity > 1 ‰) exhibited

relatively high dissolved sulfide concentrations (i.e., S(-II) > 200 µM) that generally

increased with depth. The pore waters underlying brackish waters were less alkaline with

pH ranging from 6.8 – 7.5. In April 2014, due to the infiltration of saltwater into Falgout

Canal, pore waters from TBW-1 had pH ~7, and sulfide concentrations increased with

depth, similar to TBW-9. Pore waters collected in April included those from the

sediment-water interface, allowing for complete pore water profiles for W, Mo, Fe, Mn,

and sulfide with depth to be plotted (Fig. 3.4). Fig. 3.5 illustrates W and Mo pore water

concentrations as a function of dissolved sulfide concentrations. The decrease of Mo at

~11 µM $[H_2S]_{(aq)}$ occurs near the "geochemical switch" at which molybdate (MoO_4^{2-}) is

converted to tetrathiomolybdate (MoS_4^{2-}) by thiolation (Helz et al., 1996; Erickson and

Helz, 2000). The subsequent decrease in Mo concentrations to relatively low, stable

concentrations between 1-8 nM is similar to previous reports of Mo in coastal pore waters

(e.g., Dellwig et al., 2007). Unlike Mo, which occurs primarily as MoO_4^{2-} or MoS_4^{2-}

(Helz et al., 1996; Erickson and Helz, 2000), intermediate species of thiotungstates are predicted to predominate for the dissolved sulfide concentrations measured in these pore waters (Fig. 3.5b; Mohajerin et al., 2014a).

Manganese exhibited a maximum concentration of 43 µM near the sediment-water interface of core TBW-1 and decreased to 7 µM by ~6 cm depth (Fig. 4a). For both sampling periods, Mn pore water concentrations generally decreased with depth. Iron concentrations in pore waters varied from $0.2 - 16$ µM and were highest in pore waters with low dissolved sulfide concentrations. For example, pore waters with S(-II) > 25 µM averaged 1 ± 0.9 µM of dissolved Fe. Maximum concentrations of Mo, Mn, and Fe were observed in pore water samples within 4 cm of the sediment-water interface in April for both TBW-1 and TBW-9 cores.

3.5 Discussion

3.5.1 Trace elements in surface waters

Tungsten and Mo concentrations as a function of salinity in northern Terrebonne Bay estuary are similar to reports from other estuaries (Van der Sloot et al., 1985, 1989; Audry et al., 2007; Rahaman et al., 2010). Specifically, W exhibits non-conservative (i.e., chemically reactive) behavior, whereas Mo concentrations in the surface waters of the studied estuary generally demonstrate conservative mixing between low Mo fresh waters and high Mo seawater (Fig. 3.3a and 3.3b inset). Unlike Mo, W exhibits a low correlation with salinity in estuary waters, which is indicative of reactive behavior (Hoede et al., 1987; Van der Sloot et al., 1985, 1989; this study). Tungsten concentrations reach a maximum at low salinities (< 15 ‰), and then sharply decrease at higher salinities (Fig. 3.3b). Surface water concentrations of W and Fe in northern Terrebonne Bay estuary
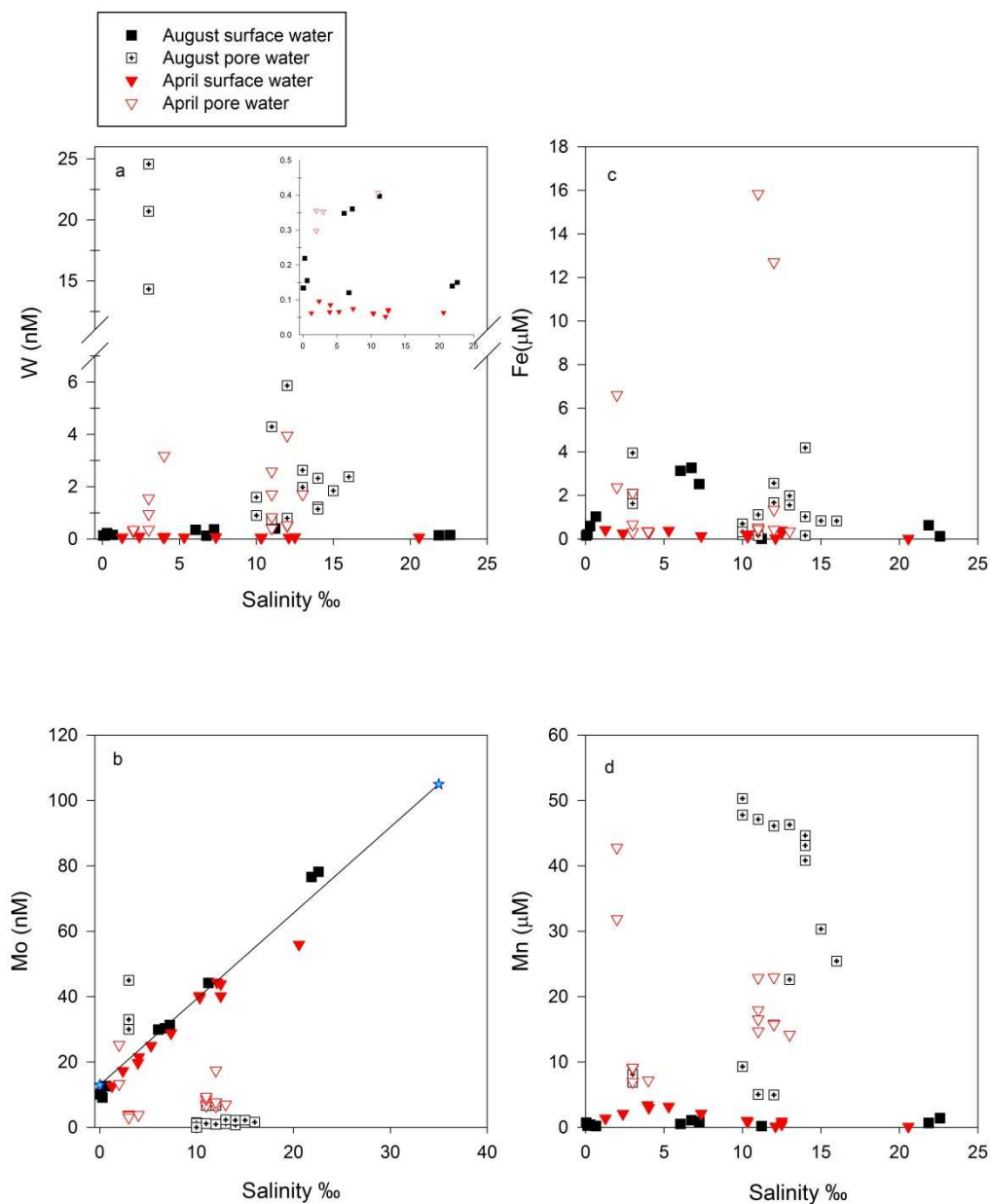
Figure 3.3: Trace element concentrations are plotted against salinity. **a)** Tungsten, inset is a close-up of low W concentrations to illustrate surface water variation with salinity. **b)** Mixing of Mo in surface waters is depicted by the linear regression using a freshwater (Mo = 13 nM) and seawater (Mo = 110 nM) endmember, which are depicted by the blue stars. **c)** Iron; **d)** Manganese

April 2014
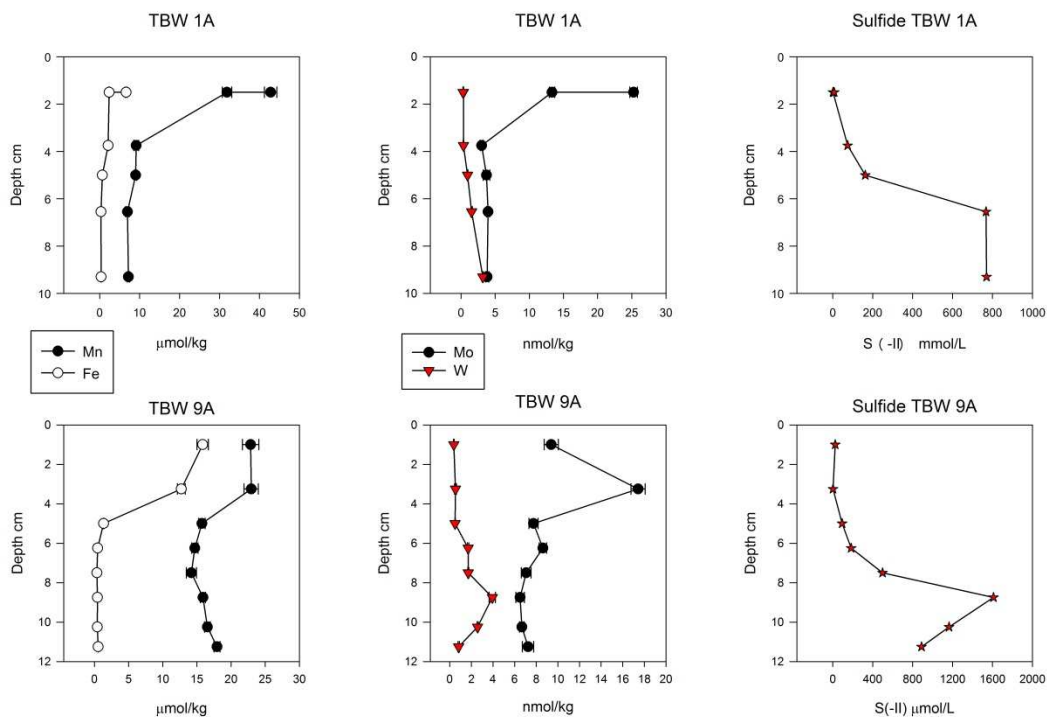
Figure 3.4: April 2014 pore water profiles illustrating trace element and total dissolved sulfide concentrations with depth **a)** Pore water concentrations of Mn and Fe from core TBW-1 **b)** Pore water concentrations of Mo and W from core TBW-1 **c)** Pore water concentrations of total dissolved sulfide from core TBW-1 **e)** Pore water concentrations of Mn and Fe from core TBW-9 **b)** Pore water concentrations of Mo and W from core TBW-9 **c)** Pore water concentrations of total dissolved sulfide from core TBW-9

showed a positive, statistically significant correlation in surface waters ($r = 0.47$, $p <$ 0.05) suggesting that the affinity for W for Fe oxides/oxyhydroxides may be removing W from surface waters to the sediments. Coagulation and removal of dissolved/colloidal Fe that occurs as salinity increases in estuaries (Boyle et al., 1977) could preferentially scavenge dissolved W over Mo from the water column **(**Takematsu et al., 1990; Gustafsson, 2003; Kashiwabara et al., 2013). Furthermore, Van der Sloot et al. (1989)

Table 3.6: Pore water samples collected August 2013.

Sample	[a]Depth cm	S(-II) μM	[b]Salinity ‰	pH	W nM	Mo nM	Mn μM	Fe μM
TBW-1.1	9.8 - 15.5	2.3	3	7.78	24.6 ± 0.4	30 ± 10	6.91 ± 0.08	3.95 ± 0.04
TBW-4.2	0 - 5.2	2.46	3	7.83	20.7 ± 0.4	33 ± 3	8.1 ± 0.07	1.62 ± 0.02
TBW-4.1	5.2 - 11.3	2.46	3	7.83	14.3 ± 0.5	45 ± 6	7.99 ± 0.08	2.06 ± 0.02
TBW-5.7	4.5 - 5.5	411.65	10	7.30	1.6 ± 0.1	1.0 ± 0.2	47.8 ± 0.7	0.7 ± 0.01
TBW-5.6	5.5 - 6.5	795.23	10	7.29	0.90 ± 0.07	1.2 ± 0.3	50.3 ± 0.9	0.19 ± 0.01
TBW-5.5	6.5 - 7.5	1172.58	11	7.08	0.74 ± 0.08	0.9 ± 0.2	47.1 ± 0.9	0.16 ± 0.01
TBW-5.4	7.5 - 9.8	746.37	12	7.25	0.79 ± 0.08	0.5 ± 0.1	46.1 ± 0.5	2.56 ± 0.03
TBW-5.3	9.8 - 12	1269.26	13	7.21	2.6 ± 0.2	0.9 ± 0.4	46.3 ± 0.8	1.99 ± 0.04
TBW-5.2	12.0 – 13.0	1749.52	14	7.32	1.1 ± 0.1	0.6 ± 0.1	43.1 ± 0.6	0.16 ± 0.01
TBW-5.1	13.0 - 14.0	1166.34	14	7.22	1.22 ± 0.07	1.2 ± 0.6	44.6 ± 0.7	1.03 ± 0.02
TBW-7.4	2.2 - 4.7	779.64	13	7.41	2.0 ± 0.2	2.0 ± 0.4	22.6 ± 0.3	1.55 ± 0.02
TBW-7.3	4.7 - 6.0	977.67	16	7.51	2.4 ± 0.2	1.32 ± 0.3	25.4 ± 0.5	0.82 ± 0.02
TBW-7.2	6.0 - 7.5	1387.76	15	7.61	1.8 ± 0.1	1.9 ± 0.3	30.3 ± 0.6	0.83 ± 0.02
TBW-7.1	7.5 - 9.3	760.93	14	7.37	2.3 ± 0.3	1.9 ± 0.3	40.8 ± 0.4	4.18 ± 0.06
TBW-9.4	0.5 - 2.2	1827.48	10	6.90	1.6 ± 0.1	<1	9.29 ± 0.09	0.32 ± 0.01
TBW-9.3	2.2 - 3.4	1805.65	11	6.89	4.3 ± 0.2	6.4 ± 0.6	5.04 ± 0.07	1.11 ± 0.02
TBW-9.2	3.4 - 4.5	202.08	12	6.83	5.9 ± 0.3	6.3 ± 0.9	4.94 ± 0.09	1.66 ± 0.03

[a]Depth from the sediment-water interface. [b]Salinity was estimated using a refractometer. [184]W values reported

Table 3.7: Pore waters samples collected in April 2014.

Core	[a]Depth cm	S(-II) µM	[b]Salinity ‰	pH	W nM	Mo nM	Mn µM	Fe µM
9A7	0 - 2	24.64	11	6.80	0.41 ± 0.03	9.4 ± 0.7	23 ± 1	15.8 ± 0.8
9A8	2 - 4.5	2.49	12	6.99	0.53 ± 0.06	17.4 ± 0.7	23 ± 1	12.7 ± 0.6
9A6	4.5 - 5.5	94.02	12	6.73	0.5 ± 0.04	7.8 ± 0.4	15.7 ± 0.5	1.34 ± 0.04
9A5	5.5 - 7	183.68	11	6.80	1.7 ± 0.07	8.6 ± 0.3	14.7 ± 0.5	0.46 ± 0.02
9A4	7 - 8	498.35	13	6.95	1.71 ± 0.1	7.1 ± 0.5	14.2 ± 0.7	0.35 ± 0.02
9A3	8 - 9.5	1609.18	12	6.94	4.0 ± 0.2	6.5 ± 0.4	15.9 ± 0.4	0.43 ± 0.01
9A2	9.5 - 11	1164.79	11	6.98	2.6 ± 0.1	6.7 ± 0.2	16.5 ± 0.4	0.41 ± 0.01
9A1	11 - 11.5	888.79	11	6.96	0.84 ± 0.05	7.2 ± 0.5	17.9 ± 0.5	0.53 ± 0.01
1A15	0 - 3	1.40	2	[c]7.22	0.3 ± 0.02	25.3 ± 0.6	43 ± 2	6.6 ± 0.2
1A14	0 - 3	6.86	2	7.14	0.36 ± 0.02	13.3 ± 0.4	32 ± 1	2.4 ± 0.1
1A13	3 - 4.5	74.85	3	[c]7.25	0.35 ± 0.05	3.0 ± 0.2	9 ± 0.6	2.1 ± 0.1
1A12	4.5 - 5.5	162.48	3	7.04	0.95 ± 0.06	3.7 ± 0.5	9.0 ± 0.3	0.66 ± 0.02
1A10	5.5 - 7.6	767.17	3	6.96	1.6 ± 0.1	4.0 ± 0.2	7.0 ± 0.5	0.32 ± 0.02
1A11	7.6 - 11	770.29	4	6.92	3.18 ± 0.09	3.8 ± 0.2	7.2 ± 0.3	0.35 ± 0.02

[a]Depth from the sediment-water interface. [b]Salinity was estimated using a refractometer. [c]Oxidation of aliquots used for pH measurements of 1A15 and 1A13 may have occurred resulting erroneous measured pH values. Aliquots of these samples for sulfide determination were not affected. [184]W values reported
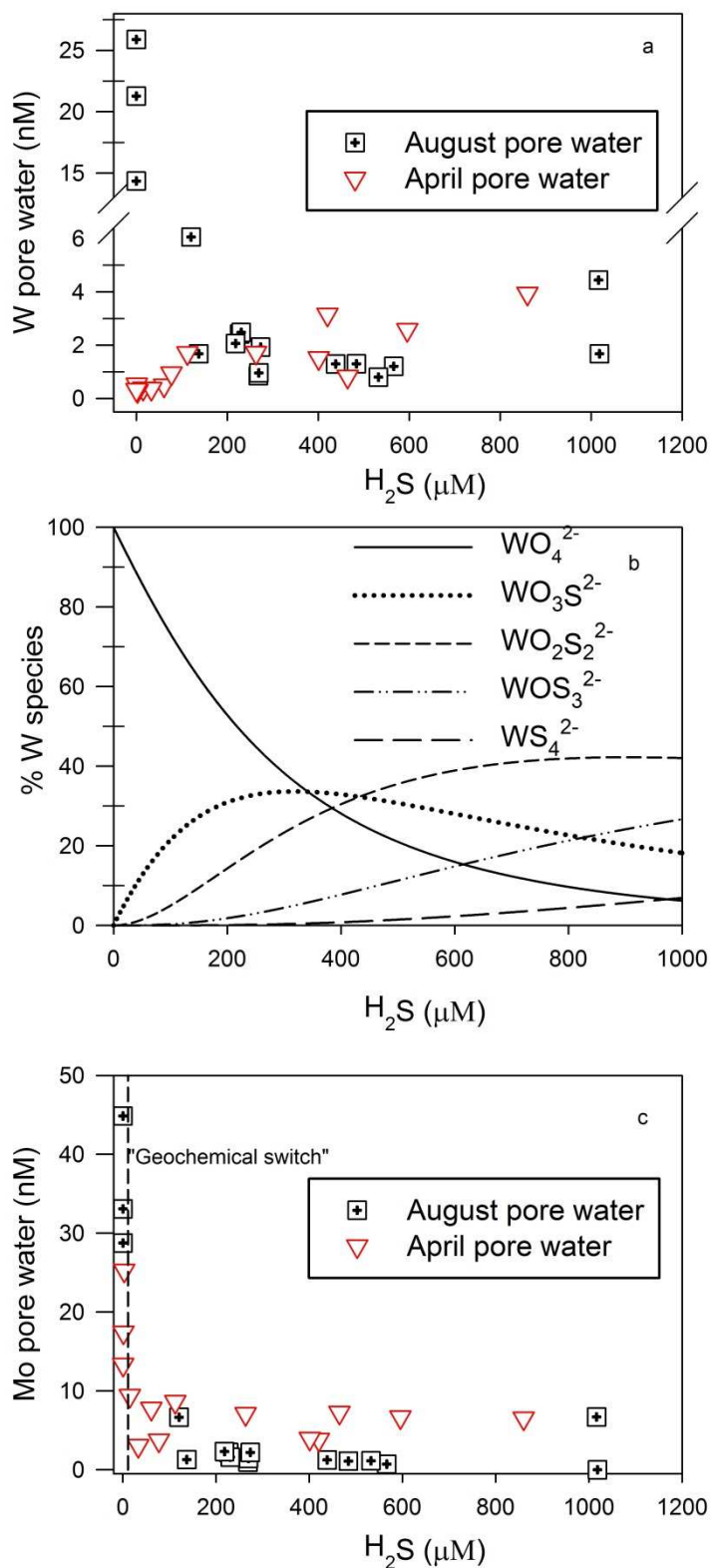
Figure 3.5: Trace element pore water concentrations (y-axis) against $[H_2S]_{(aq)}$; **a)** Tungsten; **b)** Depicts predicted thiotungstate speciation based on stability constants in Mohajerin et al. (2014a); **c)** Molybdenum, "geochemical switch" corresponds to predicted transition of MoO_4^{2-} to MoS_4^{2-} (Helz et al., 1996; Erickson and Helz, 2000).

related the decrease of dissolved W concentration in the Scheldt and Solo estuaries to uptake of W onto SPM in waters where S > 10 ‰, followed by deposition to the sediments. Further evidence includes ultrafiltration of natural river samples that exhibit a relationship between W and Fe/organic colloids in river waters, whereas Mo occurs primarily in the dissolved form (Porkrovsky and Schott, 2002). Finally, filtration studies of the Sacramento River and its tributaries showed that more than half of the W in waters from a majority of the sites sampled (i.e., 8 out of 10) occurred in colloidal form (Taylor et al., 2012).

Dissolved Mo concentrations from northern Terrebonne Bay estuarine surface waters are generally consistent with the conservative mixing of terrestrial water and seawater (Fig. 3.3a). The observed depletion of Mo in April 2014 (depicted by the sample plotted below the conservative mixing line Fig. 3.3a) can be explained by a model Dellwig et al. (2007) postulated, where in the Wadden Sea, depleted Mo concentrations are associated with enrichment of Mo onto Mn-rich SPM that aggregate and subsequently settle out of the water column. The relationship between bacterial abundance on aggregates has a negative correlation to dissolved Mo ($r = -0.88$) and positive correlation to dissolved Mn ($r = 0.69$) concentrations in the Wadden Sea. Bacterial activity can produce oxygen-depleted micro-zones enabling Mo fixation onto organic-rich SPM and release of Mn from SPM via reductive dissolution (Dellwig et al., 2007). In April, dissolved Mo in northern Terrebonne Bay estuarine surface waters had a negative and statistically significant correlation to dissolved Mn ($r = -0.78$, $p < 0.05$) suggesting a similar mechanism could explain Mo depletion.
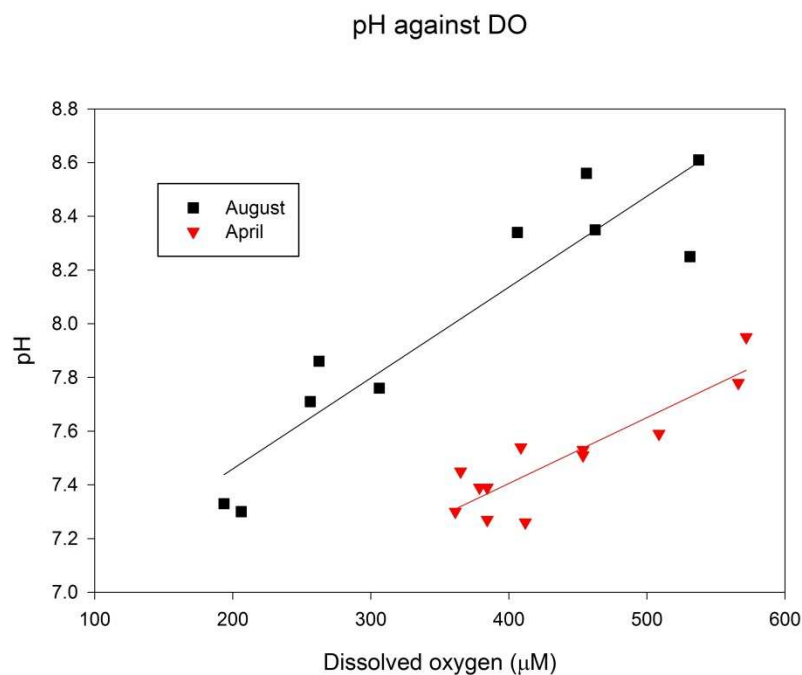
pH against DO

Fig. 3.6 Plots of pH against dissolved oxygen concentration for surface waters collected in August 2013 and April 2014.

3.5.2 Dissolved Oxygen and pH of surface waters

Plotting pH as a function of dissolved oxygen (DO) in surface waters (Fig. 3.6) depicts

the strong and statistically significant correlation between these two parameters ($r = 0.93$

August, $p < 0.0001$; $r = 0.89$ April, $p < 0.0001$). The correlation is a result of the control

photosynthesis and respiration have on DO and CO_2 in surface waters. Fig. 3.7 illustrates

both daily and seasonal changes in DO provided by the monitoring station at LUMCON

by TBW-10 (LUMCON weather station, 2014). High DO (i.e, 94-120% DO), as

observed in 83% of the brackish waters in August 2013 and 42% of the brackish April

2014 waters, indicates high levels of primary productivity compared to respiration and

possible eutrophication (O'Boyle et al., 2013 and references therein). As discussed in

section 3.5.5 and depicted in Fig. 3.7, DO in such eutrophic systems can change from supersaturated DO, to minimal DO concentrations with accompanying pH changes of up to one pH unit at night (O'Boyle et al., 2013).

Like other oxyanions, WO_4^{2-} is strongly influenced by pH, adsorbing at pH 4 to ~7 and desorbing under alkaline conditions (Johannesson et al., 2000; Gustaffson, 2003; Seiler et al., 2005; Johannesson et al., 2013; Mohajerin et al., 2014b). Both dissolved W and Fe were positively associated with pH in surface waters collected in August 2013 (W and pH: $r = 0.44$, $p > 0.05$; Fe and pH: $r = 0.71$, $p < 0.05$). In April 2014, however, W and Fe were inversely related with pH (W and pH: $r = -0.33$, $p > 0.05$; Fe and pH: $r = -0.49$, $p > 0.05$). Surface water dissolved W concentrations in August may have been influenced by W desorption from Fe particulates due to the mildly alkaline pH values of these waters, whereas in the more neutral pH waters sampled during April 2014, W adsorption to Fe oxide/oxyhydroxide particulate surfaces is favored. Thus, our data suggest the bioavailability and toxicity of W may be influenced by the trophic status of the waters that controls pH values. Further studies are necessary, however, to clarify if pH or other processes such as photoreduction of $Fe(OH)_3$ could be responsible for the increased Fe and W concentrations in these surface waters (McKnight et al., 1988; Kieber and Helz, 1992).
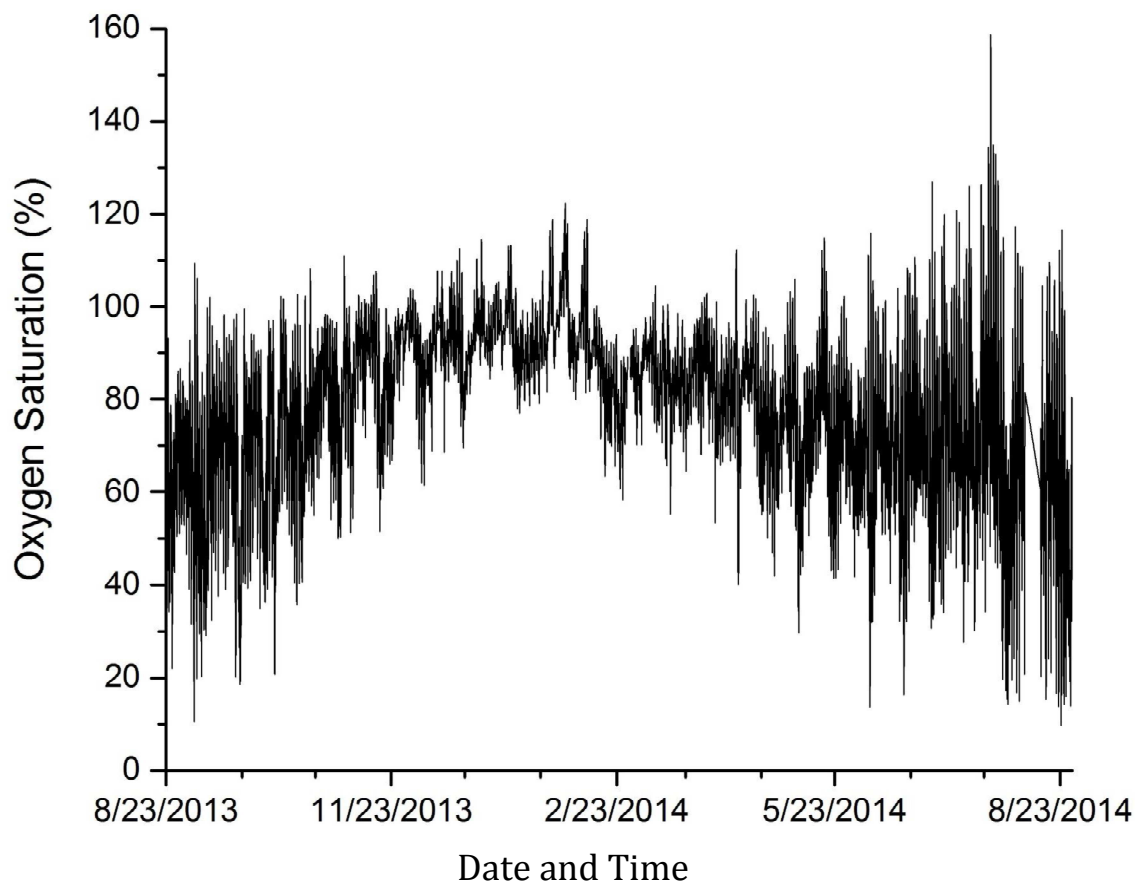
Figure 3.7 Dissolved oxygen concentration (DO) plotted against time for a period of 1 year. Data from LUMCON environmental monitoring station by point TBW-10 (Fig. 1c).

3.5.3 Pore waters

Previous measurements of pore water W concentrations are scarce. Indeed, the only reports of W in pore waters appear to be for anthropogenically impacted areas (i.e., tungsten mining; Petrunic and Al, 2005; and shooting ranges; Clausen et al., 2007, Clausen and Korte, 2009), methane seeps (Glass et al., 2014), or groundwaters (Seiler et al., 2005; Arnórsson and Óskarsson, 2007; Johannesson et al., 2013). To the best of our knowledge, no values of pore water W concentrations in an estuary or coastal salt marsh have been published. Elevated concentrations of W in hydrothermal vents that are associated with low Mo concentrations have been attributed to the higher solubility of

W compared to Mo in sulfidic waters (Kletizin and Adams, 1996; Ivanova, 1986; Kishida et al., 2004). Tungsten pore water concentrations in low temperature methane seeps (0.3 – 8 nM) are similar to our observed estuarine pore water concentrations (Tables 3.6 & 3.7), but Mo concentrations in the studied methane seeps reach 5000 nM within 15 cm of the sediment-water interface and dissolved sulfide concentrations vary from a few mM to almost 25 mM (Glass et al., 2014). These high Mo and S(-II) concentrations from methane seeps contrast sharply to the concentrations reported from estuarine pore waters estuary (e.g., Morford et al., 2007; Audry et al., 2007) as well as our measurements from the northern Terrebonne Bay. Furthermore, Glass et al. (2014) focused on microbial utilization of trace elements as opposed to geochemical controls on W cycling.

3.5.4 Redox stratification of pore waters

The pore water profiles for the April 2014 sampling campaign demonstrate vertical redox stratification consistent with other studies of marine influenced pore waters (Froelich et al., 1979; Hong et al., 1995). The relatively shallow Fe and Mn reducing zone in these sediments (0 – 4 cm) is likely due to the abundance of labile organic matter and sulfate that is available in these marine-influenced waters (e.g., Lord and Church, 1983; Koretsky et al., 2006). For example, mean annual dissolved organic carbon (DOC) concentrations for surface waters in Terrebonne Bay are 300 µM ± 200 µM in the central basin, and 414 µM ± 46 µM in the upper marshes (Bianchi et al., 2009). In pore waters with relatively low dissolved sulfide concentrations (S(-II) ≤ 2.5 µM), dissolved concentrations of Fe and Mn are enriched from the reductive dissolution of Fe/Mn oxides/oxyhydroxides (Duchart et al., 1973). In the sulfidic pore waters, total dissolved Fe and Mn concentrations are similar to other estuary pore waters with high

sulfide concentrations, suggesting removal of Fe in the pore water by formation of Fe-sulfide minerals (Berner, 1984; Morse and Luther, 1999; Koretsky et al., 2005). Thermodynamic calculations of mineral saturation states suggest that pore waters are close to equilibrium with respect to mackinawite (e.g., mean absolute values for the saturation index for mackinawite in April: $\log (SI) = 0.43 \pm 0.41$). The higher concentrations of dissolved Mn compared to Fe in pore waters is consistent with similar observations from ponded marshes reported by Koretsky et al. (2005)**.**

Profiles of Mo with depth in the April 2014 pore waters resemble the corresponding Mn and Fe profiles with maximum Mo pore water concentrations occurring near the sediment-water interface. A strong, positive correlation between Mo and Mn in the April 2014 pore water samples ($r = 0.94$, $p < 0.05$) and to a lesser degree between Mo and Fe ($r = 0.55$. $p > 0.05$), also supports an association between Fe/Mn cycling and dissolved Mo concentrations. We suggest that diagenesis of Mn and possibly Fe oxides releases Mo into these pore waters, which is subsequently co-precipitated or adsorbed as Fe and/or Mn are re-precipitated at depth (Morford et al., 2005, 2007). Conversely, W was inversely associated with Mo, Mn, and Fe, and instead had a positive correlation to dissolved sulfide ($r = 0.84$, $p < 0.05$) discussed in the following section 5.2.2. We note that we observed a positive correlation between W and S(-II) in sulfidic groundwaters from a deep, regional confined aquifer that shares little in common with the coastal marsh sediment pore waters of the current study other than the broadly similar anoxic redox conditions (Johannesson et al., 2013).

3.5.5 *W and sulfide in pore waters*

Tungsten concentrations and controls are analogous to Mo in pore waters underlying fresh surface waters. Tungsten and Mo enrichment in these pore waters is likely due to desorption and subsequent release of dissolved W and Mo from Fe/Mn oxides/oxyhydroxides at the observed pH values ~7.8 (e.g., Sohrin et al., 1999; Gustafsson, 2003). Compared to overlying fresh waters, however, W pore water concentrations are ~100 fold higher, whereas Mo in pore water concentrations only exhibit a 3 fold increase (Tables 3.4 & 3.6). Hence, our data favor a model in which proportionately more W than Mo is removed from the water column and deposited to the sediments. This is supported by the enrichment of W in all pore waters compared to overlying surface waters (Fig. 3.3b). Preferential removal of W over Mo from overlying surface waters into the sediments can be explained by the stronger affinity of W for Fe/Mn oxides/oxyhydroxides (Gustafsson, 2003; Kashiwabara et al., 2013). Field studies also demonstrate the occurrence of W primarily in the particulate phase and/or associated with Fe colloids in river waters, whereas Mo exists primarily in the dissolved phase in surface waters (Van der Sloot et al., 1989; Porkrovsky and Schott, 2002; Vasyukov et al., 2010; Taylor et al., 2012). To rule out the possibility of enrichment due to dissolution from sediments, however, sediment analysis is necessary.

Further evidence of the divergent geochemical behavior of W and Mo in sulfidic pore waters is depicted in Fig. 3.5. In contrast to the Mo depletion we observe in pore waters underlying surface waters of similar salinity, likely due to formation of particle reactive tetrathiomolybdate, dissolved W generally increases with increasing sulfide concentrations in the northern Terrebonne Bay estuarine pore waters. Fig. 3.5b presents the predicted speciation of (thio)tungstate as well as the percentage of total

thiotungstates in pore waters as a function of increasing $H_2S_{(aq)}$ concentrations. The

increase in total dissolved W, as tungstate forms thiotungstate species, suggests that

thiotungstate formation may increase W solubility in sulfidic waters similar to

thioarsenate species (Lee et al., 2005; Helz et al., 2011; Mamindy-Pajany et al., 2013).

Therefore, our data and geochemical modeling suggest that the divergent behavior of W

and Mo in these sulfidic pore waters is the result of differential particle reactivity of

thiotungstates and thiomolybdates toward Fe-sulfide minerals. The tungstate oxyanion

appears to be more particle reactive than the molybdate oxyanion with Fe/Mn

oxides/oxyhydroxides. In contrast, our data point to thiotungstate anions being less

particle reactive that than thiomolybdate anions toward minerals in sulfidic aquatic

environments. Thus, pore waters are depleted in Mo and enriched in W compared to

surface waters of similar salinity in northern Terrebonne Bay estuary.

Given the enriched W and depleted Mo pore water concentrations, release

of these elements from pore waters to surface waters (e.g, from diffussion or from

sediment resuspension during cold fronts) would lead to a decrease in Mo and an increase

in W in overlying surface waters, but this was not observed. Instead, W and Mo released

in pore waters may be adsorbed or precipitated at the sediment-water interface, or diffuse

downward to be incorporated into sulfidic sediments (e.g., Huerta-Diaz and Morse,

1992). Water column measurements in April 2014 indicated that the bottom waters were

oxic. Although no bottom water DO concentrations were obtained during our August

2013 sampling, continuous monitoring at a station near TBW-10 demonstrates that in

summer surface water DO concentrations in August 2014 fluctuated from saturated

oxygen concentrations of ~460 µM during the day to ~70 µM at night (Fig. 3.7;

LUMCON weather station). It is plausible that if bottom waters become anoxic at night in summer, trace elements, such as W, could be released to surface waters accounting for their higher W concentrations in August 2013 compared to April 2014 (Fig. 3.3a). Despite the relatively high solubility of W in sulfidic pore waters, W appears to be trapped in the sediments, possibly due to a Fe/Mn oxide/oxyhydroxide layer near the sediment-water interface, making this estuary a sink for W.

3.5.6 Mo and sulfide in pore waters

Unlike the strong relationship between Mo and salinity observed in surface waters, pore water Mo concentrations exhibited a low correlation with salinity (Fig. 3.3b). Instead, dissolved sulfide concentration appears to exert controls on the Mo concentration. Figure 3.5c illustrates Mo pore water concentrations plotted against dissolved sulfide concentrations. The enriched Mo concentrations observed in pore waters with low dissolved sulfide concentrations that were underlying fresh surface waters (Fig. 3.3a, 3.5b) is likely due to desorption and release of Mo from Fe/Mn oxides/oxyhydroxides at slightly alkaline pH ~7.8 (e.g., Morford et al., 2007). Transition of molybdate to the particle reactive tetrathiomolybdate (MoS_4^{2-}) at the "geochemical switch" (i.e., $[H_2S]$ ~11 µM; Helz et al., 1996; Erickson and Helz, 2000) was followed by low (i.e., < 10 nM), relatively constant Mo concentrations with increasing dissolved sulfide concentrations. Although there is general consensus regarding thiolation as the first step in removing Mo from sulfidic waters (e.g., Tribovillard et al., 2006), ideas about mechanisms leading to Mo enrichment in sulfidic sediments are still evolving (e.g, see Helz et al., 2011; Dahl et al., 2013; Chappaz et al., 2014). It is likely that a combination of mechanisms such as reduction of Mo(VI) to Mo(IV) or Mo(V) followed by

precipitation, formation of FeMoS nanoparticles, or complexation of Mo with organic matter control Mo sequestration into sulfidic sediments (Bostick et al, 2003; Vorlicek et al., 2004; Wang et al., 2011; Helz et al., 2011, 2014; Dahl et al., 2013; Chappez et al., 2014).

Similar pore water Mo concentrations between spatially separated sites and over a wide range of dissolved sulfide values indicate chemical mechanisms and not random variation, controls Mo in pore waters from northern Terrebonne Bay estuary. The independence of Mo concentrations relative to increases in $[H_2S]_{(aq)}$ from ~11 µM to 800 µM in the northern Terrebonne Bay estuarine pore waters suggests that free sulfide is not involved in chemical reactions controlling Mo concentrations. Furthermore, lower Mo concentrations in August 2013 pore waters that had higher pH values than April 2014 pore waters is inconsistent with control of dissolved Mo by solubility of FeMoS particulates, which would increase with increasing pH. Studies have demonstrated an association between Mo and organic carbon in sulfidic environments (e.g., Brumsack and Gieskes, 1983; Chappez et al., 2014), and Mo has been shown to be primarily in the colloidal form in swamp waters rich in Fe and organic matter (Vasyukov et al., 2010). Recent measurements of Mo speciation in salt marsh pore waters suggests ~10-13% of the dissolved Mo is reduced from Mo(VI) to Mo(V) in pore waters with dissolved sulfide > 25 µM (Wang et al., 2011). Furthermore, laboratory experiments measured increasing percentages of MoO_2^+ formation with decreasing pH (Bertine, 1972), which supports a conceptual model that includes a reduced form of Mo (i.e., $Mo^{(V)}O_2^+$ cation) binding to organic matter in the sediments following a reaction of the form:

$$C_{org}\text{-}(COO^-)_2(Mo^{(V)}O_2^+) + 2\ H^+ \ \leftrightarrow\ C_{org}\text{-}(COOH)_2\ + Mo^{(V)}O_2^+{}_{(aq)} \qquad (1)$$

in which C_{org} represents organic matter. Wichard et al. (2009) have reported that Mo

binds to organic matter over a wide pH range in soils. The complexation of Mo(V) to

organic matter could stabilize small (i.e., $< 0.45\ \mu m$) colloidal Mo in these pore waters

(Brumsack and Gieskes, 1983) explaining the near-constant Mo concentrations observed.

3.6 Conclusions

      Although W and Mo share many chemical similarities, our work in the

northern Terrebonne Bay estuary of southern Louisiana illustrates how geochemical

differences may control W and Mo concentrations in the hydrosphere. First, our data

clearly indicate enrichment of W in pore waters compared to surface waters, whereas Mo

is depleted in all pore waters except for those underlying fresh surface waters (Figs.

3.3a,b). Suspended particulate matter may remove W at relatively higher rates than Mo

due to the stronger affinity of W for Fe/Mn oxides/oxyhydroxides. Second, in contrast to

Mo, which was scavenged in the salt marsh's sulfidic pore waters to low (< 10 nM)

concentrations, dissolved W concentrations increased with increasing dissolved sulfide

concentrations suggesting that thiotungstates could be more soluble than thiomolybdates.

Thus, thiotungstate geochemical behavior resembles thioarsenates, and is divergent from

particle-reactive thiomolybdate behavior. Despite the solubility of W in the sulfidic pore

waters, the low concentrations of W in surface waters imply that any W that diffuses

from pore waters into the surface waters is likely scavenged by Fe/Mn

oxides/oxyhydroxides at the sediment-water interface making this estuary a sink for W.

Molybdenum surface water concentrations are generally consistent with conservative

mixing, although minor deviations from the conservative mixing line could be due to adsorption onto SPM.

Acknowledgements

Chapter 4:

Enrichment and degree of pyritization of tungsten and other trace elements in estuarine sediments

Abstract

Total sediment digestions and sequential extractions were performed on sediments from a coastal marsh in Louisiana to investigate the degree of enrichment and pyritization of W, Mo, Fe, and Mn. Total W concentrations were strongly correlated to both Al and Fe (r = 0.87 and r = 0.95, respectively) suggesting W is controlled by terrestrial input from weathering of crustal sources as well as Fe redox cycling. To explain observations of W and Fe enrichment and depletions, we propose a model in which W and Fe accumulate in intermediate marsh sediments (i.e., marshes characterized with fresh and brackish water vegetation) underlying fresh waters. For brackish and more saline conditions, introduction of higher sulfate concentrations and the availability of labile organic carbon favor reductive dissolution of Fe/Mn oxides/oxyhydroxides and sulfate reduction, and subsequently release of W and Fe from sediments into solution. Although some pore water W and Fe are re-precipitated by the pyrite fraction in the intermediate marsh sediments, some dissolved W and Fe are likely released into surface waters and transported laterally to salt marsh sediments where W and Fe contents are enriched in comparison to the upper continental crust. The sequential extraction studies indicate that W is likely sequestered into estuarine sediments and is cycled between the reactive and

pyrite fractions similarly to Mo and Fe. Specifically, the distribution of W, Mo, and Fe

with depth was similar for the reactive fraction (composed of carbonates, Fe/Mn

oxides/oxyhydroxides, and Fe monosulfides) and pyrite fractions in both cores examined,

indicating that both W and Mo are likely re-precipitated with Fe into pyrite bearing

sediments.

4.1 Introduction

Although investigation of tungsten (W) is increasing, a paucity of research

on W chemical reactivity and diagenetic processes precludes understanding the

geochemical cycle of W in the hydrosphere. Tungsten shares many chemical similarities

with molybdenum (Mo), another group VIB element (Cotton et al., 1999), and as such,

careful study of both W and Mo in natural systems may elucidate our understanding of W

geochemistry in the environment. In most natural, oxic waters W and Mo exist in the +VI

oxidation state as the tungstate (WO_4^{2-}) and molybdate (MoO_4^{2-}) oxyanions (Baes and

Mesmer, 1976). Both W and Mo form isostructural minerals such as scheelite and

powellite ($CaM^{VI}O_4^{2-}$ where M = W and Mo, respectively; Hazen et al., 1985), and the

sulfide minerals tungstenite and molybedenite ($M^{IV}S_2$) are also structurally analogous.

However, unlike molybedenite, tungstenite is rare (Hsu, 1977; Kletzin and Adams, 1996).

Other differences between W and Mo are exemplified by the fact that despite similar

molar ratios in the upper continental crust (UCC; Mo/W = 1.3 ± 0.5; Hu and Gao, 2008

and references therein), the dissolved molar Mo/W ratio in seawater is ≈ 2000 (Sohrin et

al., 1987, 1999; Firdaus et al., 2008), suggesting that there must be geochemical

processes that fractionate W from Mo during chemical weathering on the continental

crust and/or during transport in rivers from the continents to the oceans. The mean

residence time of W in the ocean is estimated to be between 14,000 – 61,000 years, which is substantially lower than that for Mo, which is estimated to be 440,000 – 800,000 years for Mo suggesting that W is more reactive than Mo (Firdaus et al., 2008; Miller et al., 2011).

Although W and Mo demonstrate conservative profiles in the ocean (Sohrin et al., 1987, 1998, 1999), both are enriched in oceanic ferromangese crusts (W: 0.10-0.64 mmol/kg; Mo: 3.94-9.84 mmol/kg (Takematsu et al., 1990; Kuzendorf and Glasby, 1992; Kochinsky and Hein, 2003; Kashiwabara et al., 2013) compared to the UCC (W and Mo ~ 0.01 mmol/kg; Hu and Gao, 2008). Comparing molar W and Mo contents in oceanic ferromanganese crusts to their dissolved concentrations in seawater [i.e., (µmol/kg ferromangase crust)/(µmol/L seawater)] show that W is enriched by ~ 1.1 x 10^7 in the crusts compared to a 5 x 10^4 fold enrichment of Mo (Takematsu et al., 1990). Similar to other oxyanions, adsorption of W and Mo onto Fe and Mn oxides is pH dependent with the strongest adsorption occurring at pH ~ 5 and desorption occurring at pH > 8 (Gustaffson, 2003; Seiler et al., 2005; Johannesson and Tang, 2009; Johannesson et al., 2013). Furthermore, formation of inner-sphere complexes of W onto ferrihydrite compared to outer-sphere complexes of Mo onto ferrihydrite results in a stronger affinity of W for ferrihydrite and may play a role in the fractionation of these two elements (Gustafsson, 2003; Kashiwabara et al., 2010, 2013).

Previous studies have also shown that Mo(VI) has a higher reduction potential than W(VI), leading to the prevalence of molybdenite and the rarity of tungstenite in ore bodies as well as differences in the biochemical properties of W and Mo enzymes (Hsu, 1977; Ivanova, 1986; Kletzin and Adams, 1996; Stiefel, 2002; Gonzalez et al., 2013).

Formation of tetrathiomolybdate (MoS_4^{2-}) could be one step in the mechanism leading to Mo removal from euxinic (i.e., anoxic and sulfidic) waters to sulfidic sediments, which may be followed by Fe-Mo-S particulate formation, adsorption to Fe sulfides, reduction from $Mo^{VI}S_4^{2-}$ to $Mo^{V}S_4^{2-}$, or complexation with organic matter or polysulfides (Erickson and Helz, 2000; Zheng et al., 2000; Bostick et al., 2003; Helz et al., 2004; Tribovillard et al., 2006; Helz et al., 2011; Dahl et al., 2013; Chappaz et al., 2014). Laboratory studies demonstrate that although both W and Mo form thioanions ($MO_x S_{4-x}^{2-}$, in which M = W or Mo and $1 \leq x \leq 4$) in sulfidic solutions, thiotungstates form at slower rates and require ~40 fold higher dissolved sulfide concentrations than Mo (Müller et al, 1969; Aymonino et al., 1969b; Erickson and Helz, 2000; Mohajerin et al., 2014a). Thus, in euxinic waters such as the Black Sea, Mo is predicted to occur primarily as MoS_4^{2-}, whereas only ~10% of tungstate is expected to form thioanions (Erickson and Helz, 2000; Mohajerin et al., 2014a). Despite these geochemical differences, reported W concentrations from recent Black Sea sediments of > 100 ppm W(Pilipchuck and Volkov, 1966) indicate that W may also be enriched in sulfidic sediments similar to Mo (e.g., Calvert and Pedersen, 1993; Zheng et al., 2000; Sundby et al., 2000; Adelson et al., 2001). Increases of both W and Mo content in suspended particulate matter (SPM) at the oxic-euxinic interface compared to W and Mo content in SPM in the oxic water columns in the Tyro and Bannock basins also support the notion that W is removed from sulfidic water columns and sequestered in sulfidic sediments (Van der Sloot et al., 1990; DeLange et al., 1990).

Dissolved sulfide in natural waters is produced by microbial reduction of dissolved sulfate using organic matter as a reducing agent. Thus, in freshwater lakes and groundwaters total sulfide concentrations are limited due to low sulfate concentrations

(i.e., SO_4^{2-} generally < 1 mM; Holmer and Storkholm, 2001 and references therein). In estuaries, sulfate concentration has a linear relationship with salinity (seawater: salinity = 35 ‰ and SO_4^{2-} = 28 mM; e.g. Audry et al., 2007). Thus, in estuarine areas dominated with freshwater, low dissolved sulfide concentrations occur in pore waters (Morse et al., 2007). In salt marshes with brackish waters and sediments rich in organic matter, however, dissolved sulfide concentrations can reach concentrations > 10 mM (Koretsky et al., 2005), which would be expected to thiolate both W and Mo at circumneutral pH (Erickson and Helz, 2000; Mohajerin et al., 2014a). Although water column salinity at a specific location in an estuary can change daily owing to tidal cycles or freshwater runoff, as well as seasonally due to wind-driven effects (Feng and Li, 2010), in sediments 10 - 20 cm below the water surface, pore water salinity represents the average annual salinity (Holdren et al., 1975).

In a previous study, we investigated W and Mo in surface and pore waters from northern Terrebonne Bay estuary, a Louisiana coastal marsh exhibiting salinity concentrations from < 1 ‰ to ~ 22 ‰, and pore water sulfide concentrations ranging from ~ 2.5 µM to 1830 µM (Mohajerin et al., in prep). Pore waters furthest from the coast line exhibited W concentrations 100 fold higher and Mo concentrations 3 fold higher than the overlying fresh water concentrations in August 2013, but pore waters collected from the same area in April 2014 only had a 3 and 2 fold W and Mo enrichment, respectively, compared to overlying brackish surface waters (salinity = 1.3 ‰). Furthermore, sulfidic pore waters were all depleted in Mo, but were enriched with W compared to overlying waters with similar salinity. Thus, results from northern Terrebonne Bay estuary agree with previous literature demonstrating that sulfidic sediments sequester Mo, but unlike

reports suggesting W is removed from euxinic water and trapped in sulfidic sediments (Pilipchuck and Volkov, 1966; Van der Sloot et al., 1990; DeLange et al., 1990), observations from northern Terrebonne Bay estuary suggest that sulfidic sediments could provide a source of W to the overlying water.

To improve our understanding of W mobilization and sequestration in sediments, and W phase associations, this study focuses on examining W enrichment in sediments and measures the degree of W pyritization with depth in two sediment cores. We compare the geochemical behavior of W to Mo, and analyze how W and Mo are influenced by Fe/Mn cycling. Furthermore, trace element redox geochemistry is analyzed by comparing the sediment core furthest from the coast to the sediment core located in Cocodrie salt marsh near Terrebonne Bay, which has the highest dissolved sulfide concentrations in pore waters collected (Mohajerin et al., in prep). Total W, Mo, Fe, and Mn content were measured to determine depletion or enrichment compared to the upper continental crust (UCC). In addition, a commonly used sequential leaching method was employed to investigate W and Mo distribution in the sediments in terms of their degree of trace metal pyritization (DTMP; Huerta-Diaz and Morse, 1990). Results from this study have implications for W fluxes to the ocean and for assessing the bioavailability of W, a potential toxin, in natural waters (Koustopyros et al., 2006 and references therein; Strigul et al, 2010, Strigul, 2010; Witten et al., 2012; Butcher, 2012; Tyrrell et al., 2013).

4.2 Study Area

Sediment cores were collected in northern Terrebonne Bay estuary from a salt marsh in the vicinity of Cocodrie, LA as well as in an intermediate marsh (i.e., a
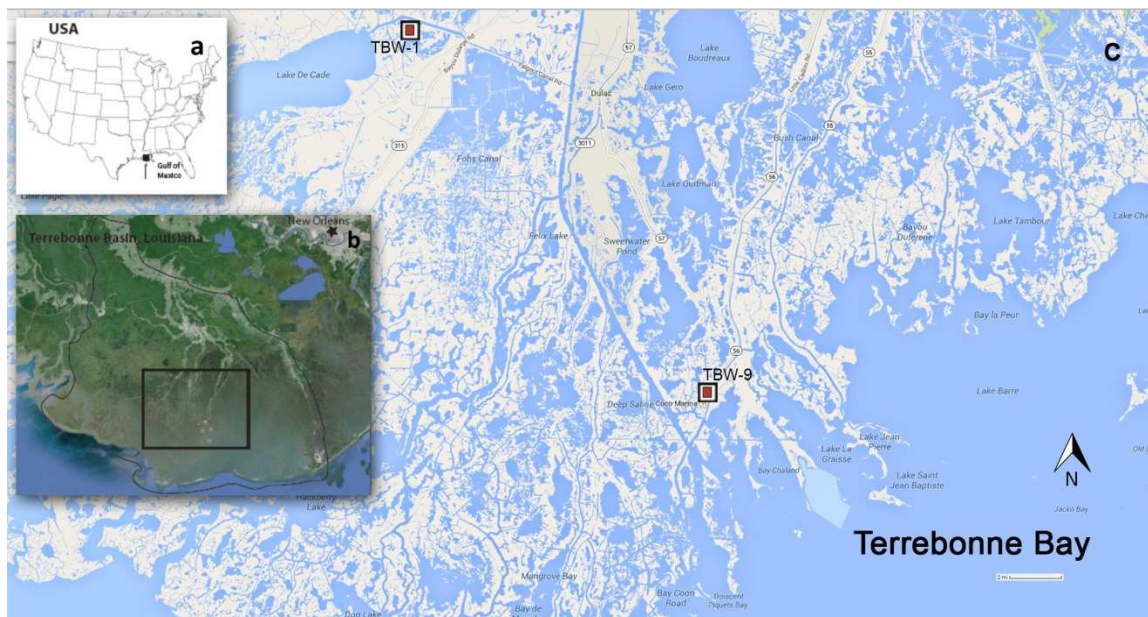
Figure 4.1: a) Map of the United States of America, arrow points to our study site in Louisiana near the Gulf of Mexico; **b**) Close up of Terrebonne Basin with a square capturing the study area and star indicating location of New Orleans near the Mississippi River. **c**) Image of study area. Filled red squares indicate the location of the two analyzed sediment cores. Images from Google Earth (**b**) and Google Maps (**c**).

marsh characterized with fresh and brackish water vegetation) near Falgout Canal, a source of fresh water input (Fig. 4.1). Northern Terrebonne Bay estuary is located within an abandoned lobe of the Mississippi River, which was an active part of the Mississippi River delta roughly 800 -1200 BP (Penland et al., 1987). Canals and levees constructed in the 19th and 20th centuries have cut-off this estuary from fluvial input from the Mississippi and Atchafalaya Rivers. Consequently, the sediment supply to the site is limited to terrestrial run-off, marine input, and redistribution of sediments within the estuary (DeLaune et al., 1981; Prager, 1992). Core TBW-1 was collected from Falgout Canal in an intermediate marsh characterized by fresh and brackish vegetation (e.g., Baustian and Turner, 2006). Falgout Canal is connected to low salinity water from Lake De Cade to the west and marine water intrusion from Houma Navigation Canal to the

east. Sediment accretion near this site is 0.30 ± 0.09 cm/yr (average $\pm 1\sigma$; Cahoon, 1994) with a high content of organic matter ($35\% \pm 4.3\%$ of dry weight sample; Baustian and Turner, 2006). Hence, core TBW-1 represents ~ 25 yrs. of sediment accumulation. Core TBW- 9, in the Cocodrie salt marsh, is dominated by *Spartina alterniflora* and sediments consist primarily of silts and clays along with ~ 2.5% organic carbon and have a median grain size of 38 µm (Millward et al., 2001). Sedimentation rates vary in Terrebonne Bay such that accumulation rates near the marshes are 1.69 cm/yr, compared to 0.69 cm/yr for Terrebonne Bay in the marine influenced central basin (McKee et al., 1994). Thus, our core of ~ 10 cm represents roughly one decade of sediment accumulation at TBW-9. Suspended sediment matter is ~ 30 mg/L near the mouth of the Houma Navigation Canal (HNC), where it empties into Terrebonne Bay and decreases to ~ 8 mg/L near Cat Island Pass where it opens to the Gulf of Mexico (McKee et al., 1994). Although daily microtidal events do not provide the critical shear stress necessary to suspend sediments, strong winds from winter cold fronts mobilize marine sediments from Terrebonne Bay and flood interior marshes resulting in sediment deposition (Wang et al., 1993; Reed, 1989). Further evidence of seasonal sediment cycling is the accumulation of sediments in Terrebonne Bay from February to September from terrestrial run-off that redistributes marsh sediments and sediment removal from the bay in winter that coincides with the period of sediment accumulation in the marsh (Reed, 1989; McKee et al., 1994). Relative sea-level rise and subsidence due to sediment compaction is ~ 1cm/yr resulting in frequent salt marsh flooding and reducing sediments (Penland and Ramsey, 1990; Nyman et al., 1995). Examination of sediment toxicity for Terrebonne Bay and Lake De Cade sediments demonstrate spatial variability and possible environmental effects from high

As and Ni concentrations, but sediment concentrations for common metal pollutants (e.g., Pb, Hg, Zn, and Cu) are well below levels of environmental concern (Rabalais, 1995). Furthermore, measurements of W, Mo, Mn, and Fe in surface waters during two sampling periods suggest minimal anthropogenic input of these elements (Mohajerin et al., in prep).

4.3 Materials and methods

Sediment cores were collected April 30, 2014 in acid rinsed acrylic tubes (i.e., 2 mm thick, 6.5 cm inner diameter, and 15 cm in length) using a push core sampler. The sediment cores were sealed inside the acrylic tubes with caps and tape then placed in anaerobic bags under a carbon dioxide atmosphere and stored on ice during transport back the lab of Tulane University. The bagged cores were transferred into a nitrogen filled glove box within 10 hours after collection. Cores were sectioned roughly every 1.75 cm into 50 mL trace metal clean polyethylene centrifuge tubes in the glove box under the inert N_2 atmosphere. Six sediment aliquots were collected from core TBW-1 and nine aliquots were obtained from core TBW-9, which allowed us to capture from the sediment-water interface to a depth of ~10 cm in each core. After pore waters were anoxically removed, the sediment tubes were capped and sealed with parafilm and stored frozen. Sediment aliquots were then freeze-dried the following day in order to preserve the pyrite fraction (Huerta-Diaz and Morse, 1990). One sediment sample from a core that was underlying fresh water (core TBW-4.2; Mohajerin et al., in prep), collected in August 2013, was also freeze-dried for analysis. Freeze-dried sediment aliquots were ground using an agate mortar and pestle, then homogenized. The following calculations all refer to dry sediment weight.

To compare trace metal enrichment between low sulfide and sulfide-rich sediments, a sub-sample of the sediment cores underwent total digestion using concentrated HNO_3 and HF (Tang et al., 1999). Specifically, two sediment aliquots from Core-1 and four sediment aliquots from Core-9 with a triplicate at 4.5 cm, were analyzed for total trace element (W, Mo, Mn, and Fe) content as well as Al content. One sediment aliquot from ~7 cm depth obtained in August 2013 that exhibited low dissolved sulfide concentrations and relatively high pH (7.8) in the associated pore waters also underwent digestion and trace element analysis. Trace metal enrichment factors (EF) were determined using the formula:

$$EF = \frac{[TM/Al]_{sample}}{[TM/Al]_{UCC}} \qquad (1)$$

where $[TM/Al]_{sample}$ is the mole ratio of the trace metal [TM = W, Mo, Fe, or Mn] content to Al content in the sediment sample collected in this study and $[TM/Al]_{UCC}$ is the corresponding mole ratio in the upper continental crust (Wedepohl, 1995).

Aliquots of sediment samples from the cores collected in April 2014 were sequentially leached using methods developed by Huerta-Diaz and Morse (1990), based on Lord (1982), to determine pyrite Fe. Aliquots from core TBW-4.2 were not subjected to sequential extraction because the pyrite fraction may have been compromised from exposure to the atmosphere. All liquid reagents were ultra-pure (Baseline, Seastar chemicals; Optima, Fisher), and the boric acid was ACS grade. A subsample of 2 g from each sediment section was subjected to a sequential extraction procedure designed to target: 1) a reactive phase, comprised of dissolved amorphous and crystalline iron and

manganese oxides/oxyhydroxides, carbonates, amorphous iron monosulfides, as well as

most mackinawite (~ 90%) and some greigite (40-67%); and 2) a pyrite phase (Cornwell

and Morse, 1987; Huerta-Diaz and Morse, 1990). First, sediment aliquots were leached

using 1 M HCl solution to remove trace elements associated with the reactive phase. The

solid portion of the remaining sediment aliquots were then leached with 10 M

hydrofluoric acid combined with 5 g boric acid to remove trace elements associated with

the silicate phase, which is comparatively non-reactive, and then the remaining sediment

aliquots were leached with concentrated sulfuric acid to remove organic matter (Huerta-

Diez and Morse, 1992). Leachate solutions targeting the silicate and organic matter

phases were discarded. Finally, the remaining sediment aliquots were leached using

concentrated HNO_3 to remove trace elements associated with the pyrite phase. The

degree of (trace metal) pyritization was calculated using the concentration of the trace

metal in the two operationally defined phases, a reactive phase and a pyrite phase, such

that:

$$DOP \text{ or } DTMP = TM_{pyrite}/(TM_{reactive} + TM_{pyrite}) \qquad (2)$$

in which TM = Fe for the degree of pyritization (DOP) and TM = W, Mo, or Mn for

degree of trace metal pyritization (DTMP) in this study.

Trace element concentrations were measured directly using magnetic

sector inductively-coupled plasma mass spectroscopy (ICP-MS; Thermo Fisher Element

2) at Tulane University using diluted leachates of the reactive and pyrite fractions as well

as the solutions from the total sediment digestions. A minimum of seven standards of

known trace element concentrations were freshly (daily) prepared using serial dilutions of certified standards (CertiPrep and Peak Performance) with 2% HNO_3 (Optima, Fisher) in doubly distilled (Milli-Q 18 MΩ cm) water. Using low resolution mode for increased sensitivity and ^{103}Rh as an internal standard, ^{182}W, ^{184}W, ^{97}Mo, and ^{100}Mo were measured in the various sample aliquots. Using medium resolution and ^{45}Sc as an internal standard, ^{27}Al, ^{55}Mn, and ^{56}Fe were quantified in the samples.

4.4 Results

4.4.1 Water Content

Comparison of sediments before pore water extraction and freeze drying show that both sediment cores had high water contents [i.e.,((wet sediment weight - dry sediment weight)/wet sediment weight) x 100% = water content; core TBW-1 average = 91% ± 4%; core TBW-9 average = 72% ± 3%).

Table 4.1: Results of total sediment digestions

Core	Depth (cm)	W nmol/g	Mo nmol/g	Mn μmol/g	Fe μmol/g	Al μmol/g
TBW-4	5.2 – 8.6	9.20	8.55	22.81	625.15	1774.35
TBW-1	0 - 3	3.82	16.84	12.46	250.88	1347.30
TBW-1	5.5 – 7.6	0.66	22.67	3.82	112.93	1075.40
TBW-9	2 – 4.5	7.98	30.7	4.25	592.17	1797.58
TBW-9	7.5 - 8.5	8.42	28.77	5.00	642.92	2002.21
TBW-9	8.5 – 9.5	7.59	24.35	5.06	540.27	1648.89
TBW-9	11 – 11.5	7.71	23.55	5.71	557.02	1876.18

4.4.2 Total concentrations and EF

Table 4.1 presents total element contents for the estuarine sediment core samples. Triplicate analysis (i.e., sediment digestion of 3 sediment aliquots from the same core section) show W contents vary by 11.8%, Mo by 5.6%, Mn by 3.8%, Fe by 10.4%, and Al by 10.4% within a section core. Calculated enrichment factors are given in Table 4.2.

Table 4.2: Enrichment factors using [a]UCC as reference material (eq. 2 in text; Wedepohl, 1995).

Core	Depth interval (cm)	W EF	Mo EF	Mn EF	Fe EF	$\frac{Al_{sample}}{Al_{UCC}}$	Pore water Dissolved Sulfide (µM)	Pore water Salinity ‰
TBW-4	5.2 – 8.6	1.95	0.95	3.84	1.82	1.5	2.5	3
TBW-1	0 - 3	1.07	2.46	2.77	0.97	1.18	6.9	2
TBW-1	5.5 – 7.6	0.23	4.15	1.06	0.54	0.94	767	3
TBW-9	2 – 4.5	1.69	3.40	0.71	1.73	1.57	2.5	12
TBW-9	7.5 - 8.5	1.59	2.83	0.75	1.67	1.75	498	13
TBW-9	8.5 – 9.5	1.73	2.9	0.92	1.7	1.44	1609	12
TBW-9	11 – 11.5	1.55	2.47	0.91	1.54	1.64	889	11

[a]UCC references from Wedepohl (1995) in (TM ppm)/(Al ppm):
W = 2.65 x 10^{-6}; Mo = 5.08 x 10^{-6}; Mn 3.34 x 10^{-3}; Fe = 0.192

Similar trends were observed for W and Fe in the examined sediments as shown by the plot of W content versus Fe content in Fig. 4.2. Specifically, both W and Fe exhibited lower contents in core TBW-1 compared to core TBW-9 that had substantially higher dissolved sulfide concentrations. Furthermore, both W and Fe were depleted in core 1 at ~ 6 cm depth, whereas this sediment sample exhibited the highest EF for Mo. In contrast to the trends observed for W, Fe, and Mo that were enriched in the sulfidic sediments of core TBW-9, Mn was depleted in sediments for this core. Manganese, however, was enriched in the less sulfidic sediments of core TBW-1. Although the lowest concentration, and only observation of Mo depletion, occurred in a sediment sample with pore waters that exhibited low dissolved sulfide concentrations underlying fresh water, this sediment aliquot exhibited the highest W, Fe, and Mn enrichment factors (core 4, Table 4.2).
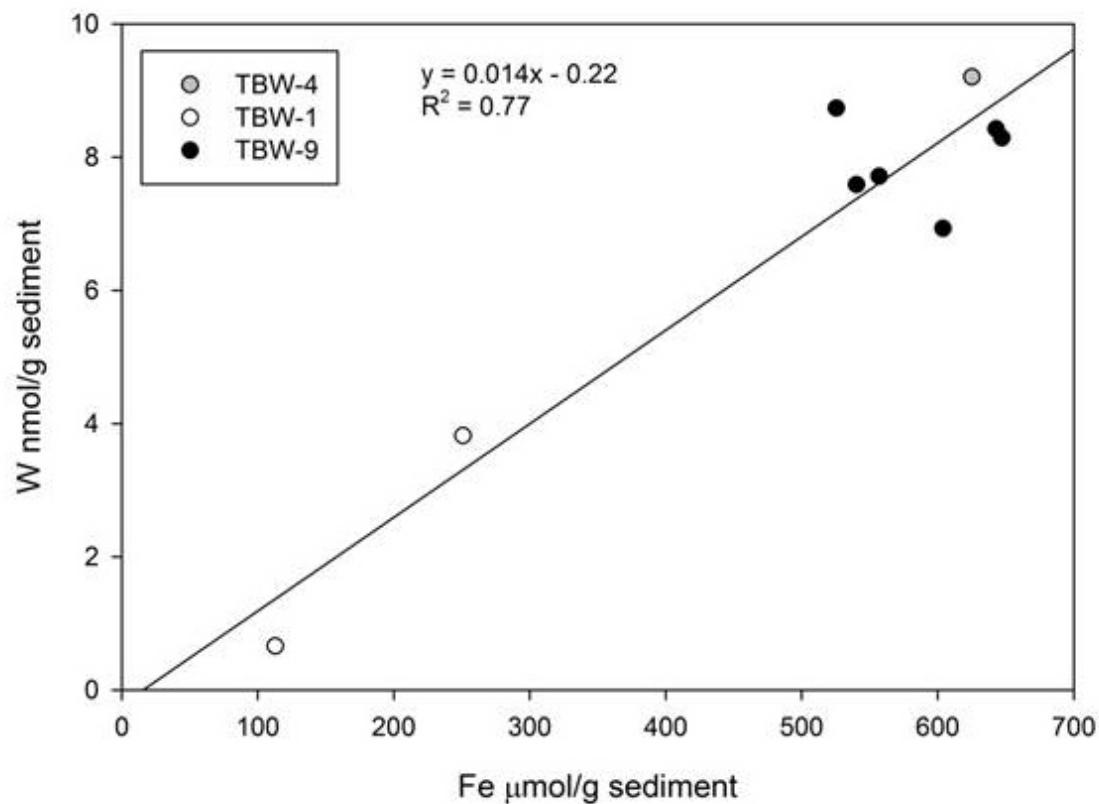
Figure 4.2: Total tungsten contents are plotted against total Fe contents for digested sediment aliquots

4.4.2 DTMP

Figs. 4.3 and 4.4 illustrate trace metal concentrations in the reactive and pyrite fractions with depth in cores 1 and 9, respectively. The molar ratios for W/Fe, Mo/Fe, and W/Mo are presented for the reactive and pyrite fractions of both cores in Appendix G along with a tabulation of the data presented in Figs. 4.3 and 4.4. We note that, with respect to the reactive fraction, no shell fragments or other large carbonates

were observed in either core. In the reactive fraction of core TBW-1, all measured trace metals exhibited similar patterns such that the highest concentrations occurred near the sediment-water interface, and then decreased to low, relatively constant concentrations at ≥ 4 cm depth (Fig. 4.3). The pyrite fraction of core TBW-1 was generally > 10 times the W and Mo reactive fraction contents. In contrast, the pyrite fraction of Mn in core TBW-1 was over an order of magnitude less that the reactive fraction, similar to Mn concentrations in the reactive and pyrite fractions reported for Atchafalaya Bay sediments (Huerta-Diaz and Morse, 1992). Pyrite fractions of Mo and Fe in core TBW-1 mirrored the reactive fractions and exhibited minimum concentrations near the surface that increased with depth. In contrast to Mo, however, reactive Fe for sediments near the sediment-water interface exceeded the maximum pyrite Fe (Fig. 4.3d).

The reactive fractions of W, Mo, Mn, and Fe in core TBW-9 also exhibited similar patterns to each other with increasing depth in the sediments. In contrast to core TBW-1, trace element concentrations in the reactive fractions were relatively constant with depth, although the minimum reactive Fe and Mn contents were observed ~5 cm depth (Fig. 4.4). Despite the relatively constant reactive W and Mo contents, the pyrite fractions of W and Mo in core 9 displayed nearly identical and variable concentrations with depth and were ~ 10 times greater than the reactive fraction contents (Fig. 4.4a, 4.4b). Concentrations of Mo in reactive and pyrite fractions for core TBW-1 and core TBW-9 were similar to reported Mo reactive and pyrite concentrations from organic-rich Atchafalaya Bay sediments (Huerta-Diaz and Morse, 1992). Manganese in the pyrite fraction of core TBW-9 increased from a minimum at the top of the core to a
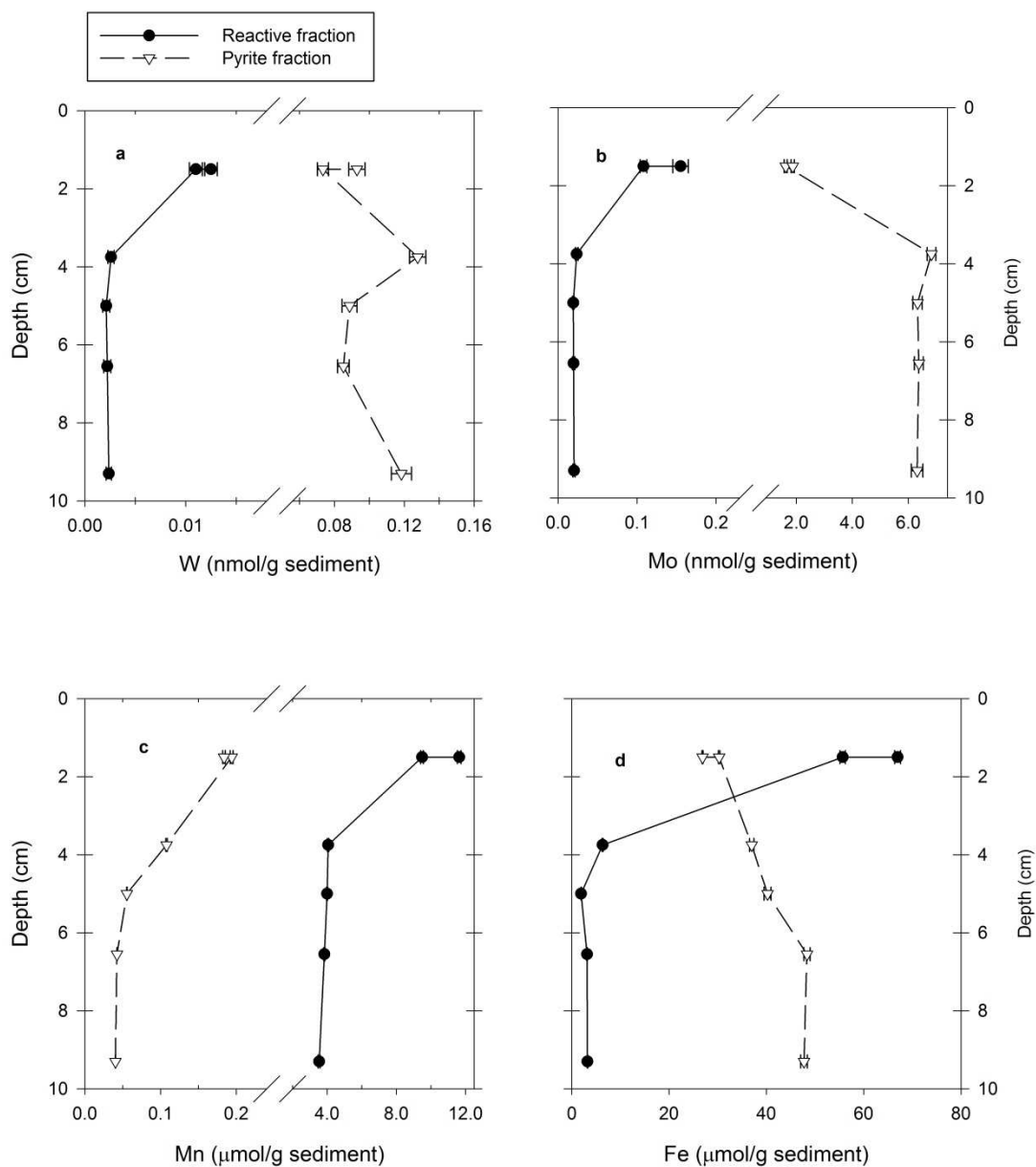
Figure 4.3 Distribution of trace element contents in the reactive and pyrite fractions with depth in core TBW-1. **a)** Tungsten, **b)** Molybdenum, **c)** Manganese, **d)** Iron
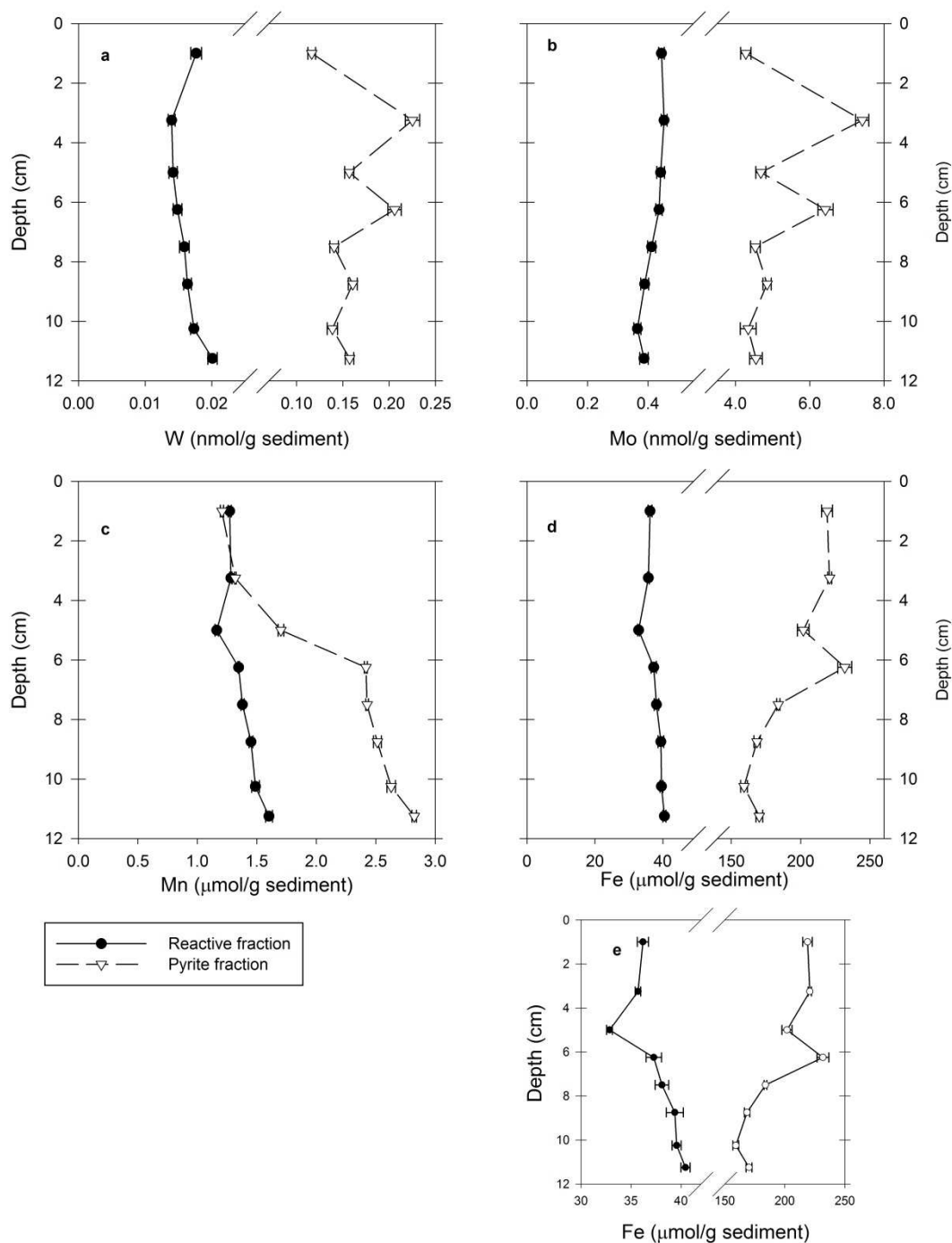
Figure 4.4 Distribution of trace element contents in the reactive and pyrite fractions with depth in core TBW-9. **a)** Tungsten, **b)** Molybdenum, **c)** Manganese, **d)** Iron, **e)** Same as d, but focuses on measured Fe reactive concentrations on the x-axis to better show reactive Fe changes with depth.

concentration of the reactive Fe fraction (Fig. 4.4d).

maximum that exceeded the reactive fraction at depth (Fig. 4.4c). Pyrite Fe distribution in

core TBW-9 mirrored the reactive Fe, with a maximum near 6 cm, but was ~ 5 times the

Fig. 4.5 illustrates DTMP and DOP with depth for cores 1 and 9, respectively, and DTMP

for W, Mo, and Mn are plotted as a function of DOP for core 1 and core 9 in Figs. 4.5a

and 4.5c, respectively. Despite changes in DOP and low DTMP for Mn, DTMP for W

and Mo were high (i.e., 0.8 – 0.99) for all sediment aliquots (Fig. 4.5). Only a small

portion of Mn occurred in the pyrite fraction of core TBW-1 such that the average DTMP

for Mn was 0.016 ± 0.01 ($\pm 1\sigma$), whereas DOP in core TBW-1 increased with depth from

0.28 at the surface to a maximum of 0.95 at ~ 5 cm. Unlike the pattern of increasing DOP

with depth observed in core TBW-1 (Huerta-Diaz and Morse, 1992), core TBW-9 DOP

was high (i.e., 0.84 ± 0.02) in all sediment samples including those near the sediment-

water interface.

4.5. Discussion

4.5.1 Total concentrations and enrichment factors

Bayous and wetlands adjacent to the coast that characterize much of

southern Louisiana may act as trace metal sinks and under certain conditions may serve

as a source of trace metals. Salt marshes, rich in organic matter and sulfate are ideal for

sulfide production and subsequent pyrite formation (Berner, 1984). Given the W

enrichment measured in sediments underlying both fresh water and brackish (i.e., salinity

> 1 ‰) water, we suggest that northern Terrebonne Bay estuary is likely a sink for W.

Total sediment contents of W are strongly correlated with total Fe and Al contents (Fig.

4.2; r = 0.88 and 0.92, respectively). We postulate that once W is leached from the

continental shelf during chemical weathering, it sorbs to Fe oxides/oxyhydroxides and

clay colloids into the hydrosphere. Ionic strength increases in this estuary can induce

colloid flocculation and subsequent removal from the water column to the sediments
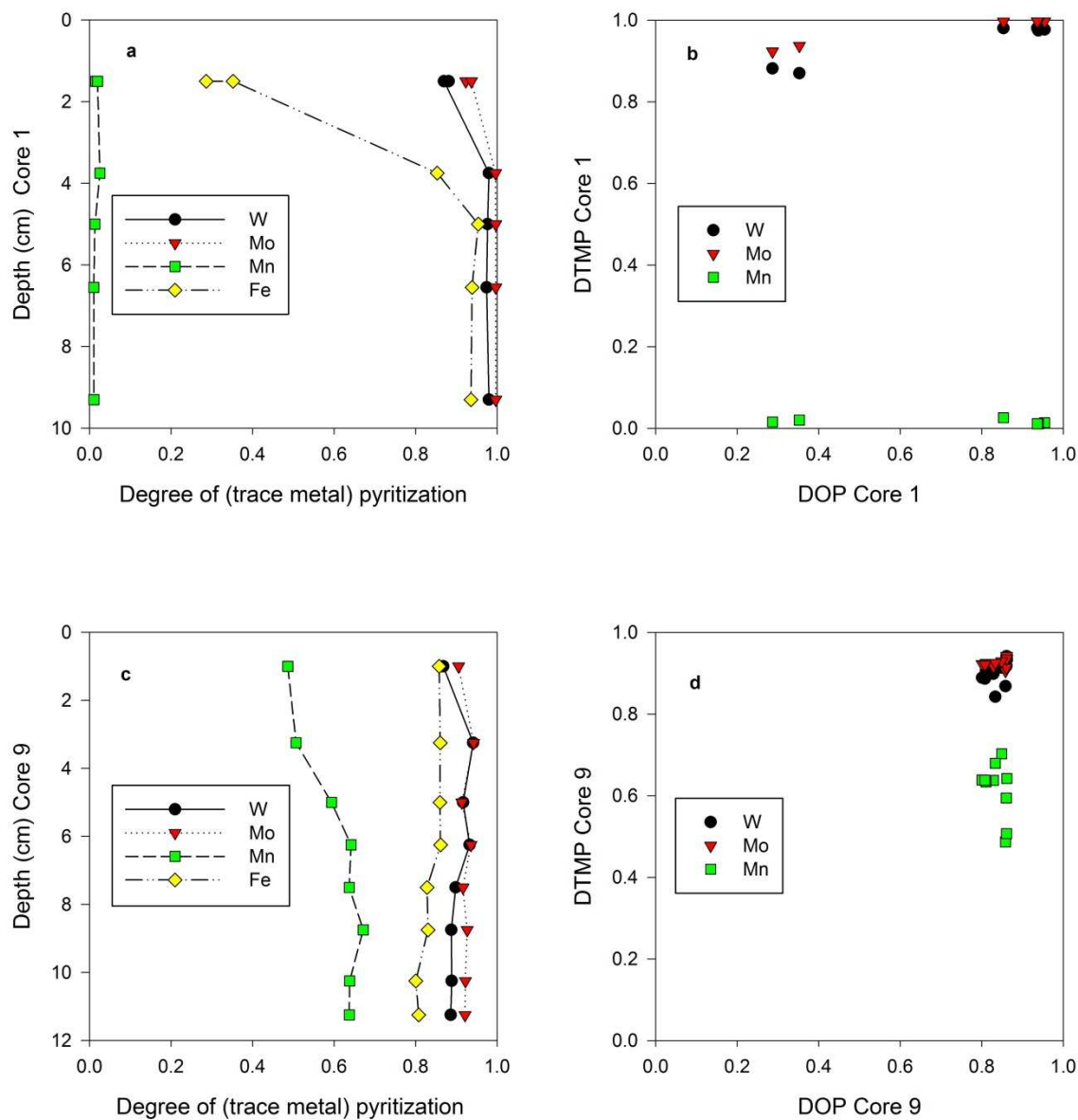
Figure 4.5 a) DTMP for W, Mo, and Mn and DOP (Fe) is plotted as a function of depth for core TBW-1; **b)** DTMP for W, Mo, and Mn is plotted against DOP for core TBW-1; **c)** DTMP for W, Mo, and Mn and DOP (Fe) is plotted as a function of depth for core TBW-9; **d)** DTMP for W, Mo, and Mn is plotted against DOP for core TBW-1

(Boyle, 1977). A strong, positive correlation (r ~ 0.88) calculated using Pearson's formula to estimate correlation between ratios with a common denominator (Kim, 1999) persists between W and Fe concentrations normalized to Al, suggesting W is cycled with Fe.

Luther et al. (1992) proposed a model in which: 1) Fe(III) is solubilized by organic ligands such as those produced by *S. alterniflora*.; 2) solubilized Fe is then reduced to Fe(II) through abiotic reduction by sulfur species or microbially mediated reduction; 3) Fe(III) minerals oxidize Fe(II) to Fe(III); and 4) precipitation of Fe(II) and Fe(III) occurs in the presence of dissolved sulfide (Luther et al., 1992). In the absence of dissolved sulfide, however, solubilized Fe may be re-precipitated as Fe(III)oxides/oxyhydroxides at the sediment-water interface (e.g., Scholz and Neumann, 2007) or diffuse into the overlying water column (e.g., Severmann et al., 2010). Iron isotope signatures from the Black Sea imply that Fe from sediments underlying oxic shelf waters undergoes reductive dissolution and is released from sediments to the water column causing a depleted Fe_T/Al ratio in oxic shelf sediments and is subsequently laterally transported to the euxinic basin resulting in enriched Fe_T/Al ratio in the sulfidic sediments (Severman et al., 2008; Scholz et al., 2014). In northern Terrebonne Bay estuary, dissolved sulfide and salinity concentrations are only valid for the time of collection and can change as marine water input varies seasonally usually by wind-driven changes (Reed, 1989; Wang et al., 1993; Mohajerin et al., in prep). For example, pore water from a core close to core TBW-1 that was collected in August 2013 exhibited low sulfide concentrations and pH ~ 7.8, similar to Core 4.2 (Mohajerin et al., in prep). In contrast, Core 9, located close to Terrebonne Bay, is always in contact with marine water,

and pore waters from a core collected in this area in August 2013 exhibited dissolved

sulfide concentrations between 200 – 1850 µM (Mohajerin et al., in prep).

Figure 4.6 illustrates a hypothesized model of how Fe cycling may affect W

sequestration and mobilization in the studied coastal system. During periods of low

salinity, when sulfate supply is limited and restricts production of dissolved sulfide in the

intermediate marsh, W sorbed to Fe oxides/oxyhydroxides is deposited in the sediments

(Fig. 4a). Deposition of W to the sediments by this process can explain the enrichment of

W and Fe in core TBW 4.2 that was underlying fresh water. Furthermore, the depletion of
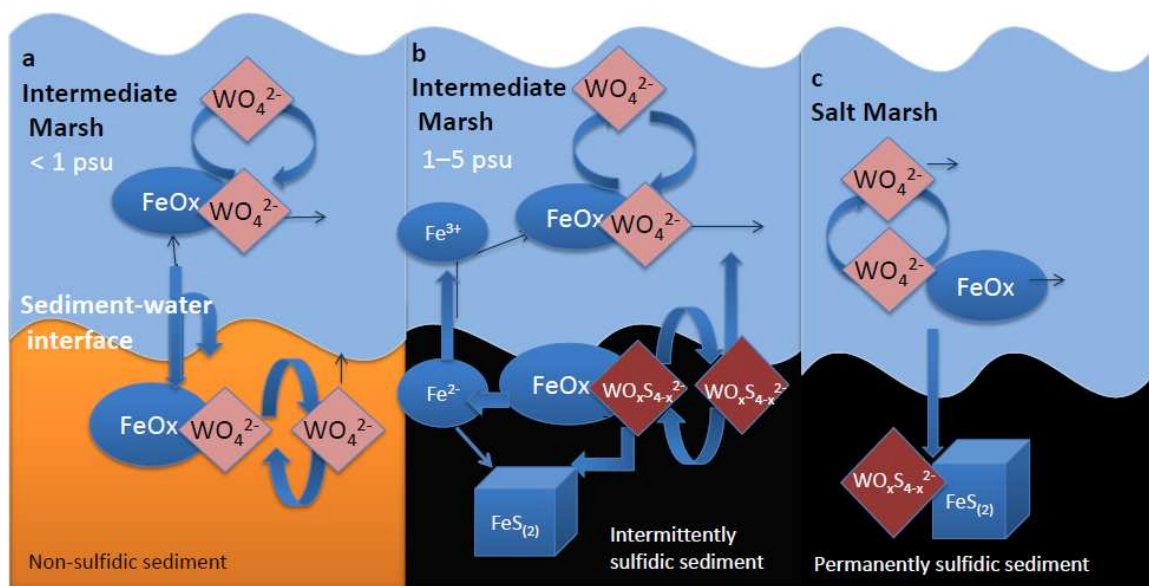
Figure 4.6 Schematic model of proposed mechanisms controlling W mobilization and sequestration in northern Terrebonne Bay estuarine sediments. **a)** In intermediate marsh sediments underlying fresh water, W adsorbed to Fe oxides/oxyhydroxides (FeOx) are tranported from the water column to sediments. Release of W and Fe into overlying waters results in some re-precipitation of FeOx at the sediment-water interface, resulting in seasonal W and Fe enrichments in the sediments, which likely occur in the reactive fraction (see text). **b)** Periods of marine water intrusion into the intermediate marsh can induce reducing conditions causing reductive dissolution of FeOx, releasing W and Fe. Although a portion of the released W and Fe are re-precipitated in the pyrite fraction, some W and Fe escapes into overlying waters where they are transported laterally towards the coast causing a seasonal depletion in intermediate marsh sediments. **c)** In salt marsh sediments that are likely permanently sulfidic, both Fe and W are sequestered in the sediments.

Mo in core 4.2 sediments suggests sediments underlying fresh waters may be a source of Mo to fresh waters, whereas the observed enrichment of W, Fe, and Mn suggest that sediments underlying fresh waters sequester W in the reactive fraction (Fig. 4a; Table 4.2). Although some W and Fe may be released into overlying fresh waters, our data indicate that W and Fe are more likely released into solution when intrusion of saline waters to the marsh facilitates the production of high dissolved sulfide concentrations owing to the increased SO_4^{2-} reduction (Fig. 4b). Although a portion of the dissolved W and Fe released by this mechanism are likely re-precipitated into the pyrite fraction (Fig. 3), some W and Fe probably diffuse into overlying surface waters and are then transported laterally, causing a seasonal depletion of W and Fe in the intermediate marsh sediments. This is consistent with the seasonal cycling of solid phase Fe in which HCl extractable Fe (i.e., solid-phase reactive Fe) decreases with increases in sulfide (Kostka and Luther, 1995; Rozan et al., 2002). In contrast, salt marsh sediments near the coast are always overlain by brackish waters. Thus, salt marsh sediments are likely always conducive to pyrite formation and are rarely, if ever under oxidizing conditions that would dissolve sulfide minerals (Kostka and Luther, 1995). Enrichment of W, Mo, and Fe in core TBW-9 indicates sulfidic sediments in Cocodrie salt marsh are a sink for W, Mo, and Fe.

Despite the generally recognized chemical similarities between W and Mo (e.g., Cotton et al., 1999), W exhibited an inverse correlation with Mo (r ~ -0.35) and had a low association with Mn (r ~ 0.2), suggesting differences between W and Mo sequestration in the northern Terrebonne Bay estuary. Previous investigations have related Mo to Mn cycling, including examination of pore waters associated with these

sediments (e.g., Adelson et al., 2001; Morford 2005, 2007; Kashiwabara et al., 2013; Mohajerin et al., in prep). Molybdenum displayed a strong, negative correlation with Mn ($r \sim -0.78$) for Al normalized values. These relationships suggest that Mo may be adsorbed or co-precipitated with Mn oxides at the sediment-water interface. Reduction of Mn oxides would then release Mo, which is consistent with the high dissolved pore water Mo concentrations near the sediment-water interface (Mohajerin et al., in prep). Release of Mo from dissolution of Fe/Mn oxides is likely followed by re-precipitation of Mo with sulfide minerals (e.g., Helz et al., 2004; Dahl et al., 2013), whereas Mn exhibited depletion in the sulfidic sediments of core TBW-9 (Table 4.2). Studies of Mn in sediments and pore waters have demonstrated that Mn is soluble under reducing conditions and solid-phase Mn typically shows a maximum near the sediment-water interface due to precipitation of Mn-oxides/oxyhydroxides (e.g., Froelich et al., 1979, Scholz and Neumann, 2007). Furthermore, studies have shown that solubilized Mn diffuses from sediments into the overlying water column (Thamdrup et al., 1994; Scholz and Neumann, 2007), which explains the Mn depletion observed in core TBW-9 (Table 4.2).

4.5.2 Degree of trace metal pyritization

Examining trace element partitioning between refractory pyrite and more labile Fe/Mn oxides/oxyhydroxides and iron monosulfides is useful for understanding trace element sequestration into sediments. The geochemical cycling of Fe is recognized as one of the dominant processes controlling diagenetic reactions in salt marsh sediments (Kostka and Luther, 1995). The DOP of sediments provides a measure of how much reactive Fe has re-precipitated as pyrite, and the DTMP provides an additional qualitative

measure of the affinity of other trace elements. The enrichment of W and Mo in ferromanganese crusts (Takematsu et al., 1990; Kuzendorf and Glasby, 1992; Kochinsky and Hein, 2003; Kashiwabara et al., 2013) suggests that Mn cycling may also affect W and Mo cycling in the environment. Furthermore, several studies have suggested Mo is influenced by Mn cycling such that Mo is adsorbed onto Mn oxides/oxyhydroxides and is released to solution during Mn reduction (e.g., Adelson et al., 2001; Morford et al., 2005, 2007). Under sulfidic conditions, Mo is re-mineralized into the pyrite fraction, whereas Mn only enters the pyrite fraction in sediments with ≥ 0.5 DOP either because Mn precipitation requires higher sulfide concentrations or because the high dissolved Mn/Fe ratio that occurs as Fe is precipitated out of solution favors Mn incorporation into the pyrite fraction (Huerta-Diaz and Morse, 1992).

Pore waters obtained from core TBW-1 showed mildly sulfidic (i.e., S(-II) $< 8 \, \mu M$) conditions that increased to almost $800 \, \mu M$ dissolved sulfide at a depth of ~ 6 cm (Table 4.2). The rise in dissolved sulfide from between $1 - 7 \, \mu M$ in the upper 3 cm near the sediment-water interface to $75 \, \mu M$ around 4 cm depth corresponds to decreases in W, Mo, Fe, and Mn in the reactive fraction (Fig. 4.3). The related rise in pyrite Fe and Mo suggests re-mineralization of reactive Fe minerals, such as iron monosulfides, to pyrite Fe along with Mo in core TBW-1, similar to previous studies (Huerta-Diaz and Morse, 1992). Furthermore, Fig. 4.5 illustrates a marked increase in DOP at ~ 4 cm also suggesting transfer of reactive Fe to pyrite Fe. However, Fig. 4.5d illustrates that reactive Fe was not quantitatively re-mineralized to pyrite Fe, but instead supports the notion that a portion of the reactive Fe was removed from the sediment. Reductive dissolutions and subsequent diffusion of Fe from the sediments into the water column is implied by the

depletion of total Fe from ~ 10 cm depth in core TBW-1, as discussed in section 4.5.1

(Fig. 4.6b; Table 2). Despite low DOP (~0.3) near the sediment-water interface, DTMP

for both W and Mo was > 0.85 similar to DTMP of Mo reported for sediments from the

Atchafalaya Bay, and sediments from Green Canyon, a hydrocarbon seep in the Gulf of

Mexico (Huerta-Diaz and Morse, 1992). Previous research has demonstrated the affinity

of W and Mo for Fe/Mn oxides/oxyhydroxides that occur at the sediment-water interface,

thus Fe/Mn oxides/oxyhydroxides are likely a source of W and Mo (e.g., Gustaffson,

2003; Adelson et al., 2001; Kashiwabara et al., 2013; Mohajerin et al., in prep). Because

W and Mo have higher degrees of pyritization than Fe, however, indicates that W and Mo

are derived from additional sources (e.g., organic matter or the water column) in addition

to Fe/Mn oxides/oxyhydroxides and Fe monosulfides that became re-mineralized with-in

the sediment core to pyrite (Canfield, 1989; Morse, 1994). The divergent behavior of Mn

DTMP compared to W and Mo DTMP, however, suggests that mineralization of Mn does

not sequester W or Mo in this estuary.

In contrast to W and Mo, the DTMP for Mn was below 0.03 throughout

core 1, indicating that solubilized Mn oxides/oxyhyroxides remained in the dissolved

form or were re-precipitated back to the reactive fraction in this core, similar to reports of

Mn in the Atchafalaya Bay sediments (Huerta-Diaz and Morse, 1992) and estuarine

sediments from San Simón Bay in Spain (Álvarez-Iglesias and Rubio., 2009). Morse and

Luther (1999) related the DTMP of several trace elements to thermodynamics that predict

the metal-sulfide solubility and the kinetics of water exchange. Reductive dissolution of

Mn oxides/oxyhydroxides predominantly occurs prior to sulfate reduction, which releases

dissolved sulfide, as well as the affinity of Mn for carbonates (part of the reactive

fraction) could explain the low DTMP observed for Mn in this core (Morse and Luther, 1999).

Core TBW-9, located in a salt marsh near Terrebonne Bay exhibited high DOP values even near the sediment-water interface (Fig. 4.5c). Dissolved sulfide concentrations for the pore waters associated with sediments from the sediment-water interface (0 - 2 cm) of core TBW-9 were 25 μM and reached a maximum of ~ 1600 μM S(-II) near 8 cm depth (Table 4.2). We suggest that the availability of sulfide in pore waters from core TBW-9 led to high DOP and DTMP for W and Mo both at depth and near the sediment-water interface (Fig. 4.5c). In contrast to core TBW-1, the DTMP for Mn was between 0.5 -0.7 for core TBW-9, similar to the high DTMP of Mn (up to 0.75) reported for anoxic, sulfidic sediments from the coastal lagoon Baffin Bay in Texas (Huerta-Diaz and Morse, 1992). The high DTMP for Mn in core TBW-9 may be due to adsorption of Mn to FeS phases that became pyritized (Morse and Luther, 1999). Recent studies have also emphasized the role of Mn(III) in the sub-oxic zone of sediments near the sediment-water interface. Specifically, Madison et al. (2013) proposed that Mn(III) complexation with organic and/or inorganic ligands stabilize it in solution, which may explain the similarity between the reactive and pyrite fractions of Mn for both cores from northern Terrebonne Bay estuary. Although the reactive phase of Mn in cores TBW-1 and TBW-9 was similar to Fe, the pyrite phase of Mn in both cores closely tracked the reactive phase of Mn (Fig 4.3c and 4.4c). In core TBW-1, Mn in both the reactive and pyrite fractions decreased with depth, whereas in core TBW-9, pyrite Mn increased with depth to 0.5-0.7 DTMP similar to previous reports from Baffin Bay (Huerta- Diaz and Morse, 1992). In core TBW-9, solubilized Mn(III) may be reduced and subsequently

incorporated into both the reactive fraction as a carbonate (e.g., rhodochrosite, $Mn(II)CO_3$) as well as into the pyrite fraction as Mn/Fe pore water ratios increase at ~ 5 cm depth due to Fe removal from the pore water as Fe sulfides precipitate (Mohajerin et al., in prep).

Reactive W, Mn, and Fe generally increased with depth in core TBW-9 (Fig. 4.4). The general increase of reactive Fe with depth in core TBW-9 could be due to the presence of buried plant material as well as active plant roots, which can release organic ligands that solubilize Fe and release oxidants (Hines et al., 1989). Data from northern Terrebonne Bay estuary supports such a model as illustrated in Fig. 4.2e, where the increase of the reactive Fe corresponds to a decrease in the pyrite Fe. It should be noted that pyrite mineral grains may not be controlling sequestration of Mo into the pyrite fraction, as suggested by laboratory experiments (Bostick et al., 2003). Recent studies using laser ablation-inductively coupled plasma-mass spectrometry (LA-ICPMS) have detected that the majority of Mo in sulfidic sedimentary rocks is associated with the pyrite matrix, but post-lithification re-distribution of Mo may have contributed to this finding (Chappaz et al., 2014). Using LA-ICPMS on sedimentary pyrite, Large et al. (2014) have also shown Mo is included in both the pyrite structure as well as in the matrix, whereas W is predominantly in the pyrite matrix material. The almost identical pattern of W and Mo in the pyrite fraction of core 9 from northern Terrebonne Bay estuary suggests that mechanisms controlling Mo sequestration, such as precipitation via a polysulfide or organic matter pathway are likely the same for W (e.g., Vorlicek et al., 2004; Chappaz et al., 2014).

4.6 Conclusions

Results from total digestions and calculation of the DTMP of W and Mo in northern Terrebonne Bay estuarine sediments demonstrate both similarities and differences between W and Mo. Total W sediment contents are controlled primarily by terrestrial input and Fe redox cycling, whereas total Mo content is likely related to Mn cycling in these coastal marsh sediments. To explain the observed enrichment and depletion of W and Fe in intermediate marsh sediments collected at different times, we propose a model in which W is coupled to Fe redox cycling. We predict that measured enrichments of W and Fe in sediments underlying fresh waters collected in August are concentrated in the reactive fraction. We propose depletion of W and Fe in intermediate marsh sediments underlying brackish (i.e., S >1 ‰) surface waters is caused by reductive dissolution of Fe oxides/oxyhydroxides that releases Fe and W into solution. Although a portion of W and Fe are re-precipitated into the pyrite fraction, some W and Fe escapes to overlying waters and is transported laterally towards the coast. In the nearly permanently sulfidic Cocodrie salt marsh sediments, W, Fe, and Mo are sequestered causing enrichment of these elements compared to the UCC. Furthermore, the observation of W and Mo enrichment in 6 out of 7 of the measured sediment aliquots suggest northern Terrebonne Bay estuary is a likely sink for both elements.

Despite differences in total enrichment, DTMP for W and Mo was > 0.85 for both cores. These results indicate W has a high affinity for pyrite similar to other trace metals including Mo, As, and Hg that show high DTMP even at low DOP levels (Huerta-Diaz and Morse, 1992) and imply that W and Mo are likely derived from sources such as organic matter and possibly the water column in addition to reactive Fe minerals. Furthermore, the low DTMP measured for Mn in core TBW-1 demonstrates that re-

mineralization of Mn into minerals associated with the reactive fraction, does not sequester W and Mo. Finally, nearly identical patterns of W and Mo in the pyrite fraction of core 9 suggest that W and Mo are sequestered into the pyrite fraction by similar mechanisms.

Acknowledgements

CHAPTER 5: CONCLUSIONS

This work has broadened our understanding of W geochemistry especially in sulfidic environments, and deepened our knowledge of mechanisms that control dissolved W and Mo concentrations in natural waters. First, measured stability constants of the four thiotungstate anions are approximately two orders of magnitude lower than analogous thiomolybdate stability constants. Analysis of W and Mo in estuarine surface and pore waters demonstrated that W is enriched in pore waters, whereas Mo is depleted in pore waters compared to overlying brackish (i.e., 1 – 22 ‰) surface waters. Finally, based on data from sediment digestions, we propose a model describing the seasonal cycling of W in northern Terrebonne Bay estuary.

Laboratory investigations demonstrate that thiotungstates require ~ 40-fold higher sulfide concentrations and form at slower rates than thiomolybdates under similar conditions (Erickson and Helz, 2000; Mohajerin et al., 2014b). Therefore, thiomolybdates are predicted to occur over a broader range of environmental conditions compared to thiotungstates. Natural waters with sufficient dissolved sulfide concentrations conducive to thiotungstate formation can occur in pore waters where sulfate reduction produces mM concentrations of dissolved sulfide. Estuarine sediments with high organic matter content and variable sulfate concentrations exhibit pore waters with a range of dissolved sulfide concentrations over relatively short distances.

Analysis of W, Mo, Fe, and Mn in northern Terrebonne Bay estuary captured oxic surface waters with salinity < 1 ‰ up to ~ 22 ‰ in Terrebonne Bay near the Gulf of

Mexico. In surface waters from this shallow, wind-driven estuary, dissolved Mo concentrations displayed a linear relationship with relationship to salinity indicative of conservative mixing. In contrast, W exhibited a reactive path that exhibited a positive and statistically significant correlation with dissolved Fe (r = 0.47, p < 0.05). Furthermore, analysis of pore waters also demonstrate differences between W and Mo geochemistry. For all samples analyzed, compared to overlying surface waters W was enriched in pore waters. In contrast, Mo was enriched in pore waters underlying fresh waters that had pH ~ 7.8 and dissolved sulfide concentrations ~ 2.5 μM, but was depleted in sulfidic pore waters underlying brackish (1 – 22 ‰) surface waters. Furthermore, unlike Mo concentrations that decreased to low, stable concentrations in pore waters with S (-II) > 200 μM, dissolved W generally increased with increasing dissolved sulfide concentrations for pore waters with pH ≤ 7.5. Hence, our data suggest thiotungstates are more soluble compared to tungstate. In addition, the association of W and Fe along with the elevated concentrations of W in pore waters compared to surface waters indicates that Fe may act as a particulate shuttle such that W is adsorbed to Fe oxides/oxyhydroxides in the water column that are then deposited in the sediments. Sequestration of W in sediments underlying fresh waters was confirmed using sediment digestions.

Finally, using data from sediment digestions we propose mechanisms to explain modes of W sequestration and mobilization in northern Terrebonne Bay estuary. Our data support a model in which W is controlled by Fe redox cycling. We suggest that W is scavenged from surface waters onto colloidal or suspended particulate matter and is subsequently sequestered in Fe/Mn oxides/oxyhydroxides in estuarine sediments explaining the observed enrichment of W, Fe, and Mn, compared to concentrations in the upper continental crust (UCC) in sediments underlying fresh surface waters. During periods of salt water intrusion, associated with passing cold fronts in northern Terrebonne Bay estuary, W is released from Fe/Mn minerals when dissolved sulfide concentrations rise causing reductive dissolution of oxide minerals and allowing W and Fe release into surface waters as well as re-mineralization of Fe and W in sulfidic sediments. The loss of W and Fe to surface waters is implied by the depletion of W and Fe observed in sediments from the intermediate region of the marsh collected when overlying surface waters were brackish (> 1 ‰). Furthermore, we attribute the enrichment of W and Fe in coastal salt marsh sediments to lateral transport of W and Fe in the overlying waters. Unlike intermediate marsh sediments, Cocodrie salt marsh sediments likely exhibit permanently sulfidic conditions. Observed W enrichment in the salt marsh sediments demonstrate that although W may become more soluble as dissolved sulfide concentrations increase, W is trapped to some degree in sulfidic sediments, similar to arsenic (Lee et al., 2005; Helz et al., 2011; Mamindy-Pajany, 2013; Neumann et al., 2013).

Table 5.1: W/Mo molar ratios reported in this study

Sample type	W/Mo molar ratio
Surface water average	0.005
Pore water average	0.42
Reactive fraction average	0.07
Pyrite fraction average	0.03
Total sediment content average	0.34

The work in this manuscript also broadens our knowledge of mechanisms leading to W concentrations ~ 1800 fold less than Mo in oxic oceans, despite their similar molar concentrations in the UCC. Table 5.1 summarizes the W/Mo molar ratios observed in this study. The higher affinity of W for Fe/Mn oxides/oxyhydroxides has been demonstrated in laboratory experiments and reports on naturally occurring ferromanganese crusts in oxic oceans indicate W is sequestered to a greater extent than Mo (Takematsu et al., 1990; Gustaffson, 2003; Kashiwabara et al., 2013). Our data also demonstrate that sediments underlying fresh waters are enriched in W, Fe, and Mn, whereas Mo is slightly depleted in comparison to the UCC. Thus, in northern Terrebonne Bay estuary, W is sequestered in sediments underlying fresh waters, unlike Mo, but both W and Mo are trapped in permanently sulfidic sediments near the coast.

Observations in Chapter 3 suggest higher W solubility in sulfidic waters, whereas Chapter 4 demonstrates W is sequestered in permanently sulfidic sediments. To reconcile these observations we suggest a mechanism of ligand induced reduction of W by polysulfide in pyrite that leads to the incorporation of W into the pyrite phase, similar to

the mechanism proposed for Mo capture by pyrite. The mechanism of polysulfide

reduction requires a thiometallate precursor (Vorlicek et al., 2004). As we have

demonstrated in this work, thiotungstates are less likely to form compared to

thiomolydates in the pore waters studied (Erickson and Helz, 2000; Mohajerin et al.,

2014a), which could explain the greater Mo concentration in the pyrite phase compared

to W in the pyrite phase.

Appendix A: Characterization of thiotungstate salts

The electronic spectra of thiotungstates and thiomolybdates was initially characterized by Müller et al. (1969). For example, Müller et al. (1969) show the differences in the peak wavelengths of all four analogous thiotungstate and thiomolybdate anions (e.g. $\lambda_{max}MoO_3S^{2-}$ - $\lambda_{max}WO_3S^{2-}$) is nearly 200 nm. The consistency of the wavelength difference for analogous thioanions indicates the spectra are influenced by the difference in electronegativities between Mo and W. The peak wavelengths of thiotungstate and thiomolybdate thioanions have since been confirmed in subsequent publications (e.g. Tsigdinos, 1978; McDonald et al., 1983; Basu et al., 2009). Although the thioutungstate salts were analyzed in conjuction with associated cations (i.e. $(Et_4N)_2$, K_2, and $(NH_4)_2$), the absorbance of the associated cations occurs at wavelengths less than 240 nm and did not interfere with the previously described absorbance of the associated thiotungstates (Table 2; Müller et al., 1969; Tsigdinos, 1978; McDonald et al., 1983; Basu et al., 2009).

Figures show XRD pattern of synthesized salt as well as the peak positions for the salt found in the ICDD database. Note that the ICDD database measurements do not provide measurements at the higher 2-Theta values.
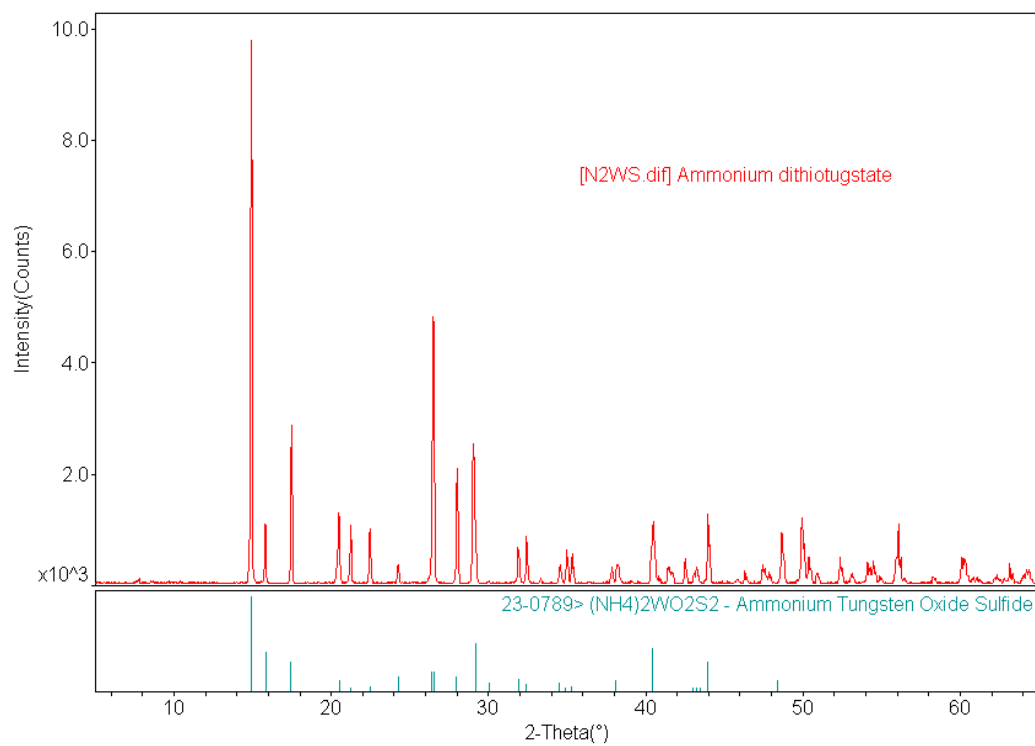
Figure A.1: XRD pattern of the prepared $(NH_4)_2WO_2S_2$ salt. Bottom pattern indicates peak positions found in the ICDD, 2003 database of the pure material
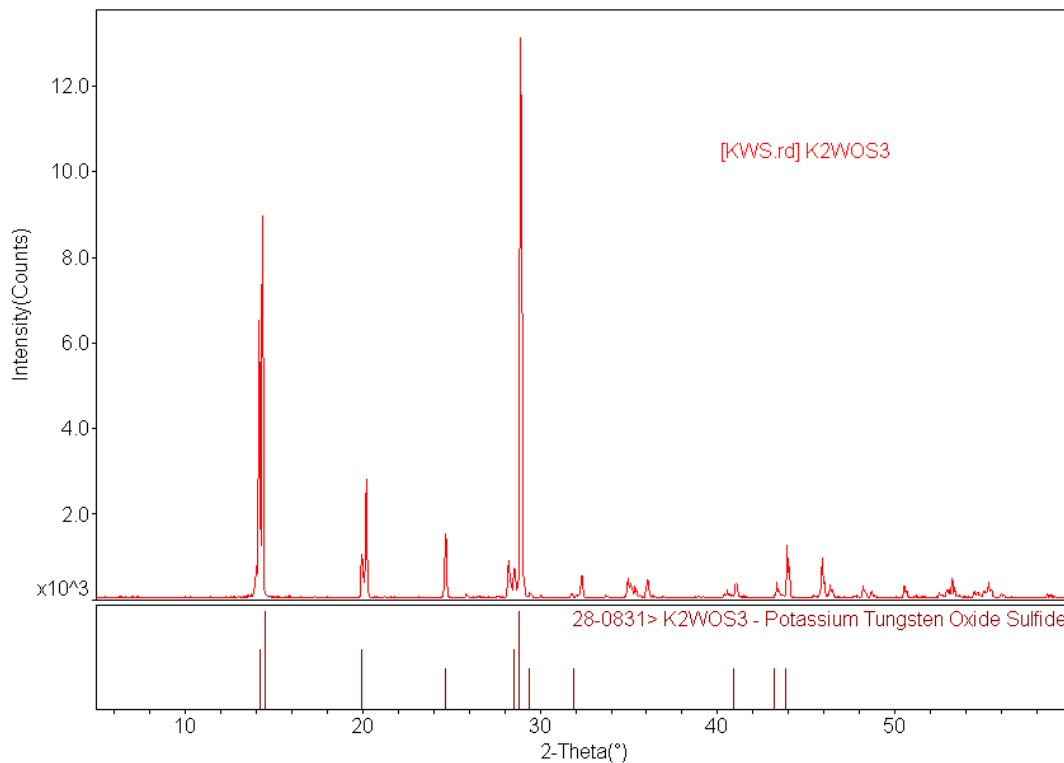
Figure A.2: XRD pattern of the prepared K_2WOS_3 salt. Bottom pattern indicates peak positions found in the ICDD, 2003 database of the pure material
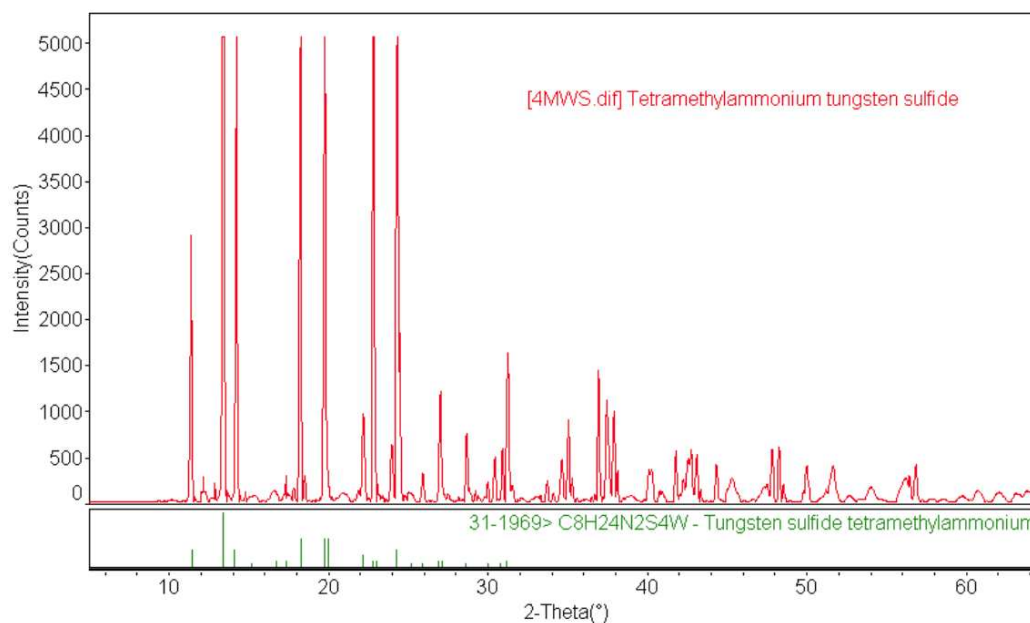
Figure A.3: XRD pattern of the prepared $[Et_4N]_2[WS_4]$ salt. Bottom pattern indicates peak positions found in the ICDD, 2003 database of the pure material

Appendix B: Determination of molar absorption coefficients

Thiotungstate standards were made using measured weights of the pure, synthesized

individual thiotungstate salts and known volumes and serial dilutions were made using

Milli-Q water.

Table B.1: Concentrations (nM) used to determine molar absorption coefficients

$[NH_4]_2[WO_2S_2]$	$K_2[WOS_3]$	$[Et_4N]_2[WS_4]$
221.5	149.6	107.7
191.8	116.5	77.5
178.3	101.2	56.9
119.1	70.2	30.0
72.5	47.0	17.4
50.5	32.1	7.4
24.2	20.7	4.0
11.1		1.5
4.6		

Because monothiotungstate salt could not be synthesized, we were only able to use a

narrow range of WO_3S^{2-} (~ 90 nM) concentrations. To determine the monothiotungstate

concentration, we followed the approach of Aymonino et al. (1969a,b), who argued for

the existence of monothiotungstate. We observed that spectrophotometric scans displayed

an isosbestic point between WO_3S^{2-} and dithiotungstate ($WO_2S_2^{2-}$) at ~255 nm. Thus, ε

must be identical for both species at this wavelength. Using scans from solutions C1 and C2 (Table 1) taken shortly after mixing tungstate and hydrogen sulfide, and before the formation of dithiotungstate, wavelengths between 254 nm to 260 nm were used to calculate the concentration of monothiotungstate using the absorption coefficient of dithiotungstate. To mitigate the interference with sulfide at these wavelengths, absorbance of sulfide for each experimental solution was recorded before tungstate was injected, and then the response was subtracted from the scans used to determine the monothiotungstate concentration. For wavelengths near the isosbestic point (ie. 250 -260 nm), the absorbance of the sulfide was at least 10 times less than the absorbance after tungstate was injected. The standard deviation (σ) of the average concentration of monothiotungstate for a given scan was less than 10% using wavelengths 254 – 260 nm.

Appendix C: Determining the order of thiotungstate reaction

For each thiotungstate equilibrium reaction we made a plot of $y = \ln(C_{eq} - C_t)$, where C_{eq} is the equilibrium concentration for the thiotungstate and C_t is the concentration of that thiotungstate at a given time, versus time on the x-axis. The linearity of these plots (i.e. $R^2 \geq 0.97$) indicates these reactions are first order with respect to W and H_2S_{aq}. Below is an example of the plots.
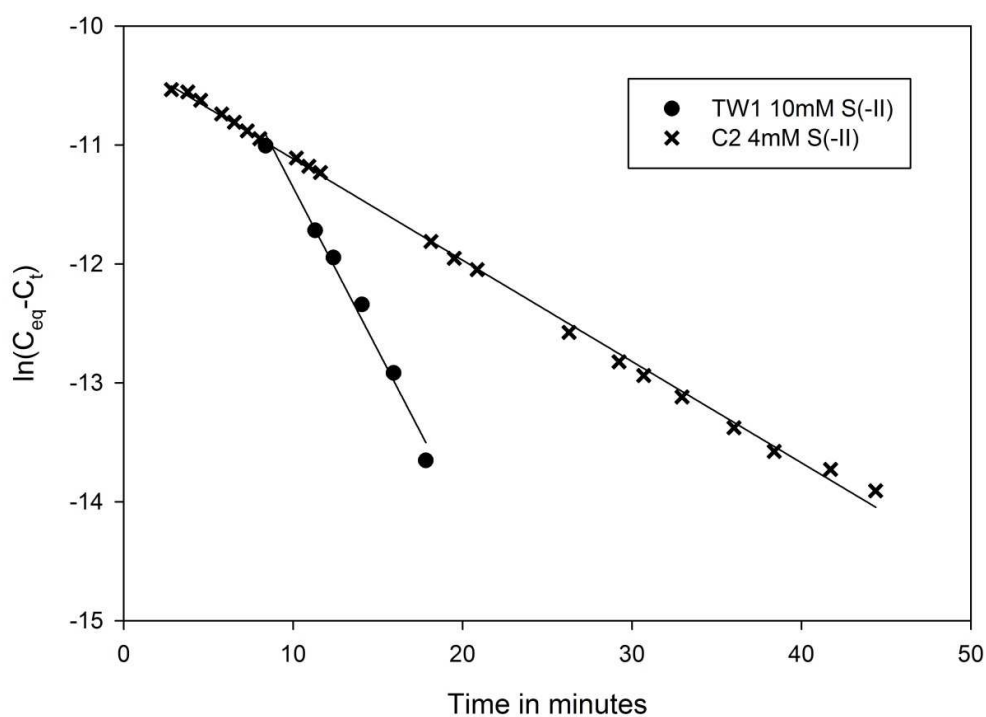
Figure C.1 Formation of dithiotungstate ($WO_2S_2^{2-}$) in two solutions TW1 ($R^2=0.98$) and C2 ($R^2 > 0.99$; Table 1), both with 0.1 mM W and different amounts of sulfide.

Appendix D: Methods and results of isotope dilution measurements of August 8, 2013 water samples

Methods: Certified isotope enrichments [183]W and [97]Mo were purchased from Isoflex isotopes in San Francisco, CA. Briefly, powdered tungsten oxide, enriched with 78% [183]W, was dissolved in ultrapure ammonium hydroxide then diluted with Milli-Q water to 13% w/w. The concentration of the enriched isotope solution was determined in triplicate using 1 ppb W prepared from a certified standard (CertiPrep) and checked using a 100 ppt standard solution for W for quality assurance. Diluted pore water (20 fold dilution) and surface samples (10 fold dilution) were then spiked with an appropriate amount of isotope enriched solution in order to obtain isotope ratios of [182]W /[183]W close to the geometric mean of the natural and enriched isotope ratios. Isotope ratios were then measured by ICP-MS and employed to calculate W concentrations in surface and pore waters for elemental IDMS (equation 2.7, Alonso and Rodríguez-González, 2013). Measurement of W by ICP-MS was optimized by rinsing with ultrapure ammonium and nitric acid after some samples to avoid carryover of W in the ICP-MS (Clausen et al., 2010). Several surface samples (i.e. TWB-6, 7, and 8) had high uncertainty for W; hence, they were also measured using standard additions. Isotope dilution mass spectrometry was also used to determine Mo concentrations in separate sample aliquots using the above methods, except the molybdenum oxide enriched Mo-97 (96.6%) in was dissolved in 10% w/w ultra-pure nitric acid to make the enriched isotope solution (Alonso and Rodríguez-González, 2013). After determining the Mo concentration of the enriched standard using a 1 ppb Mo certified standard (Peak Performance), Mo was measured in SLRS-4 and SLEW-3

reference materials using IDMS to check for accuracy. Certified values are in

parenthesis.

Table D.1 August surface water IDMS results

Sample	Mo nmol/kg	W nmol/kg
TBW-1	8 ± 2	0.12 ± 0.02
TBW-2	10 ± 3	0.13 ± 0.04
TBW-3	12 ± 2	0.11 ± 0.05
TBW-4	14 ± 3	0.20 ± 0.06
TBW-5	25 ± 8	0.12 ± 0.05
TBW-6	35 ± 5	0.60 ± 0.05
TBW-7	58 ± 9	0.15 ± 0.02
TBW-8	61 ± 9	0.33 ± 0.08
TBW-9	26 ± 5	0.12 ± 0.05
TBW-10	25 ± 3	0.12 ± 0.06
SLEW-3	57 ± 17 (53.15)	0.27 ± 0.05
SLRS-4	2.25 ± 0.0 (2.29)	0.14 ± 0.02

Certified values are in parentheses.

Table D.2: August pore water IDMS results

Core sample	Depth cm	Mo nmol/kg	W nmol/kg
TBW-1	9.8	30 ± 10	26 ± 3
TBW-4	5.2	33 ± 3	22 ± 2
TBW-4	11.3	45 ± 6	13 ± 1
TBW-5	5.5	1.0 ± 0.2	0.3 ± 0.1
TBW-5	6.5	1.2 ± 0.3	0.9 ± 0.2
TBW-5	7.5	0.9 ± 0.2	0.8 ± 0.2
TBW-5	9.8	0.5 ± 0.1	0.8 ± 0.2
TBW-5	12.0	0.9 ± 0.4	1.3 ± 0.3
TBW-5	13.0	0.6 ± 0.1	1.5 ± 0.2
TBW-5	14.0	1.2 ± 0.6	0.9 ± 0.2
TBW-7	4.7	2.0 ± 0.4	1.5 ± 0.3
TBW-7	6.0	1.32 ± 0.3	2.1 ± 0.2
TBW-7	7.5	1.9 ± 0.3	1.7 ± 0.3
TBW-7	9.3	1.9 ± 0.3	1.7 ± 0.3
TBW-9	2.2	< 0.5	0.9 ± 0.10 (0.9)
TBW-9	3.4	6.4 ± 0.6	1.8 ± 0.2 (2.1)
TBW-9	4.5	6.3 ± 0.9	2.3 ± 0.4 (2.4)

TBW-9 samples were also measured using standard additions yielding the values in parentheses

The following Figures illustrate differences between measurements using dilution and isotope dilution for Mo and W August water samples. The axes are adjusted to illustrate how analytical variation changes with concentration.

Interference of Mn55Ar40 was likely present in measuring Mo95 in diluted pore water samples in August accounting for the elevated concentrations.

W in August
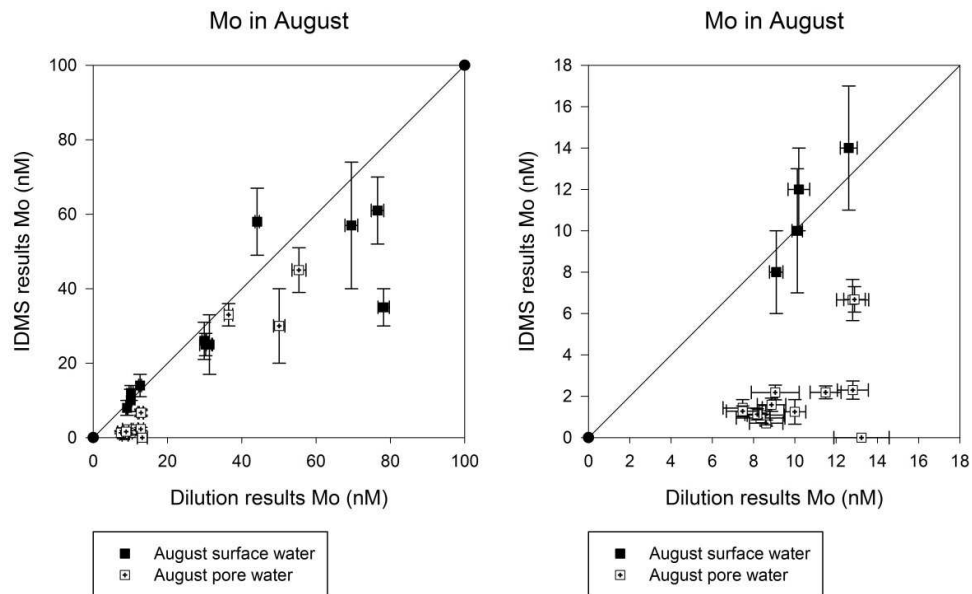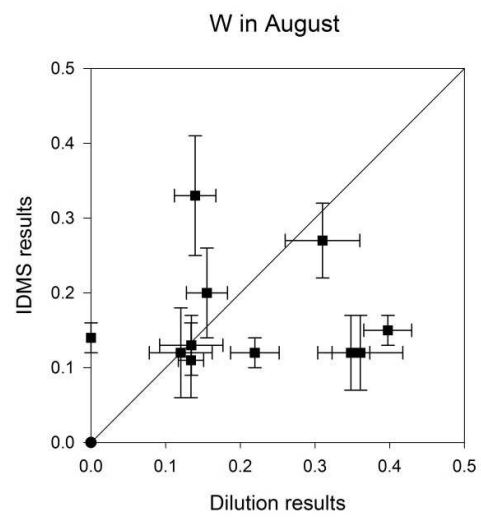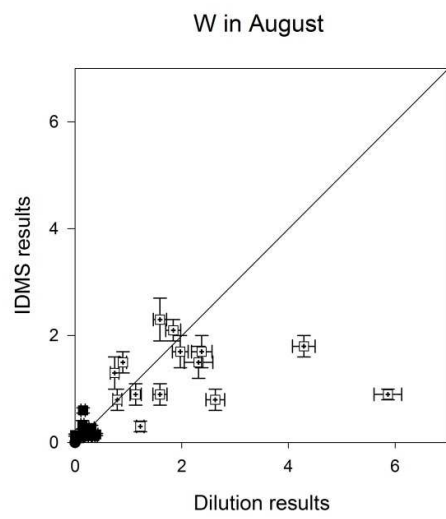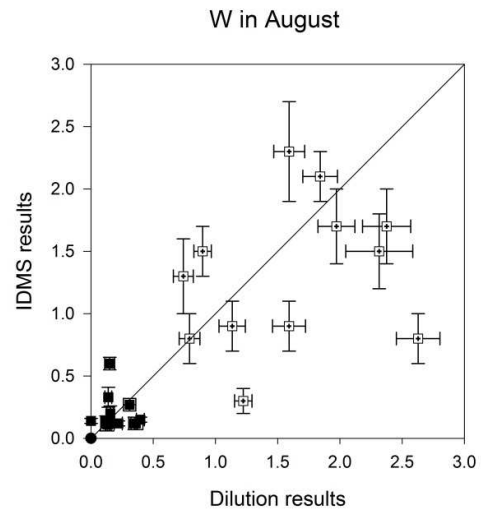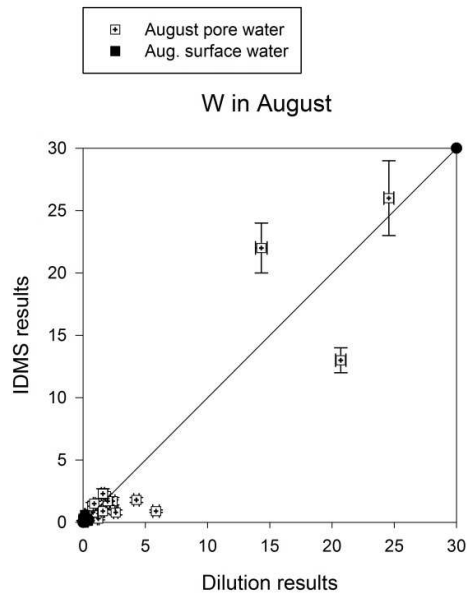
Appendix E: Dilution vs. Standard additions for April 2014 water samples

Comparison of measurements using diluted samples calibrated with a standard curve

and standard additions using a one addition. Most values are similar and patterns and

trends remain relatively stable. The use of a standard curve using 5 – 7 known

standards and internal standards to mitigate instrument drift, I have more confidence

in the dilution data. Furthermore, diluted measurements had less analytical uncertainty

and were more accurate as demonstrated by measurement of SLEW-3.

Fe standard addition

Fe Dilution

Mn standard addition

Mn dilution

Using Dilution concentrations

Mn and Fe

Core 9 A

Mo and W

Using Standard additionconcentrations

Mn and Fe

Core 9 A

W and Mo
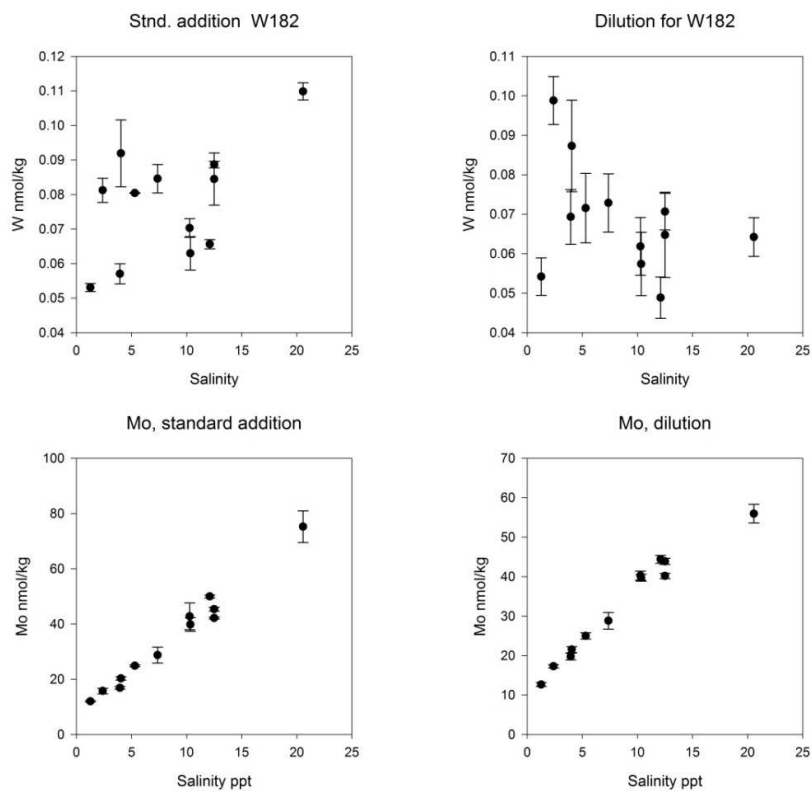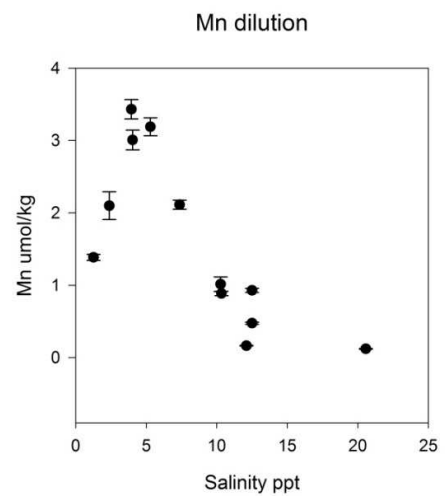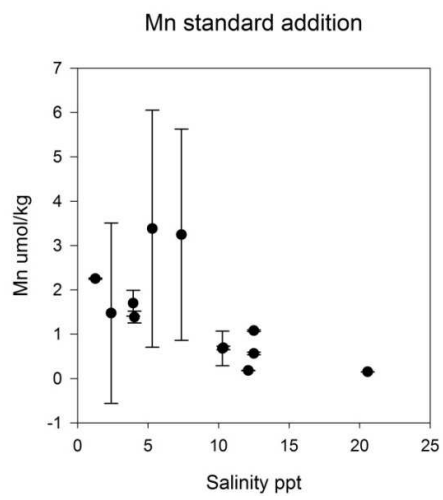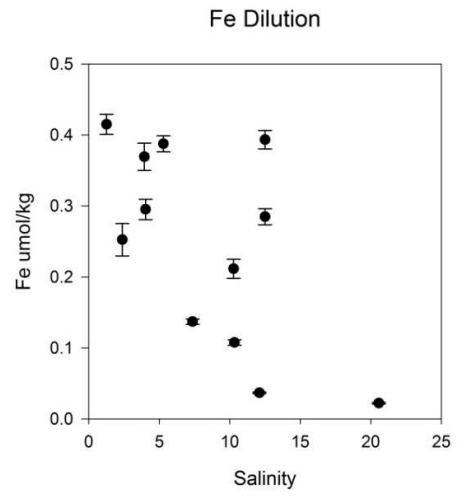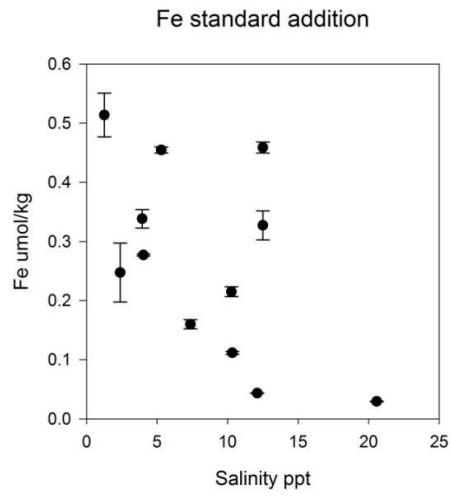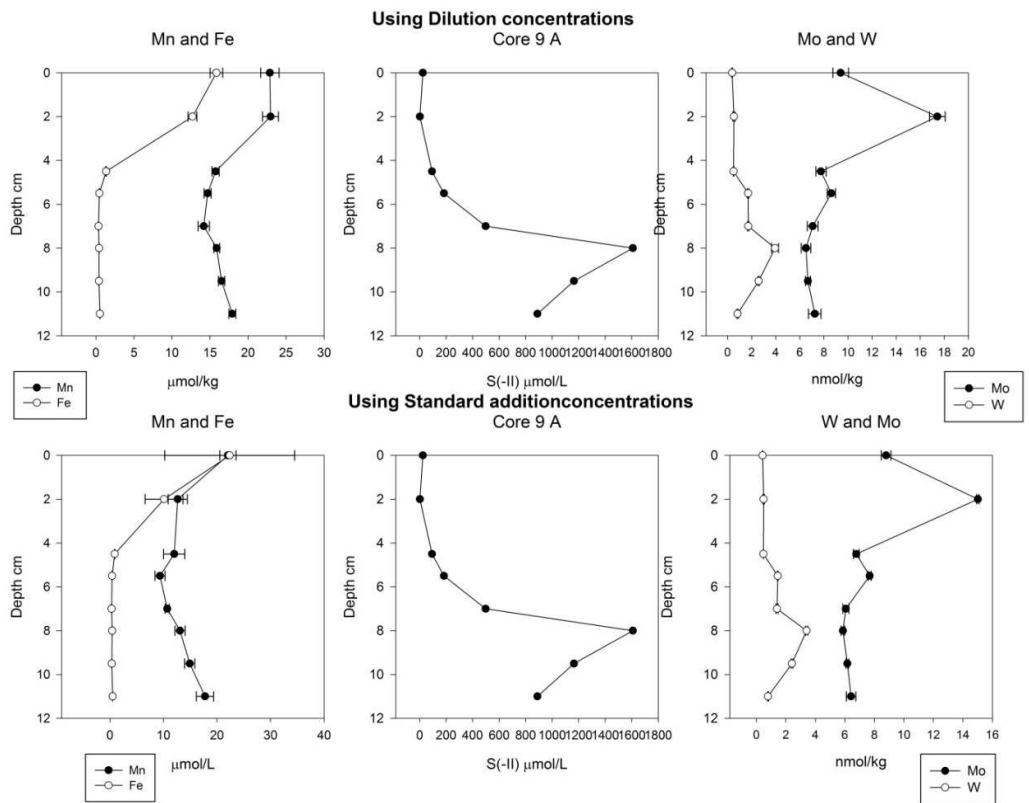
Appendix F

Appendix F: April 30, 2014 Vertical Profiles

	TBW-1	TBW-1	TBW-1	TBW-3	TBW-3	TBW-3	TBW-3
Depth m	Temperature	Salinity per m	Dissolved O2	Temperature	Salinity per m	pH	Dissolved O2 %
0.25	24.4	1.27	99.8	24.4	5.3	7.32	81.2
0.5	24.3	1.27	87	24.4	5.29	7.28	78.5
0.75				24.4	5.27	7.27	77
1				24.4	5.24	7.28	76.8
1.25				24.4	5.25	7.25	76.6
1.5				24.4	5.25	7.25	76.3
1.75				24.4	5.24	7.24	78.1

	TBW-4	TBW-4	TBW-4	TBW-5	TBW-5	TBW-5
Depth m	Temperature	Salinity per m	Dissolved O2	Temperature	Salinity per m	Dissolved O2 %
0.25	25.7	7.37	78.2	27.7	11	95.5
0.5	25.6	7.32	77.6	27.3	11.04	94.8
1	25.6	7.35	78.5			
1.25	25.6	7.35	76.4			

	TBW-6	TBW-6	TBW-6	TBW-7	TBW-7	TBW-7
Depth m	Temperature	Salinity per m	Dissolved O2	Temperature	Salinity per m	Dissolved O2 %
0.25	27.4	12.5	98.8	26.8	12.1	121.2
0.5	27.2	12.54	94	26.6	12.09	112.1
0.75				26.6	12.09	114.2
1	27	12.63	94.2			

	TBW-8	TBW-8	TBW-8	TBW-9	TBW-9	TBW-9
Depth m	Temperature	Salinity per m	Dissolved O2	Temperature	Salinity per m	Dissolved O2 %
0.25	26.4	20.57	127.4	28.6	10.28	80.8
0.5	26.4	21	126.5			

	TBW-10	TBW-10	TBW-10	TBW-11	TBW-11	TBW-11
Depth m	Temperature	Salinity per m	Dissolved O2	Temperature	Salinity per m	Dissolved O2 %
0.25	26.7	10.34	81	24.8	3.95	75.3
0.5	26.7	10.33	82.4	24.7	3.87	70.5
1	26.7	10.34	83.4	24.8	3.97	70.7
1.5	26.7	10.34	82.1	24.8	3.99	70.5
2	26.7	10.35	83.3	24.8	4.23	66.7
2.5				24.6	4.65	63.5

	TBW-12	TBW-12	TBW-12	TBW-13	TBW-13	TBW-13
Depth m	Temperature	Salinity per m	Dissolved O2	Temperature	Salinity per m	Dissolved O2 %
0.25	25.1	2.39	80.9	24.6	4.04	71.21
0.5	25.1	2.53	81.9	25	4.04	71
1				24.6	4.07	70
1.5				25.1	3.89	76.6
2				25	4.08	75
2.75				24.7	4.13	70.3

Appendix G: Trace elements in sediment fractions
W/Fe x 10^6 and Mo/Fe x 10^6 as well as W/Mo molar ratios in the reactive and pyrite fractions, and concentration of trace elements (nmol or µmol/gram dry weight sediment) in reactive and pyrite fractions.

Reactive M/Fe molar ratios

Core	Depth cm	W182/Fe	W184/Fe	Mo97/Fe	Mo100/Fe	W ave of W184 and W182 / Mo ave of Mo97 and Mo100 Wave/Moave
1	0 - 3	0.27	0.20	1.94	2.15	0.11
1	0 - 3	0.25	0.18	2.31	2.49	0.09
1	3 - 4.5	0.63	0.47	3.77	5.98	0.11
1	4.5 - 5.5	1.55	1.03	9.80	17.53	0.09
1	5.5 - 7.6	0.95	0.63	6.35	10.15	0.10
1	7.6 - 11	0.92	0.62	6.16	10.47	0.09
9	0 - 2	0.61	0.50	12.30	11.80	0.05
9	2 - 4.5	0.53	0.39	12.69	12.49	0.04
9	4.5 - 5.5	0.61	0.43	13.45	13.03	0.04
9	5.5 - 7	0.54	0.40	11.72	11.40	0.04
9	7 - 8	0.55	0.42	10.81	10.47	0.05
9first	8 - 9.5	0.56	0.41	9.87	9.57	0.05
9OUP	8 - 9.5	0.59	0.43	11.62	11.46	0.04
9TRIP	8 - 9.5	0.77	0.63	10.45	10.13	0.07
9	9.5 - 11	0.61	0.43	9.22	8.87	0.06
9	11 - 11.5	0.67	0.49	9.57	9.49	0.05

Pyrite M/Fe molar ratios

Core	Depth cm	W182/Fe	W184/Fe	Mo97/Fe	Mo100/Fe	W ave of W184 and W182 / Mo ave of Mo97 and Mo100 Wave/Moave
1	0 - 3	2.4	2.4	53.4	52.8	0.05
1	0 - 3	3.5	3.5	69.5	68.9	0.05
1	3 - 4.5	3.5	3.5	184.7	178.7	0.02
1	4.5 - 5.5	2.2	2.2	157.4	155.0	0.01
1	5.5 - 7.6	1.7	1.8	131.9	132.8	0.01
1	7.6 - 11	2.5	2.5	132.4	132.1	0.02
9	0 - 2	0.5	0.5	19.5	19.5	0.03
9	2 - 4.5	1.0	1.0	33.6	34.2	0.03
9	4.5 - 5.5	0.8	0.8	23.2	23.0	0.03
9	5.5 - 7	0.9	0.9	27.7	27.4	0.03
9	7 - 8	0.8	0.8	24.6	24.9	0.03
9first	8 - 9.5	0.9	1.0	28.8	29.1	0.03
9OUP	8 - 9.5	0.8	0.8	27.3	27.0	0.03
9TRIP	8 - 9.5	0.7	0.7	26.0	25.5	0.03
9	9.5 - 11	0.9	0.9	27.2	27.0	0.03
9	11 - 11.5	0.9	0.9	26.7	26.4	0.04

Reactive — All values given per gram dry sediment

Core	Depth cm	Midpoint depth	g wt. of sed	W182 nmol/g	error W182	W184 nmol/g	error W18, Mo97	Mo97 nmol/g	error Mo97, Mo100	Mo100 nmol/g	error Mo100, Mn	Mn umol/g	Mn error	Fe umol/g	Fe error
1	0 - 3	1.5	2.006	0.015	0.001	0.011	0.001	0.108	0.004	0.12	0.006	9.49	0.08	55.7	0.5
1	0 - 3	1.5	1.996	0.017	0.001	0.012	0.001	0.155	0.01	0.167	0.005	11.6	0.1	67.0	0.6
1	3 - 4.5	3.75	1.954	0.004		0.003		0.024	0.002	0.038	0.002	4.06	0.05	6.4	0.1
1	4.5 - 5.5	5	2.012	0.003		0.002		0.019	0.001	0.034	0.001	4.00	0.04	1.94	0.02
1	5.5 - 7.6	6.55	1.952	0.003		0.002		0.02	0.001	0.032	0.002	3.84	0.04	3.15	0.07
1	7.6 - 11	9.3	2.002	0.003		0.002		0.02	0.001	0.034	0.001	3.54	0.06	3.25	0.04
9	0 - 2	1	2.006	0.022	0.001	0.018	0.001	0.45	0.01	0.43	0.01	1.27	0.01	36.2	0.5
9	2 - 4.5	3.2	2.022	0.019	0	0.014	0.001	0.45	0.01	0.45	0.01	1.28	0.01	35.7	0.3
9	4.5 - 5.5	5	1.99	0.02	0.001	0.014	0.001	0.44	0.01	0.43	0.01	1.16	0.01	32.9	0.3
9	5.5 - 7	6.25	2.006	0.02	0.001	0.015	0.001	0.41	0.01	0.40	0.02	1.38	0.007	37.3	0.8
9	7 - 8	7.50	2.029	0.021	0.001	0.016	0.001	0.39	0.01	0.38	0.01	1.45	0.02	39.4	0.9
9first	8 - 9.5	8.75	2.041	0.022	0.001	0.016	0.001	0.38	0.01	0.37	0.01	1.19	0.02	32.3	0.3
9OUP	8 - 9.5	8.75	2.037	0.019	0.001	0.014	0.001	0.40	0.01	0.38	0.01	1.35	0.03	37.8	1.0
9TRIP	8 - 9.5	8.75	1.998	0.029	0.001	0.024	0.001	0.40	0.01	0.38	0.01	1.49	0.03	39.5	0.5
9	9.5 - 11	10.25	2.036	0.024	0.001	0.017	0	0.37	0.01	0.35	0.01	1.60	0.03	40.5	0.5
9	11 - 11.5	11.25	1.952	0.027	0.001	0.02	0.001	0.39	0.01	0.38	0.01				
9A3 ave			2.03	0.02		0.02		0.39		0.38		1.3		36		
9A3 stdev			0.02	0.01		0.01		0.01		0.01		0.1		3		
%stdev			1.17	22.10		28.08		2.58		1.62		9.0		8		

Appendix G (cont.)

All values given per gram dry sediment

sample	Depth cm	nmol/g in pyrite fraction W182	error W182	nmol/g in pyrite fraction W184	error W184	nmol/g in pyrite fraction Mo97	error Mo97	nmol/g in pyrite fraction Mo100	error Mo100	umol/g in pyrite fraction Mn	Mn error	umol/g in pyrite fraction Fe	Fe error
1A15	0 - 3	0.074	0.003	0.073	0.003	1.62	0.06	1.599	0.07	0.194	0.002	30.3	0.2
1A14	0 - 3	0.093	0.004	0.093	0.005	1.87	0.06	1.85	0.07	0.184	0.002	26.9	0.1
1A13	3 - 4.5	0.128	0.006	0.128	0.005	6.8	0.2	6.6	0.2	0.108	0.001	37.0	0.5
1A12	4.5 - 5.5	0.09	0.003	0.089	0.004	6.3	0.2	6.2	0.2	0.055	0.000	40.2	0.7
1A10	5.5 - 7.6	0.084	0.004	0.085	0.003	5.4	0.2	6.4	0.2	0.042	0.000	48.4	0.6
1A11	7.6 - 11	0.118	0.005	0.118	0.006	6.3	0.2	6.3	0.2	0.040	0.000	47.7	0.7
9A7	0 - 2	0.115	0.004	0.116	0.004	4.3	0.1	4.3	0.2	1.21	0.01	219	4
9A8	2 - 4.5	0.223	0.007	0.225	0.008	7.4	0.2	7.6	0.2	1.320	0.007	221	1
9A6	4.5 - 5.5	0.156	0.006	0.157	0.005	4.7	0.1	4.6	0.1	1.70	0.02	202	4
9A5	5.5 - 7	0.205	0.009	0.206	0.007	5.4	0.2	6.3	0.3	2.42	0.01	232	5
9A4	7 - 8	0.138	0.005	0.141	0.005	4.5	0.1	4.6	0.1	2.43	0.01	184	1
9A3	8 - 9.5	0.159	0.005	0.161	0.005	4.8	0.1	4.9	0.1	2.51	0.03	169	2
9A3DUP	8 - 9.5	0.15	0.007	0.151	0.006	4.9	0.2	4.9	0.2	2.80	0.02	181	4
9A3TRIP	8 - 9.5	0.13	0.006	0.128	0.005	4.9	0.2	4.8	0.2	2.85	0.02	189	2
9A2	9.5 - 11	0.138	0.006	0.139	0.006	4.3	0.2	4.3	0.2	2.63	0.04	159	2
9A1	11 - 11.5	0.16	0.005	0.157	0.005	4.5	0.2	4.5	0.1	2.82	0.02	170	2
9A3 ave		0.15		0.15		4.90		4.88		2.2		206	
9A3 stdev		0.02		0.02		0.05		0.05		0.4		24	
%stdev		10.23		11.42		1.03		1.06		19.0		12	

Appendix G (cont.)

Degree of (trace metal) pyritization (DTMP)

sample	Depth cm	DTMP W182	DTMP W184	DTMP Mo97	DTMP Mo100	DTMP Mn	DOP (Fe)
1A15	0 - 3	83.2%	87.0%	93.7%	93.0%	2.0%	35.2%
1A14	0 - 3	84.5%	88.1%	92.3%	91.7%	1.6%	28.6%
1A13	3 - 4.5	97.2%	98.0%	99.7%	99.4%	2.6%	85.3%
1A12	4.5 - 5.5	97.0%	97.7%	99.7%	99.5%	1.4%	95.4%
1A10	5.5 - 7.6	96.8%	97.5%	99.7%	99.5%	1.1%	93.9%
1A11	7.6 - 11	97.5%	98.0%	99.7%	99.5%	1.1%	93.6%
9A7	0 - 2	83.8%	86.8%	90.6%	90.9%	48.7%	85.8%
9A8	2 - 4.5	92.2%	94.2%	94.2%	94.4%	50.7%	86.1%
9A6	4.5 - 5.5	88.9%	91.7%	91.4%	91.6%	59.4%	86.0%
9A5	5.5 - 7	91.0%	93.3%	93.6%	93.7%	64.2%	86.1%
9A4	7 - 8	86.8%	89.8%	91.7%	92.0%	63.8%	82.8%
9A3	8 - 9.5	87.8%	90.8%	92.6%	92.9%	63.4%	81.1%
9A3DUP	8 - 9.5	88.7%	91.4%	92.9%	93.0%	70.3%	84.9%
9A3TRIP	8 - 9.5	81.6%	84.2%	92.5%	92.6%	67.9%	83.3%
9A2	9.5 - 11	85.4%	88.9%	92.2%	92.4%	63.8%	80.1%
9A1	11 - 11.5	85.6%	88.7%	92.2%	92.1%	63.8%	80.8%
9A3 ave		0.86	0.89	0.927	0.928	0.62	0.85
9A3 stdev		0.04	0.04	0.002	0.002	0.03	0.02
%stdev		4.49	4.45	0.244	0.181	4.24	2.20

LIST OF REFERENCES

Adams Jr, C. E., Xu, L., Walker, N. D., Murray, S. P. (1997). Flow and sediment transport in a shallow bar-built estuary, northern Gulf of Mexico. *Journal of coastal research*, 164-180.

Adelson, J. M., Helz, G. R., & Miller, C. V. (2001). Reconstructing the rise of recent coastal anoxia; molybdenum in Chesapeake Bay sediments. *Geochimica et Cosmochimica Acta*, *65*(2), 237-252.

Algeo, T. J., & Lyons, T. W. (2006). Mo–total organic carbon covariation in modern anoxic marine environments: Implications for analysis of paleoredox and paleohydrographic conditions. *Paleoceanography*, *21*(1).

Alonso J.I.G. and Rodríguez-González P. (2013) *Isotope Dilution Mass Spectrometry*. Cambridge, UK: The Royal Society of Chemistry

Álvarez-Iglesias, P., & Rubio, B. (2009). Redox status and heavy metal risk in intertidal sediments in NW Spain as inferred from the degrees of pyritization of iron and trace elements. *Marine pollution bulletin*, *58*(4), 542-551.

Andreesen, J. R. and Makdessi, K. (2008). Tungsten, the surprisingly positively acting heavy metal element for prokaryotes. *Ann. N.Y. Acad. Sci.* 1125, 215-229.

Arnórsson, S. and Óskarsson, N. (2007). Molybdenum and tungsten in volcanic rocks and in surface and <100ºC ground waters in Iceland. *Geochim. Cosmochim. Acta* 71, 284-304.

Audry, S., Blanc, G., Schäfer, J., Robert, S. (2007). Effect of estuarine sediment resuspension on early diagenesis, sulfide oxidation and dissolved molybdenum

and uranium distribution in the Gironde estuary, France. *Chemical geology*, *238*(3), 149-167.

Aymonino, P. J., Ranade, A. C., Müller, A. (1969a). Evidence for the existence of MoO_3S^{2-} and WO_3S^{2-} ions in aqueous solution. *Z. Anorg. Allgem. Chem.* 371*, 295-299.

Aymonino, P.J., Ranade, A.C, Diemann, E., and Müller, A. (1969b). Study of formation and relative reaction rates of different thioanions of molybdenum and tungsten. *Z. Anorg. Allgem. Chem* 371*, 300-305.

Baes, C. F. Jr. and Mesmer, R. E. (1976). *The Hydrolysis of Cations*. John Wiley and Sons, New York.

Basu, P., Perera, E., Sengar, R. S., Bole, M., Dagget, J., Matosziuk, L., Sajdak, S. (2009). Chapter 7: Syntheses and Properties of Thiomolybdates and Thiotungstates. In: *The Integrated Approach to Chemistry Laboratory.* DEStech Publications, Inc., Lancaster, PA.

Baustian, J. J., & Eugene Turner, R. (2006). Restoration success of backfilling canals in coastal Louisiana marshes. *Restoration Ecology*, *14*(4), 636-644.

Beasley, M.L. (1995). Falgout Canal Protection (TE-02). LDNR. (http://dnrucm.dnr.state.la.us/ucm/groups/coastalprotectionrestoration/documents/ocpr/3890981.pdf, accessed Nov. 22, 2014).

Boyle, E. A., Edmond, J. M., & Sholkovitz, E. R. (1977). The mechanism of iron removal in estuaries. *Geochimica et Cosmochimica Acta*, *41*(9), 1313-1324.

Bednar, A. J., Jones, W. T., Boyd, R. E., Ringelberg, D. B., and Larson, S. L. (2008).

Geochemical parameters influencing tungsten mobility in soils. *J. of Environ. Qual.* 37, 229-233.

Bednar, A. J., Jones, W. T., Boyd, R. E., Jones, W. T., McGrath, C. J., Johnson, D. R., Chappell, M. A., Ringelberg, D. B. (2009). Investigations of tungsten mobility in soil using column tests. *Chemosphere* 75, 1049-1056.

Berner, R. A. (1984). Sedimentary pyrite formation: an update. *Geochimica et Cosmochimica Acta*, *48*(4), 605-615.

Bertine, K. K. (1972). The deposition of molybdenum in anoxic waters. *Marine Chemistry*, *1*(1), 43-53.

Bethke, C. M., and Yeakel, S. (2013) *The Geochemist's Workbench®, Release 9.0.* Aqueous Solutions, LLC., Champaign, IL.

Bethke, C. M. (2008). *Geochemical and Biogeochemical Reaction Modeling. Second Edition.* Cambridge University Press, New York.

Bevers L.E., Hagedoorn P.L., Hagen W.R. (2009). The bioinorganic chemistry of tungsten. *Coordin. Chem. Rev.* 253, 269-90

Bianchi T.S., DiMarco S.F., Smith R.W., Scheiner, K.M. (2009). A gradient of dissolved organic carbon and lignin from Terrebonne-Timbalier Bay estuary to the Louisiana shelf (USA). *Marine Chemistry* 117: 32-41.

Blokhin, A. A. and Kopyrin, A. A. (2003). Kinetics and equilibrium of thiomolybdenum(VI) complex formation in solution: Equilibrium of thiomolybdate (and thiotungstate) formation. *Russ. J. Inorg. Chem.* 36, 785-787.

Bolt, A. M., Sabourin, V., Molina, M. F., Police, A. M., Silva, L. F. N., Plourde, D., Lemaire, M., Ursini-Siegel, J., Mann, K. K. (2014). Tungsten targets the

tumor microenvironment to enhance breast cancer metastasis. *Toxicological Sciences*, kfu219.

Bostick, B. C., Fendorf, S., Helz, G. R. (2003). Differential adsorption of molybdate and tetrathiomolybdate on pyrite (FeS$_2$). *Environ. Sci. Technol.* 37, 285-291.

Brüchert, V., Jørgesen, B. B., Neumann, K., Riechmann, D., Schlösser, M., Schulz, H. (2003). Regulation of bacterial sulfate reduction and hydrogen sulfide fluxes in the central Namibian coastal upwelling zone. *Geochim. Cosmochim. Acta*, 67, 4505-4518.

Brule, J. E. (1982). *Equilibria and kinetics for the formation of trithiomolybdate and tetrathiomolybdate in aqueous solution*. PhD dissertation. Brown University.

Brumsack, H. J., and Gieskes, J. M. (1983). Interstitial water trace-metal chemistry of laminated sediments from the Gulf of California, Mexico. *Marine Chemistry*, *14*(1), 89-106.

Butcher, J. (2011). New substances added to HHS report on carcinogens. National Institute of Environmental Health Sciences. Available: http://www.niehs.nih.gov/news/newsroom/releases/2011/june10/, (accessed May 30, 2013).

Butler, J. N. and Cogley, D. R. (1998). *Ionic Equilibrium: Solubility and pH Calculations*. John Wiley and Sons, New York.

Cahoon, D. R. (1994). Recent accretion in two managed marsh impoundments in coastal Louisiana. *Ecological Applications*, 166-176.

Cahoon, D.R., Reed, D.J., Day, J.W.J., Steyer, G.D., Boumans R.M., Lynch, J.C., McNally, D. Numair, L. (1995). The Influence of Hurricane Andrew on

Sediment Distribution in Louisiana Coastal Marshes. *Journal of Coastal Research*: 15

Calvert, S. E. and Pedersen, T. F. (1993). Geochemistry of recent oxic and anoxic marine sediments: Implications for the geological record. *Marine Geology* 113, 67-88.

Canfield, D. E. (1989). Reactive iron in marine sediments. *Geochimica et cosmochimica acta*, *53*(3), 619-632.

CDC. 2003. A Cross-Sectional Exposure Assessment of Environmental Exposures in Churchill County, Nevada. Final Report. Atlanta, GA:Centers for Disease Control and Prevention. Available: http://www.cdc.gov/nceh/clusters/fallon/study.htm [accessed 15 February 2013].

Chappaz, A., Lyons, T. W., Gregory, D.D., Reinhard, C.T., Gill, B.C., Li, C., Large, R.R. (2014). Does pyrite act as an important host for molybdenum in modern and ancient euxinic sediments? *Geochim. Cosmochim. Acta.* 126, 112-122.

Church, T. M., Sarin, M. M., Fleisher, M. Q., Ferdelman, T. G. (1996). Salt marshes: An important coastal sink for dissolved uranium. *Geochimica et Cosmochimica Acta*, *60*(20), 3879-3887.

Clausen, J. L., Bostick, B. C., Bednar, A., Sun, J., & Landis, J. D. (2011). *Tungsten Speciation in Firing Range Soils* (No. ERDC-TR-11-1). ENGINEER RESEARCH AND DEVELOPMENT CENTER HANOVER NH.

Clausen, J.L., Ketterer, M.E., Bednar, A.J., Koenig, M.R. (2010). Challenges and successes in using inductively coupled plasma mass spectrometry for

measurements of tungsten in environmental water and soil samples. *International Journal of Environmental Analytical Chemistry* 90: 773-83

Clausen, J.L. and Korte, N. (2009). Environmental fate of tungsten from military use. *Science of the Total Environment* 407: 2887-93

Clausen, J.L,. Taylor, S., Larson, S.L., Bednar, A.J., Ketterer, M., Griggs, C., Lambert, D..J, Hewitt, A.D., Ramsey, C.A., Bigl, S.R., Bailey, R.N., Perron, N.M. (2007). Fate and Transport of Tungsten at Camp Edwards Small Arms Ranges. ERDC TR-07-5. Cold Regions Research and Engineering Laboratory, U.S. Army Engineer Research and Development Center, 72 Lyme Road, Hanover, NH; 2007. http://www.crrel.usace.army.mil/home-products.html.

Cornwell, J. C., & Morse, J. W. (1987). The characterization of iron sulfide minerals in anoxic marine sediments. *Marine Chemistry*, *22*(2), 193-206.

Cotton, F.A., Wilkinson, G., Murillo, C.A., Bochmann, M. (1999). Advanced Inorganic Chemistry, 6th edition. John Wiley and Sons, New York.

Crusius, J., Calvert, S., Pedersen, T., Sage, D. (1996). Rhenium and molybdenum enrichments in sediments as indicators of oxic, suboxic and sulfidic conditions of deposition. *Earth and Planetary Science Letters* 145, 65-78.

Cruywagen, J.J. (2000). Protonation, oligomerization, and condensation reactions of vandate(V), molybdate(VI), and tungstate(VI). *Adv. Inorg. Chem.*49.127-182.

Cruywagen JJ, Van der Merwe FJ. 1987. Tungsten(VI) equilibria: A potentiometric and calorimetric investigation. *Journal of the Chemical Society, Dalton Transactions* 7:1701-1705

Cutler, N.K. (2011). *The geochemistry of groundwater and sediments governing tungsten concentration in the basin-fill aquifers Fallon, Nevada. Master's thesis.* University of Nevada, Reno.

Dahl, T. W., Chappaz, A., Fitts, J.P., Lyons, T.W. (2013). Molybdenum reduction in a sulfidic lake: Evidence from X-ray absorption fine-structure spectroscopy and implications for the Mo paleoproxy. *Geochim. Cosmochim. Acta* 103, 213-231.

Dalai, T. K., Nishimura, K., Nozaki, Y. (2005). Geochemistry of molybdenum in the Chao Phraya River estuary, Thailand: Role of suboxic diagenesis and porewater transport. *Chemical geology*, *218*(3), 189-202.

Day, J.W., Kemp, G.P., Reed, D.J., Cahoon, D.R., Boumans, R.M., Suhayda, J.M., Gambrell, R. (2011). Vegetation death and rapid loss of surface elevation in two contrasting Mississippi delta salt marshes: The role of sedimentation, autocompaction and sea-level rise. *Ecological Engineering*: 229-240.

Delaney, J.M., Lundeen, S.R. (1989). The LLNL thermochemical database. Lawrence Livermore National Laboratory Report UCRL-21658.

De Lange, J. J., Middelburg, C. J., Van der Weijden, C. H., Catalano, G., Luther III, G. W., Hydes, D. J., Woittiez, J. R. W., Klinkhammer, G. P. (1990). Composition of anoxic hypersaline brines in the Tyro and Bannock Basins, eastern Mediterranean. *Mar. Chem.* 31, 63-88.

DeLaune, R. D., Reddy, C. N., & Patrick, W. H. (1981). Accumulation of plant nutrients and heavy metals through sedimentation processes and accretion in a Louisiana salt marsh. *Estuaries*, *4*(4), 328-334.

Dellwig, O., Beck, M., Lemke, A., Lunau, M., Kolditz, K., Schnetger, B., Brumsack, H. J. (2007). Non-conservative behaviour of molybdenum in coastal waters: Coupling geochemical, biological, and sedimentological processes. *Geochimica et cosmochimica acta*, *71*(11), 2745-2761.

Dobbek, H. (2011). Structural aspects of mononuclear Mo/W-enzymes. *Coordination Chemistry Reviews*, *255*(9), 1104-1116.

Duchart, P., Price, N. B., & Calvert, S. E. (1973). Trace metals in sediment pore waters. *Limnol. Oceanogr*, *18*, 605-610.

Dzombak, D.A. and Morel, F.M.M. (1990). *Surface Complexation Modeling: Hydrous Ferric Oxide.* John Wiley & Sons, New York

Emerson, S. R. and Huested, S. S. (1991). Ocean anoxia and the concentrations of molybdenum and vanadium in seawater. *Mar. Chem.* 34, 177-196.

Erickson, B. E. (1998). The speciation of molybdenum in sulfidic natural waters. *Ph.D. dissertation*. College Park, MD: University of Maryland.

Erickson, B., and Helz, G. R. (2000). Molybdenum(VI) speciation in sulfidic waters: Stability and lability of thiomolybdates. *Geochim. Cosmochim. Acta*, 64, 1149-1158.

Firdaus, M. L., Norisuye, K., Nakagawa, Y., Nakatsuka, S., Sohrin, Y. (2008). Dissolved and labile particulate Zr, Hf, Nb, Ta, Mo and W in the western North Pacific Ocean. *Journal of Oceanography* 64, 247-257.

Feng, Z., & Li, C. (2010). Cold-front-induced flushing of the Louisiana Bays. *Journal of Marine Systems*, *82*(4), 252-264.

Froelich, P., Klinkhammer, G. P., Bender, M. A. A., Luedtke, N. A., Heath, G. R., Cullen, D., ... & Maynard, V. (1979). Early oxidation of organic matter in

pelagic sediments of the eastern equatorial Atlantic: suboxic diagenesis. *Geochimica et Cosmochimica Acta*, *43*(7), 1075-1090.

Fry, B. (2008). Open bays as nurseries for Louisiana brown shrimp. *Estuaries and Coasts*, *31*(4), 776-789.

Gaillardet, J., J. Viers and B. Dupre (2005): Trace elements in river waters. p. 225–272. In *Treatise on Geochemistry*, Vol.3, ed. by H. D. Holland and K. K. Turekian, Elsevier, Amsterdam.

Glass, J. B., Yu, H., Steele, J. A., Dawson, K. S., Sun, S., Chourey, K., ... & Orphan, V. J. (2014). Geochemical, metagenomic and metaproteomic insights into trace metal utilization by methane-oxidizing microbial consortia in sulphidic marine sediments. *Environmental microbiology*, *16*(6), 1592-1611.

Gonzalez, P.J., Rivas, M.G., Mota, C.S., Brondino, C.D., Moura, I., Moura, J. J.G. (2013). Periplasmic nitrate reductases and formate dehydrogenases: Biological control of the chemical properties of Mo and W for fine tuning of reactivity, substrate specificity and metabolic role. *Coordin. Chem. Rev.*257, 315-331.

Goyet C., Bradshaw A. L., Brewer P. G. (1991). The carbonate system in the Black Sea. *Deep-Sea Res.* 38 (Suppl. 2), S1049–S1068.

Gustafsson, J.P., 2003. Modelling molybdate and tungstate adsorption to ferrihydrite. *Chem. Geol*. 200, 105-115.

Hach Company. (1997). DR/4000 spectrophotometer handbook. Hach Company, Loveland, CO.

Harmer, M.A. and Sykes, A.G. (1980). Kinetics of the interconversion of sulfido- and oxomolybdate(VI) species $Mo_xS_{4-x}^{2-}$ in aqueous solutions. *Inorg. Chem.* 19, 2881-2885.

Hazen, R. M., Finger, L. W., Mariathasan, J. W. (1985). High-pressure crystal

chemistry of scheelite-type tungstates and molybdates. *Journal of Physics and

Chemistry of Solids*, *46*(2), 253-263.

Helz, G. R.; Bura-Nakic, E.; Mikac, N.; Ciglenecki, I., New model for molybdenum

behavior in euxinic waters. (2011). *Chemical Geology 284*, (3-4), 323-332.

Helz, G. R. and Dolor, M. K. (2012). What regulates rhenium deposition in euxinic

basins? *Chem. Geol.* 304-305, 131-141.

Helz, G. R., Erickson, B. E., & Vorlicek, T. P. (2014). Stabilities of thiomolybdate

complexes of iron; implications for retention of essential trace elements (Fe,

Cu, Mo) in sulfidic waters. *Metallomics*, *6*(6), 1131-1140.

Helz, G.R., Miller, C.V., Charnock, J.M., Mosselmans, J. F.W., Pattrick, R.A.D.,

Garner, C.D., Vaughn, D. J. (1996). Mechanism of molybdenum removal from

the sea and its concentration in black shales: EXAFS evidence. *Geochim.

Cosmochim. Acta,* 60, 3631-3642.

Helz, G.R., Vorlicek, T.P., Kahn, M.D., 2004. Molybdenum scavenging by iron

monosulfide. Environ. Sci. Technol. 38, 4263–4268.

Hines, M. E., Berry Lyons, W. M., Armstrong, P. B., Orem, W. H., Spencer, M. J.,

Gaudette, H. E., & Jones, G. E. (1984). Seasonal metal remobilization in the

sediments of Great Bay, New Hampshire. *Marine chemistry*, *15*(2), 173-187.

Hoede, D., Wijkstra, J., van der Sloot, H. A. (1987). Dissolved trace oxyanions and

trace elements in suspended matter and sediments in Indonesian waters. Data

report of the ECN participation in the Snellius II expedition. ECN-203,

Netherlands Energy Research Foundation, Petten.

Holdren, G. R., Bricker, O. P., & Matisoff, G. (1975).Chapter 20 In: *Marine

Chemistry in the Coastal Environment.*Church, T.M. (ed.)

Hong, J.W., Calmano, W., Förstner. (1995). Interstitial waters. In: *Trace Elements in Natural Waters*. Brit Salbu and Eiliv Steinnes (eds.). CRC Press, Boca Raton, Florida.

Howarth, R.W. (1984). The ecological significance of sulfur in the energy dynamics of salt marsh and coastal marine sediments. *Biogeochemistry,* 1, 5-27.

Hsu, L. C. (1977). Effects of oxygen and sulfur fugacities on the scheelite-tungstenite and powellite-molybdenite stability relations. *Economic Geology*, *72*(4), 664-670.

Hsu, S.C., Hsieh, H.L., Chen, C.P., Tseng, C.M., Huang S.C., Huang, C.H., Huang, Y.T, Radashevsky, V., and Lin, S.H. (2011). Tungsten and other heavy metal contamination in aquatic environments receiving wastewater from semiconductor manufacturing. *J. Hazard. Mater.,* 189, 193-202.

Hu, Z. and Gao, S. (2008). Upper crustal abundances of trace elements: A revision and update. *Chem. Geol.* 253, 205-221.

Huerta-Diaz, M. A., & Morse, J. W. (1990). A quantitative method for determination of trace metal concentrations in sedimentary pyrite. *Marine Chemistry*, *29*, 119-144.

Huerta-Diaz, M. A., and Morse, J. W. (1992). Pyritization of trace metals in anoxic marine sediments. *Geochimica et Cosmochimica Acta*, *56*(7), 2681-2702.

Inoue, M., and Wiseman Jr, W. J. (2000). Transport, mixing and stirring processes in a Louisiana estuary: a model study. *Estuarine, Coastal and Shelf Science*, *50*(4), 449-466.

Ivanova, G. F. (1986). Geochemistry of tungsten. In: Geology of Tungsten (ed. Beus,

A. A.) UNESCO, Paris. 11-43.

Johannesson, K. H., Dave, H. B., Mohajerin, T. J., Datta, S. (2013). Controls on tungsten concentrations in groundwater flow systems: The role of adsorption and thiotungstate formation. *Chem. Geol.* 351, 76-94.

Johannesson, K. H., Lyons, B. W., Graham, E. Y., Welch, K.A. (2000). Oxyanion concentrations in Eastern Sierra Nevada Rivers-3. Boron, Molybdenum, Vanadium, and Tungsten. *Aquat. Geochem.,* 6: 19-46.

Johannesson, K.H., Maest A.S., Lyons W.B. (1992) Oxyanion concentration mechanisms in eastern Sierra Nevada surface waters. In *The History of Water: Eastern Sierra Nevada, Owens Valley, White-Inyo Mtns.(eds. CA Hall, Jr., V. Doyle-Jones, and B. Widawski) White Mtn. Res. Station Symp* (Vol. 4, pp. 348-366).

Johannesson, K. H., Tang, J., Daniels, J. M., Bounds, W. J., & Burdige, D. J. (2004). Rare earth element concentrations and speciation in organic-rich blackwaters of the Great Dismal Swamp, Virginia, USA. *Chemical Geology*, *209*(3), 271-294.

Johannesson, K.H. and Tang, J. (2009). Conservative behavior of arsenic and other oxyanion-forming trace elements in an oxic groundwater flow system. *J. Hydrol.*378, 13-28.

Kalinich, J. F., Emond, C. A., Dalton, T. K., Mog, S. R., Coleman, G. D., Kordell, J. E., Miller, A. C., Widmer, D. E. (2005). Embedded Weapons-Grade Tungsten Alloy Shrapnel Rapidly Induces Metastatic High-Grade Rhabdomyosarcomas in F344 Rats. *Environ. Health Persp.*113, 729-734.

Kashiwabara, T., Takahahi, Y., Marcus, M. A., Uruga, T., Tanida, H., Terada, Y. and Usui A. (2013). Tungsten species in natural ferromanganese oxides related to

its different behavior from molybdenum in oxic ocean. *Geochim. Cosmochim. Acta* 106, 364-378.

Kashiwabara, T., Takahashi, Y., Uruga, T., Tanida, H., Terada, Y., Niwa, Y., & Nomura, M. (2010). Speciation of tungsten in natural ferromanganese oxides using wavelength dispersive XAFS. *Chemistry Letters*, *39*(8), 870-871.

Kelly, A. D. R., Lemaire, M., Young, Y. K., Eustache, J. H., Guilbert, C., Molina, M. F., Mann, K. K. (2013). *In vivo* tungsten exposure alters B-cell development and increases DNA damage in murine bone marrow. *Toxicological Sciences* 131, 434-446.

Kieber, R. J., and Helz, G. R. (1992). Indirect photoreduction of aqueous chromium (VI). *Environmental science & technology*, *26*(2), 307-312.

Kim, J. H. (1999). Spurious correlation between ratios with a common divisor. *Statistics & probability letters*, *44*(4), 383-386.

Kishida K, Sohrin Y, Okamura K, Ishibachi J. (2004). Tungsten enriched in submarine hydrothermal fluids. *Earth and Planetary Science Letters* 222: 819-27

Kletzin, A., and Adams, M.W. (1996). Tungsten in biological systems. *FEMS Microbiol. Rev.* 18, 5-63.

Koretsky, C. M., Haas, J. R., Ndenga, N. T., & Miller, D. (2006). Seasonal variations in vertical redox stratification and potential influence on trace metal speciation in minerotrophic peat sediments. *Water, air, and soil pollution*, *173*(1-4), 373-403.

Koretsky, C.M., Van Cappellen, P., DiChristina, T.J., Kostka, J.E., Lowe, K.L., Moore, C.M., Roychoudhury, A.N., Viollier, E. (2005). Salt marsh pore water

geochemistry does not correlate with microbial community structure. *Est.*

Coast. Shelf Sci. 62, 3233-251.

Koschinsky, A. and Hein, J.R. (2003). Uptake of elements from seawater by

ferromanganese crusts: solid-phase associations and seawater speciation. *Mar.*

Geol. 198, 331-351.

Kostka, J. E., & Luther III, G. W. (1995). Seasonal cycling of Fe in saltmarsh

sediments. *Biogeochemistry*, *29*(2), 159-181.

Koutsospyros, A., Braida, W., Christodoulatos, C., Dermatas, D., Strigul, N. (2006).

A review of tungsten: From environmental obscurity to scrutiny. *Journal of*

Hazardous Materials, 136, 1-19.

Krauskopf, K. B. (1970). Tungsten. In: *Handbook of Geochemistry* (ed. Wedepohl, K.

H.) Vol. II-5, Chapter 74 B-O. Springer, Berlin.

Kulmukhamedov, G. K., Zelikman, A. N., Vol'dman, G. M., Verevkin, G. V. (1991).

Thiotungstates(VI) and thiomolybdates(VI) in solutions containing Na_2S and

Na_2CO_3. *Russ. J. Inorg. Chem* 36, 1675-1677.

Kunzendorf, H., & Glasby, G. P. (1992). Tungsten accumulation in Pacific

ferromanganese deposits. *Mineralium Deposita*, *27*(2), 147-152.

Large, R. R., Halpin, J. A., Danyushevsky, L. V., Maslennikov, V. V., Bull, S. W.,

Long, J. A., ... & Calver, C. R. (2014). Trace element content of sedimentary

pyrite as a new proxy for deep-time ocean–atmosphere evolution. *Earth and*

Planetary Science Letters, *389*, 209-220.

Lassner, E., & Schubert, W. D. (1999). *Tungsten: properties, chemistry, technology of*

the elements, alloys, and chemical compounds. Springer.

Lee, M. K.; Saunders, J. A.; Wilkin, R. T.; Mohammad, S. (2005). Geochemical modeling of arsenic speciation and mobilization: Implications for bioremediation. *Advances in Arsenic Research: Integration of Experimental and Observational Studies and Implications for Mitigation*, *915*, 398-413.

Lindberg, Vern. (2001)." Uncertainties and Error Propagation: Part I of a Manual on Uncertainties, Graphing, and the Vernier Caliper." N.p., 1 July 2000. Web. 18 July 2014. <http://www.rit.edu/~w-uphysi/uncertainties/Uncertaintiespart2.html>.

Lindstedt, D.M. (2005). Renewable resources at stake: Barataria-Terrebonne estuarine system in southeast Louisiana. *Journal of Coastal Research* 44: 162-175

Lord III, C. J. (1982). A Selective and Precise Method for Pyrite Determination in Sedimentary Materials: RESEARCH-METHOD PAPER. *Journal of Sedimentary Research*, *52*(2).

Lord, C.J. III, and Church, T.M. (1983). The geochemistry of salt marshes: Sedimentary ion diffusion, sulfate reduction, and pyritization. *Geochim. Cosmochim. Acta,* 47, 1381-1391.

LUMCON weather station. (2014). Monitoring data from Terrebonne Bay and LUMCON environmental stations near Chauvin, LA. (http://weather.lumcon.edu/; last accessed Oct. 25, 2014).

Luther G.W. III and Church T. M. (1988). Seasonal cycling of sulfur and iron in porewaters of a Delaware salt marsh. *Mar. Chem.* 23, 295-309.

Luther III, G. W., Kostka, J. E., Church, T. M., Sulzberger, B., & Stumm, W. (1992). Seasonal iron cycling in the salt-marsh sedimentary environment: the importance of ligand complexes with Fe (II) and Fe (III) in the dissolution of Fe (III) minerals and pyrite, respectively. *Marine Chemistry*, *40*(1), 81-103.

Madison, A. S., Tebo, B. M., Mucci, A., Sundby, B., & Luther, G. W. (2013). Abundant porewater Mn (III) is a major component of the sedimentary redox system. *science*, *341*(6148), 875-878.

Mamindy-Pajany, Y.; Bataillard, P.; Seby, F.; Crouzet, C.; Moulin, A.; Guezennec, A. G.; Hurel, C.; Marmier, N.; Battaglia-Brunet, F. (2013). Arsenic in Marina Sediments from the Mediterranean Coast: Speciation in the Solid Phase and Occurrence of Thioarsenates. *Soil & Sediment Contamination, 22* (8), 984-1002.

Marquet, P., Francois, B., Lofti, H., Turcant, A., Debord, J., Nedelec, G., et al. (1997). Tungsten determination in biological fluids, hair and nails by plasma emission spectrometry in a case of severe acute intoxication in man. *J. Forensic Sci.* 42, 527-530.

McDonald, J. W., Friesen, G. D., Rosenhein, L. D., Newton, W. E. (1983). Syntheses and characterization of ammonium and tetraalkylammonium thiomolybdates and thiotungstates. *Inorg. Chim. Acta*, 72, 205-210.

McKee, B.A., Wiseman, W.J. Jr. Inoue, M. (1994). Salt-water intrusion and sediment dynamic in a bar-built estuary. In: *Changes in Fluxes in Estuaries: Implications from Science to Management* Olsen & Olsen: Fredensborg; 13-16.

McKnight, D. M., Kimball, B. A., Bencala, K. E. (1988). Iron photoreduction and oxidation in an acidic mountain stream. *Science*, *240*(4852), 637-640.

Miller, C. A., Peucker-Ehrenbrink, B., Walker, B. D., & Marcantonio, F. (2011). Re-assessing the surface cycling of molybdenum and rhenium. *Geochimica et Cosmochimica Acta*, *75*(22), 7146-7179.

Millward, R. N., Carman, K. R., Fleeger, J. W., Gambrell, R. P., Powell, R. T., & Rouse, M. A. M. (2001). Linking ecological impact to metal concentrations and speciation: a microcosm experiment using a salt marsh meiofaunal community. *Environmental toxicology and chemistry*, *20*(9), 2029-2037.

Mohajerin, T.J., Helz, G.R., Datta, S., Grimm, D., Kolker, A., Johannesson, K.H.(in prep). Geochemical differences of tungsten and molybdenum in coastal waters: The effects of speciation on sequestration and mobilization.

Mohajerin, T.J., Helz, G.R., White, C.D., Johannesson, K.H.(2014a). Tungsten speciation in sulfidic waters: Determination of thiotungstate formation constants and comparison of molybdenum and tungsten in euxinic basins. *Geochimica Et Cosmochimica Acta* 144, 157-172

Mohajerin, T.J., Johannesson, K., Kolker, A., Palmore, D., Datta, S. (2014c). Concentration and speciation of tungsten and molybdenum in estuarine surface and underlying porewaters. Goldschmidt conference 2014, Sacramento, CA.

Mohajerin, T. J., Neal, A. W., Telfeyan, K., Sasihharan, S. M.,Ford, S.; Yang, N., Chevis, D. A., Grimm, D. A., Satta, S., White, C. D., Johannesson, K. H. (2014b) Geochemistry of tungsten and arsenic in aquifer systems: A comparative study of groundwaters from West Bengal, India and Nevada, USA. *Water Air and Soil Polution* 225 1792

Montgomery, D. C., Peck, E. A., Vining, G. G. (2012). *Introduction to linear*

regression analysis. Wiley Series in Probability and Statistics. Wiley.

Morford, J. L., Emerson, S. R., Breckel, E. J., & Kim, S. H. (2005). Diagenesis of oxyanions (V, U, Re, and Mo) in pore waters and sediments from a continental margin. *Geochimica et Cosmochimica Acta*, *69*(21), 5021-5032.

Morford, J. L., Martin, W. R., Kalnejais, L. H., François, R., Bothner, M., Karle, I. M. (2007). Insights on geochemical cycling of U, Re and Mo from seasonal sampling in Boston Harbor, Massachusetts, USA. *Geochimica et cosmochimica acta*, *71*(4), 895-917.

Morse, J. W. (1994). Interactions of trace metals with authigenic sulfide minerals: implications for their bioavailability. *Marine Chemistry*, *46*(1), 1-6.

Morse, J. W., & Luther Iii, G. W. (1999). Chemical influences on trace metal-sulfide interactions in anoxic sediments. *Geochimica et Cosmochimica Acta*, *63*(19), 3373-3378.

Morse, J. W., Thomson, H., & Finneran, D. W. (2007). Factors controlling sulfide geochemistry in sub-tropical estuarine and bay sediments. *Aquatic Geochemistry*, *13*(2), 143-156.

Müller, A., Diemann, E., Ranade, A. C., and Aymonino, P. J. (1969). Electronic spectra of MoO_3S^{2-} and WO_3S^{2-} and their comparison with the spectra from the ions of $MoO_xS_{4-x}^{2-}$ and WO_xS_{4-x}. *Z. Naturforch.*, 24b, 1247-1249.

Müller, A., Diemann, E., and Schulze, H. (1970). Über K_2MoOS_3 und K_2WOS_3 und ihre Reaktion mit Selenwasserstoff zu Dithiomonoselenomolybdaten und – wolframaten Röntgenkristallographische Daten von Cs_2MoOS_2Se und Cs_2WOS_2Se. *Z. Anorg. Allgem. Chem.* 376, 120-124.

Müller, A., & Diemann, E. (Eds.). (1981). *Transition Metal Chemistry: Current Problems of General, Biological and Catalytical Relevance; Proceedings of a Workshop Held at Bielefeld, Germany, 14-17 July, 1980*. Verlag Chemie.

Neretin, L.N., Volkov, I.I., Böttcher, M.E., Grinenko, V.A. (2001). A sulfur budget for the Black Sea anoxic zone. *Deep-Sea Res.,* 48, 2569-2593.

Neumann, T., Scholz, F., Kramar, U., Ostermaier, M., Rausch, N., & Berner, Z. (2013). Arsenic in framboidal pyrite from recent sediments of a shallow water lagoon of the Baltic Sea. *Sedimentology*, *60*(6), 1389-1404.

Nyman, JA, DeLaune, RD, Pezeshki, SR, Patrick Jr., WH. (1995). Organic matter fluxes and marsh stability in a rapidly submerging estuarine marsh. *Estuaries* 18: 207-218

O'Boyle S, McDermott G, Noklegaard T, Wilkes R. (2013). A Simple Index of Trophic Status in Estuaries and Coastal Bays Based on Measurements of pH and Dissolved Oxygen. *Estuaries and Coasts* 36: 158-73

Penland, S., & Ramsey, K. E. (1990). Relative sea-level rise in Louisiana and the Gulf of Mexico: 1908-1988. *Journal of Coastal Research*, 323-342.

Penland, S., Suter, J. R., McBride, R. A. (1987). Delta plain development and sea level history in the Terrebonne coastal region, Louisiana. In *Coastal Sediments* (pp. 1689-1705). ASCE.

Petrunic, B.M., Al, T.A. (2005). Mineral/water interactions in tailings from a tungsten mine, Mount Pleasant, New Brunswick. *Geochimica et Cosmochimica Acta* 69: 2469-2483

Pilipchuk, M. F. and Volkov, I. I. (1966). Tungsten in Recent Black Sea sediments. Translated from: *Dokl. Acad. Nauk. SSSR* 167, 430-433.

Pilson, M.E.Q. (1998). *An Introduction to the Chemistry of the Sea.* Prentice Hall, Inc. USA.

Pokrovsky, O.S., Schott, J. (2002). Iron colloids/organic matter associated transport of major and trace elements in small boreal rivers and their estuaries (NW Russia). *Chemical Geology* 190: 141-79

Prager, EJ. (1992). *Modeling of circulation and transport in Terrebonne Bay, Louisiana and its implications for oyster harvesting management*. Baton Rouge, LA. Louisiana State University and Agricultural and Mechanical College.

R Core Team, R (2013). A language and environment for statistical computing, R Foundation for Statistical Computing, Vienna, Austria

Rabalais, N. N. (1995). *Status and trends of eutrophication, pathogen contamination, and toxic substances in the Barataria-Terrebonne estuarine system*. Barataria-Terrebonne National Estuary Program. Publication #22.

Rahaman, W., Singh, S. K., & Raghav, S. (2010). Dissolved Mo and U in rivers and estuaries of India: Implication to geochemistry of redox sensitive elements and their marine budgets. *Chemical Geology*, *278*(3), 160-172.

Reed, D. J. (1989). Patterns of sediment deposition in subsiding coastal salt marshes, Terrebonne Bay, Louisiana: the role of winter storms. *Estuaries*, *12*(4), 222-227.

Rickard, D. (2006). The solubility of FeS. *Geochimica Et Cosmochimica Acta*, *70*(23), 5779-5789.

Robie, R.A., Hemingway, B.S, Fisher, J.R. (1978). Thermodynamic properties of minerals and related substances at 298.15 K and 1 bar (10^5 Pascals) pressure and at higher temperatures. U. S. Geol. Surv. Bull. 1452, 456

Rozan, T. F., Taillefert, M., Trouwborst, R. E., Glazer, B. T., Ma, S., Herszage, J., ... & Luther III, G. W. (2002). Iron-sulfur-phosphorus cycling in the sediments of a shallow coastal bay: Implications for sediment nutrient release and benthic macroalgal blooms. *Limnology and Oceanography*, *47*(5), 1346-1354.

Rozantsev, G. M. and Sazonova, O. I. (2005). Thermodynamic parameters of interconversions of isopolyanions in solutions of tungsten(VI). *Russ. J. Coord. Chem.* 31, 552-558.

Rubin, C.S., Holmes, A.K., Belson, M.G., Jones, R.L., Flanders, W.D., et al. (2007). Investigating childhood leukemia in Churchill County, Nevada. *Environmental Health Perspectives* 115: 151-7

Scheiderich, K., Helz, G. R., & Walker, R. J. (2010). Century-long record of Mo isotopic composition in sediments of a seasonally anoxic estuary (Chesapeake Bay). *Earth and Planetary Science Letters*, *289*(1), 189-197.

Scholz, F., & Neumann, T. (2007). Trace element diagenesis in pyrite-rich sediments of the Achterwasser lagoon, SW Baltic Sea. *Marine Chemistry*, *107*(4), 516-532.

Scholz, F., Severmann, S., McManus, J., & Hensen, C. (2014). Beyond the Black Sea paradigm: The sedimentary fingerprint of an open-marine iron shuttle. *Geochimica et Cosmochimica Acta*, *127*, 368-380.

Schroeder, W.W., Wiseman, W.J. Jr. (1999). Geology and hydrodamics of Gulf of Mexico estuaries. *Biogeochemistry of Gulf of Mexico Estuaries.* In Bianchi TS, Pennock JR, Twilley, RR (Eds.), John Wiley and Sons, Inc, New York, 3-28.

Seiler, R. (2012). Physical setting and natural sources of exposure to carcinogenic trace elements and radionuclides in Lahontan Valley, Nevada. *Chemico-biological interactions*, *196*(3), 79-86.

Seiler, R. (2004). Temporal Changes in Water Quality at a Childhood Leukemia Cluster. *Ground Water*, *42*(3), 446-455.

Seiler, R., Stollenwerk, K. G., and Garbarino, J. R. (2005). Factors controlling tungsten concentrations in ground water, Carson Desert, Nevada. *Appl. Geochem.* 20, 423-441.

Severmann, S., Lyons, T. W., Anbar, A., McManus, J., & Gordon, G. (2008). Modern iron isotope perspective on the benthic iron shuttle and the redox evolution of ancient oceans. *Geology*, *36*(6), 487-490.

Sheppard, P. R., Speakman, R. J., Ridenour, G., & Witten, M. L. (2007). Temporal variability of tungsten and cobalt in Fallon, Nevada. *Environmental health perspectives*, 715-719.

Sheppard, P. R., Speakman, R. J., Ridenour, G., & Witten, M. L. (2008). Tungsten and Cobalt: Sheppard et al. Respond. *Environmental health perspectives*, *116*(5), A197.

Sheppard, P.R., Witten, M.L. Dendrochemistry of urban trees in an environmental exposure analysis of childhood leukemia cluster areas, EOS Trans. AGU, 84 (46), Fall Meet. Suppl., 2003 (Abstract B12F-07).

Smith, R.M., Martell, A.E.(2004). NIST Standard Reference Database 46: NIST critically selected stability constants of metal complexes database. US Department of Commerce Technology Admistration

Sohrin, Y., Matsui, M., and Nakayama, E. (1999). Contrasting behavior of tungsten and molybdenum in the Okinawa Trough, the East China Sea and the Yellow Sea *Geochim. Cosmochim. Acta* 63, 3457-3466.

Sohrin, Y., Fujishima, Y., Ueda, K., Akiyama, S., Mori, K., Hasegawa, H., and Matsui, M. (1998). Dissolved niobium and tantalum in the North Pacific. *Geophys. Res. Lett.*25, 999-1002.

Sohrin, Y., Isshiki, K., and Kuwamoto, T. (1987). Tungsten in North Pacific waters. *Mar. Chem.* 22, 95-103.

Solis, R.S. and Powell, G.L. (1999). Hydrography, mixing characteristics, and residence times of Gulf of Mexico estuaries. In Bianchi TS, Pennock JR, Twilley, RR (Eds.), *Biogeochemistry of Gulf of Mexico Estuaries*. John Wiley and Sons, Inc, New York, 29-61.

Stiefel, E. I. (2002). The biogeochemistry of molybdenum and tungsten. In: *Metals Ions in Biological System* (eds. Sigel, A. and Sigel, H.). Vol 39: Molybdenum

and Tungsten: Their roles in biological processes. CRC Press, New York: Marcel Dekker.

Strigul, N. (2010). Does speciation matter for tungsten ecotoxicology? *Ecotox. Environ. Safe.* 73*,*1099-1113.

Strigul, N., Galdun, C., Vaccari, L., Ryan, T., Braida, W., and Christodoulatos, C. (2009). Influence of speciation on tungsten toxicity. *Desalination* 248, 869-879.

Strigul, N., Koutsospyros, A., and Christodoulatos, C. (2010). Tungsten speciation and toxicity: Acute toxicity of mono- and poly-tungstates to fish. *Ecotox. Environ. Safe.* 73*,* 164-171.

Sundby, B., Martinez, P., and Gobeil, C. (2004). Comparative geochemistry of cadmium, rhenium, uranium, and molybdenum in continental margin sediments. *Geochim. Cosmochim. Acta* 68, 2485-2493.

Takematsu, N., Sato, Y., Okabe, S., & Usui, A. (1990). Uptake of selenium and other oxyanionic elements in marine ferromanganese concretions of different origins. *Marine chemistry*, *31*(1), 271-283.

Tang, J., Whittecar, G. R., Johannesson, K. H., & Daniels, W. L. (1999). Potential contaminants at a dredged spoil placement site, Charles City County, Virginia, as revealed by sequential extraction. *Geochemical Transactions*, *5*(4), 49.

Taylor, H. E., Antweiler, R. C., Roth, D. A., Alpers, C. N., & Dileanis, P. (2012). Selected trace elements in the Sacramento River, California: Occurrence and distribution. *Archives of environmental contamination and toxicology*, *62*(4), 557-569.

Thamdrup, B., Fossing, H., & Jørgensen, B. B. (1994). Manganese, iron and sulfur cycling in a coastal marine sediment, Aarhus Bay, Denmark. *Geochimica et Cosmochimica Acta*, *58*(23), 5115-5129.

Tribovillard, N., Algeo, T.J., Lyons, T., and Riboulleau, A. (2006). Trace metals as paleoredox and paleoproductivity proxies: An update. *Chem. Geol.* 232, 12-32.

Tsigdinos, G. A. (1978). Inorganic sulphur compounds of molybedenum and tungsten- Their preparation, structure, and properities. Ed. Boschke, F. L. *Topics in Current Chemistry.* Germany: Springer-Verlag. 65-106.

Tyrrell J., Galloway T.S., Abo-Zaid G., Melzer D., Depledge M.H., Osborne N.J. (2013). High urinary tungsten concentration is associated with stroke in the National Health and Nutrition Examination Survey 1999-2010. *Plos One* 8, 1-7 (e77546).

Van der Sloot, H. A., Hoede, D., Hamburg, G., Woittiez, J. R. W., and van der Weijden, C. H. (1990). Trace elements in suspended matter from the anoxic hypersaline Tyro and Bannock Basins (eastern Mediterranean). *Mar. Chem.* 31, 187-203.

Van der Sloot, H. A., Hoede, D., and Wijkstra, J. (1989). Trace oxyanions and their behavior in the Rivers Porong and Solo, the Java Sea and the adjacent Indian Ocean. *Neth. J. Sea Res.* 23, 379-386.

Van der Sloot, H. A., Hoede, D., Wijkstra, J., Duinker, J. C., and Nolting, R. F. (1985). Anionic species of V, As, Se, Mo, Sb, Te, and W in the Scheldt and Rhine estuaries and the Southern Bight (North Sea). *Estuar. Coast. Shelf Sci.* 21, 633-651.

Vasyukova, E.V., Pokrovsky, O.S., Viers, J., Oliva, P., Dupre, B., et al. (2010). Trace elements in organic- and iron-rich surficial fluids of the boreal zone: Assessing colloidal forms via dialysis and ultrafiltration. *Geochimica Et Cosmochimica Acta* 74: 449-68

Vorlicek, T. P., Kahn, M. D., Kasuya, Y., and Helz, G. R. (2004). Capture of molybdenum in pyrite-forming sediments: Role of ligand-induced reduction by polysulfides. *Geochim. Cosmochim. Acta* 68*,* 547-549.

Wang, D., Aller, R. C., & Sanudo-Wilhelmy, S. A. (2011). Redox speciation and early diagenetic behavior of dissolved molybdenum in sulfidic muds. *Marine Chemistry*, *125*(1), 101-107.

Wang, F. C. (1997). Dynamics of intertidal marshes near shallow estuaries in Louisiana. *Wetlands Ecology and Management*, *5*(2), 131-143.

Wang, F. C., Lu, T., & Sikora, W. B. (1993). Intertidal marsh suspended sediment transport processes, Terrebonne Bay, Louisiana, USA. *Journal of Coastal Research*, 209-220.

Hans Wedepohl, K. (1995). The composition of the continental crust. *Geochimica et cosmochimica Acta*, *59*(7), 1217-1232.

Wichard, T., Mishra, B., Myneni, S. C., Bellenger, J. P., & Kraepiel, A. M. (2009). Storage and bioavailability of molybdenum in soils increased by organic matter complexation. *Nature Geoscience*, *2*(9), 625-629.

Wiseman WJ Jr., Swenson EM, Kelly FJ. (1990). Control of estuarine salinities by coastal ocean salinity.- In: Cheng, R.T. (ed.): *Residual currents and long-term transport processes. Coastal and Estuarine Studies* 38: 184-193

Witten, M. L., Sheppard, P. R., Witten, B. L. (2012). Tungsten toxicity. *Chemico-Biological Interactions*196, 87-88.

Xu, N., Christodoulatos, C., Braida, W. (2006). Modeling the competitive effect of phosphate, sulfate, silicate, and tungstate anions on the adsorption of molybdate onto goethite. *Chemosphere* 64, 1325-1333.

Yao W, and Byrne R. (1999). Determination of trace chromium(VI) and molybdenum(VI) in natural and bottled mineral waters using long pathlength absorbance spectroscopy (LPAS). *Talanta* 48: 277 - 282

Zheng, Y., Anderson, R. F., van Geen, A., Kuwabara, J. (2000). Authigenic molybdenum formation in marine sediments: A link to pore water sulfide in the Santa Barbara Basin. *Geochim. Cosmochim. Acta* 64, 4165-4178.

BIOGRAPHY

Tahmineh Jade Mohajerin Haug was born on October 12, 1976 in Tehran, Iran to an American mother and Iranian father. She was in Texas from the time she started first grade until she graduated with a B.S. in Biology (Ecology, Evolution, and Conservation) from the University of Texas in Austin in 1998. She served in Peace Corps in Madagascar from 2000-2002 doing environmental education. After working for the National Park Service from 2003-2007, she moved to Denmark to be with her now husband, Bjarne Haug. Upon return to the U.S. in 2008, she sought to further her education in hopes of becoming involved in water quality. As a graduate student at Tulane University, she accompanied Dr. Karen Johannesson and Dr. Saugata Datta to India to study high arsenic concentrations in the groundwaters used as a drinking water source. She is currently employed as a geologist with the Bureau of Ocean and Energy Management in New Orleans, LA.